CAPITAL UNIVERSITY OF SCIENCE AND TECHNOLOGY, ISLAMABAD

MHD Prandtl-Eyring Hybrid Nanofluid Flow Over a Permeable Moving Surface with Thermal Radiation

by

Shahmer Ahmed

A thesis submitted in partial fulfillment for the degree of Master of Philosophy

in the

Faculty of Computing
Department of Mathematics

2023

I dedicate my dissertation work to my ***family*** *and dignified* ***teachers****. A special feeling of gratitude to my loving* ***parents*** *and elder brother* ***Sagheer Ahmed Abbasi*** *who have supported me in my studies.*

CERTIFICATE OF APPROVAL

MHD Prandtl-Eyring Hybrid Nanofluid Flow Over a Permeable Moving Surface with Thermal Radiation

by

Shahmer Ahmed

(MMT-193034)

THESIS EXAMINING COMMITTEE

S. No.	Examiner	Name	Organization
(a)	External Examiner	Dr. Tanvir Akbar	COMSATS, Islamabad
(b)	Internal Examiner	Dr. Muhammad Afzal	CUST, Islamabad
(c)	Supervisor	Dr. Dur-e-Shehwar Sagheer	CUST, Islamabad

Dr. Dur-e-Shehwar Sagheer
Thesis Supervisor
July, 2023

Dr. Muhammad Sagheer
Head
Dept. of Mathematics
July, 2023

Dr. Muhammad Abdul Qadir
Dean
Faculty of Computing
July, 2023

Author's Declaration

I, **Shahmer Ahmed** hereby state that my MPhil thesis titled " **MHD Prandtl-Eyring Hybrid Nanofluid Flow Over a Permeable Moving Surface with Thermal Radiation**" is my own work and has not been submitted previously by me for taking any degree from Capital University of Science and Technology, Islamabad or anywhere else in the country/abroad.

At any time if my statement is found to be incorrect even after my graduation, the University has the right to withdraw my MPhil Degree.

(Shahmer Ahmed)
Registration No: MMT-193034

Plagiarism Undertaking

I solemnly declare that research work presented in this thesis titled "**MHD Prandtl-Eyring Hybrid Nanofluid Flow Over a Permeable Moving Surface with Thermal Radiation**" is solely my research work with no significant contribution from any other person. Small contribution/help wherever taken has been dully acknowledged and that complete thesis has been written by me.

I understand the zero tolerance policy of the HEC and Capital University of Science and Technology towards plagiarism. Therefore, I as an author of the above titled thesis declare that no portion of my thesis has been plagiarized and any material used as reference is properly referred/cited.

I undertake that if I am found guilty of any formal plagiarism in the above titled thesis even after award of MPhil Degree, the University reserves the right to withdraw/revoke my MPhil degree and that HEC and the University have the right to publish my name on the HEC/University website on which names of students are placed who submitted plagiarized work.

(Shahmer Ahmed)
Registration No: MMT-193034

Acknowledgement

In the name of **Almighty Allah**, the Compassionate, the Merciful, Praise be to **Almighty Allah**, Lord of the Universe, and peace and prayers be upon his final **Prophet Muhammad (PBUH)** and Messenger.

I would like to express my sincere gratitude to my kind supervisor **Dr. Dur-e-Shehwar Sagheer** for her motivation, and continuous support in M.Phil study and research, for her patience, for her motivation, enthusiasm, and immense knowledge. Her guidance helped me a lot at the time of research and writing of this thesis. Her kind effort and motivation would never be forgotten.

I would like to express my appreciation to the Head of department **Dr. Muhammad Sagheer**, for providing us a learning and creative environment.

I am grateful to my **family and friends** for their support in completing my degree program.

I wish to thank my fellows **Muhammad Naveed Sani, Haseeb-ur-Rehman, Abdul Daim** and many others for supporting me during degree programs.

(Shahmer Ahmed)
Registration No: MMT-193034

Abstract

The purpose of the current research is to study the MHD Prandtl-Eyring Hybrid Nanofluid Flow Over a Permeable Moving Surface with Thermal Radiation. The moving surface is exposed to convective heating and surface is assumed to be permeable in an attempt to achieve the suction/injection of hybrid nanofluid boundary layer through the surface. Similarity transformations are utilized to transform the partial differential equation of momentum and thermal equations in to ordinary differential equations in non-dimensional form. It is investigated that how various flow parameters, such as the magnetic parameter, the Prandtl number, nanoparticles volume fraction, heat source/sink, Biot number, thermal radiation parameter, velocity slip parameter and suction/injection parameter effect on the temperature and velocity profiles. The variations in skin friction and heat transfer coefficient are discussed through tables. The numerical technique is incorporated by using Runge-Kutta method of order four and Newton method. Graphs are plotted to depict different significant effects. It is observed that velocity of fluid is higher for assisting flow as compared to opposing flow. Temperature is increased by increasing the volume fraction of both nano particles.

Contents

List of Figures

Abbreviations

HNF	Hybrid Nanofluid
IVPs	Initial value problems
MHD	Magnetohydrodynamics
ODEs	Ordineary differential equations
PDEs	Partial differential equations
RK	Runge-Kutta

Symbols

ρ	Density in kg $\mathtt{m}^{-3}$
ν	Kinematic viscosity in $\mathtt{m}^2\mathtt{s}^{-1}$
k	Thermal conductivity
α	Thermal diffusitivity in $\mathtt{m}^2\mathtt{s}^{-1}$
u	Velocity component in $\mathtt{ms}^{-1}$
v	Velocity component in $\mathtt{ms}^{-1}$
x	Cartesian coordinates in $\mathtt{m}$
y	Cartesian coordinates in $\mathtt{m}$
B_0	Magnetic number
C_f	Skin friction
M	Non dimensional magnetic number
Nu	Nusselt number
Pr	Prandtl number
T	Temperature
ϕ	Nanoparticle volume fraction
R	Thermal radiation parameter
γ	Inclination Angle
σ	Electrical conductivity of the nanoparticle
f	Dimensionless velocity
θ	Dimensionless temperature
η	Independent similarity variable

Chapter 1

Introduction

Now a days, a familiar research area is the analysis of hybrid nanofluid. Choi [1] originally proposed the various nanofluids that consist only unique types of nanoparticles. Tiwari, Das [2] and Buongiorno [3] reported basic models and fundamental applications for studying nanofluids. Many mathematicians have thought about using highly thermally conductive liquids, for example, Safaei et al. [4] investigated the use of the cooling of electronics with nanofluids. Hybrid nanofluids are made up of two or more solid nanoparticles suspended in any base liquid. Compared to regular nanoliquids, hybrid nanofluids have significantly better heat transfer capabilities. Hybrid nanofluids have uses in machine heat transfer coolants, electromechanical systems, optical sensors, and the field of nanomedicine.

Hybrid nanofluids have even better thermal properties than standard nanofluids. These unique nanofluids are created by mixing traditional fluid with nanoparticles of two or more different materials that can be the same size or different. Due to "synergistic effects", the "hybrid nanofluid" exhibit improved thermal properties over basic nanofluids. Synergism is a property that occurs due to interactions between molecules at the microscopic level. This interaction results better combined effect which is more that individual effect. Incorporating small amounts of metallic nanomaterials into oxide or metallic nanostructures and embedding them in the base liquid unexpectedly enhances their thermal properties. Hybrid nanofluids are defined by their high thermal conductivity, solidity, and improved heat transfer.

Better thermal conductivity results in higher energy efficiency, lower operating costs, and better performance. For more efficient space cooling and heating, better heat management in electrical devices like generators, transformers, heat pumps, refrigerators, and better heat transfer in complex devices like spacecraft, biomedical science nuclear stations, etc are just a few uses for hybrid nanofluids. Due to their superior performance over nanofluids, hybrid nanofluids are now more important and cost-effective for industry.

The boundary layer flow in hybrid nanofluids is the subject of this study. In regions where a moving fluid contacts a nearby surface, a boundary layer develops due to fluid viscosity and adhesion effects [5]. Some researchers have used the formation of boundary layers with various fluids and surfaces because it is very significant in scientific procedures like biological and chemical. Regular fluids include oil, fresh water and ethylene glycol which are classified as low heat transfer fluids. Falodun and Fadugba [6] studied viscous dissipation and thermal radiations effects on chemically reactive fluid flow through vertical plates during unsteady MHD boundary layer. Different physical properties and effects were endowed on different types of surface nanofluids with different shapes and configurations. Bachok et al. [7] used the suspension of alumina (Al_2O_3), copper (Cu) and titanium dioxide (TiO_2) . Najib et al. [8], then continued the issue by applying the thermal convective and slip conditions, where it was found that there is a trustworthy duality of solutions. Over a moving permeable surface, they investigate the mass diffusion of nanofluid and the transfer of heat. Constant surface diffusion and convective boundary conditions Brownian motion and thermophoresis effects also evaluated by them. Rawat and Kumar [9] investigated the stagnation point flow of a Cu-water nanofluid past a stretching/shrinking plate, where there was a delay in heat transfer when there was a heat generation/absorption, heat radiation, slip, suction and activation energy present. Goud et al. [10] investigated the effect of heat generation on a time-dependent MHD Casson fluid placed over a vertical vibrating plate. In the aforementioned studies [6–10], the boundary layer model was considered under the effect of nanofluids or other viscous fluids. In order to investigate boundary layer flow and its uses, many authors in the latter half of

the previous decade considered hybrid nanofluids. Waini et al. [11] investigated the heat transfer and flow independent of time of a hybrid nanofluid containing $Cu - Al_2O_3$ nanoparticles on a non-linear permeable surface. Waini extended this problem by cosidering various surfaces and numerous effects which can be seen in [12–17]. In a study by Kumar et al. [18, 19] water was used as the base fluid in a hybrid nanofluid that contained copper and magnetized ferrite nanoparticles. He also utilized the ethylene glycol as base fluid with copper and silver nanoparticles to study heat transfer characteristics. Authors also investigated the steady state analysis of improved heat transfer. Another article by Shoaib et al. [20] water is used as the primary fluid and two nanoparticles (alumina and silver) were suspended in it. This flow rotated over a streching plate. They provided a numerical solution for their model and presented it as a three-dimensional flow model. Aluminum oxide, copper, and water were used as the base fluids in Roy et al.'s investigation [21] to the flow and heat transfer of a hybrid nanofluid around a cylinder. They carried out a comparison of assisted and counterflow, and the findings demonstrated that, in contrast to assisted flow, counterflow had a significant impact on the energy fields close to the rear stagnation point. Stagnation point flow of hybrid nanofluid (MoS_2 and SiO_2) is studied by Khan et al. [22]. Several authors dealt with the hybrid nanofluid problem with the influence of various physical parameters [23–28].

In many scientific research, magnetic fields via heat transfer has always been crucial. It plays an important role in sciences, engineering and methods such as control of sand boundary layers, pumps and MHD turbines etc. One important aspect of MHD is the physical control of the coupling of momentum and heat. The MHD continuously improve the overall effectiveness of heat transfer. Davidson and Belova [29] provide a more thorough explanation of the MHD theory. The significant effects of slip and magnetic field on a stretching plate over a micropolar liquid are analyzed by Kumar et al. [30]. The heat transfer efficiency of a hybrid ferrofluid investigated by Tlili et al. [31] over an extendable plate in the presence of MHD and thermal radiation. Mishra and Kumar [32] studied the magnetic effects of the flow of water based nanofluid with silver nanoparticles on a streching

plate. Akolade [33] investigated the impact of a magnetic field on the movement of two parallel plate by keeping of one stationary with Casson fluid between them. Kumar et al. [34] created and examined a Cattaneo-Christov model in order to simulate the flow of an electrically conducting fluid past a cone and a wedge under the influence of a magnetic field .

Heat radiation, heat generation, and heat absorption effects cannot be ignored at high operating temperatures. Given that many technical procedures require operating at high temperatures hence consideration must be given to heat generation or absorption, as well as heat radiation. These effects play a big part in a lot of manufacturing applications, like building furnaces and making glass, applications related to technology such as spacecraft, rocket propulsion systems, plasma mechanics, nuclear power plant ignition processes, solar radiation , compressors and internal combustion engines for ships.

Kempananagari et al. [35] investigated the Non-Newtonian flow issue with thermal radiation on a curved, stretched-out surface. Ahmad and Nadeem [36] analyzed the effect of thermal radiation on a hybrid nanofluid made of ethylene glycol and SWCNT-MWCNT nanoparticles in a paper. The movement of a micropolar fluid near a boundary layer over a thin, stretching surface while being impacted by thermal radiation was studied by Kumar et al. [37]. A study by Alharbi et al. [38] focused on the movement of a $Cu - Al_2O_3$/blood hybrid nanofluid over a spherical stretching cylinder with potential for producing or absorbing heat.

Kumar et al. [39] studied the Casson flow over an exponentially stretched and curved surface under convective boundary conditions and radiative forcing. Due to the stretching of the plate, a water based hybrid nanofluid with two nanoparticles (copper and alumina) will flow by heat generation or absorption. Venkateswarlu and Narayana [40] modeled a numerical solution to a mathematical flow problem. For more information on studies of hybrid nanofluids that produce heat or have absorption and heat radiation effects, see for example [41–44].

1.1 Thesis Contributions

In the present work, which is motivated by the aforementioned literature contains a detail review of work done by Yaseen et al. [58]. Authors considered Magneto hydrodynamics hybrid nanofluid flow past a moving surface under the effects of thermal radiation, heat source/sink and suction/injection. We extended this work by considering the influence of Prandtl-Eyring fluid stress tensor over a permeable moving surface in two dimensions flow of a MHD hybrid nanofluid. We also develop a mathematical model of heat transfer along a permeable surface that moves with auxiliary and opposite flow cases of Prandtl Eyring nanofluid flow. Using the appropriate transformations, the governing nonlinear PDEs are transformed into a system of dimensionless ODEs. In order to solve the ODEs, the shooting technique is implemented in MATLAB. Variation of parameters for the dimensionless velocity profile $f'(\eta)$ and temperature distribution $\theta(\eta)$ are discussed with graphs.

1.2 Thesis Outlines

Four major chapters comprise this thesis:

Chapter 2 includes the fundamental terminologies and definitions that are essential to understanding the concepts discussed later.

Chapter 3 contains a thorough evaluation of the problem considered by Yaseen et al. [58] that takes into account the analysis of assisting and obstructing flow of a MHD hybrid nanofluid flow.

Chapter 4 extends the model discussed in Yaseen et al. [58] by considering the effects of Prandtl-Eyring fluid.

Chapter 5 provides a summary of the research findings and the main finding resulting from the entire study.

The **Bibliography** contains a list of all the references used in this thesis.

Chapter 2

Fundamental Terms and Laws

This chapter includes some fundamental ideas, definitions, and governing laws associated to the fluid dynamics. Dimensionless quantities are also discussed which seem to be helpful in the upcoming chapters. A concise discussion has been done for the numerical methodology adopted for the solution of governing equations.

2.1 Properties of Fluids

This section contains, some elemental terminologies and definitions from fluid dynamics which are needed for our fundamental work.

Definition 2.1.1 (Fluid)

"A fluid is a substance that deforms continuously under the application of a shear (tangential) stress no matter how small the shear stress may be." [50]

Definition 2.1.2 (Fluid Mechanics)

"Fluid mechanics is defined as science that deals with the behavior of fluids at rest or in motion, and the interaction of fluids with solid or other fluids at the boundaries." [51]

Definition 2.1.3 (Fluid Dynamics)

"The study of fluid if the pressure forces are also considered for the fluids in motion, the branch of science is called fluid dynamics." [51]

Definition 2.1.4 (Fluid Statics)

"The study of fluid at rest is called fluid statics." [51]

Definition 2.1.5 (Viscosity)

"Viscosity is defined as the property of a fluid which offers resistance to the movement of one layer of fluid over another adjacent layer of the fluid. Mathematically,

$$\mu = \frac{\tau}{\frac{\partial u}{\partial y}},$$

where μ is viscosity coefficient, τ is shear stress and $\frac{\partial u}{\partial y}$ represents the velocity gradient. SI units of viscosity is $\frac{Ns}{m^2}$." [51]

Definition 2.1.6 (Kinematic Viscosity)

"It is defined as the ratio between the dynamic viscosity and density of fluid. It is denoted by symbol ν called **nu**. Mathematically,

$$\nu = \frac{\mu}{\rho}.$$

SI unit of kinematic viscosity is $\mathtt{m^2 s^{-1}}$." [51]

Definition 2.1.7 (Thermal Conductivity)

"The Fourier heat conduction law states that the heat flow is proportional to the temperature gradient. The coefficient of proportionality is a material parameter known as the thermal conductivity which may be a function of a number of variables. Mathematically,

$$q = -K\nabla T,$$

where K stands for the second order conductivity tensor. The form of K for an isotropic material is as follows:

$$K = kI,$$

where k denotes the thermal conductivity $[W/(m.C)]$ of the medium, and I is again the unit tensor." [52]

Definition 2.1.8 (Magnetohydrodynamics)

"Magnetohydrodynamics (MHD) is concerned with the mutual interaction of fluid flow and magnetic fields. The fluids in question must be electrically conducting and non-magnetic, which limits us to liquid metals, hot ionised gases (plasmas) and strong electrolytes." [53]

Definition 2.1.9 (Porosity)

"The porosity is the relationship of the volume of void space to the bulk volume of a permeable medium. A permeable medium is often identified by its porosity." [54]

Definition 2.1.10 (Boundary Layer)

"The influence of fluid viscosity and adhesion in the area where a moving fluid comes into contact with the nearby surface causes a boundary layer to develop." [5]

2.2 Types of Fluid

In this section, different types of fluids are discussed which may be helpful to understand the nature of fluid motion. There are following categories in which we classified the fluid.

Definition 2.2.1 (Ideal Fluid)

"A fluid, which is incompressible and has no viscosity, is known as an ideal fluid. Ideal fluid is only an imaginary fluid as all the fluids, which exist, have some viscosity." [51]

Definition 2.2.2 (Real Fluid)

"A fluid which possesses viscosity is known as a real fluid. All the fluids in actual practice are real fluids." [51]

Water, diesel, petrol, honey etc, are the common examples of real fluid.

Definition 2.2.3 (Newtonian Fluid)

"A real fluid, in which the shear stress is directly proportional to the rate of shear strain (or velocity gradient) is known as a Newtonian fluid. Mathematically, it can be written as:

$$\tau_{xy} \propto \left(\frac{du}{dy}\right),$$
$$\tau_{xy} = \mu\left(\frac{du}{dy}\right),$$

where, μ = Dynamic viscosity, τ_{xy} = Shear stress exerted by the fluid, and $\frac{du}{dy}$ = Velocity gradient perpendicular to the direction of the shear." [51]
Air, water, and kerosene are some examples.

Definition 2.2.4 (Non-Newtonian Fluid)
"A real fluid in which the shear stress is not directly proportional to the rate of shear strain (or velocity gradient), is known as a non-Newtonian fluid. It has the following mathematical expression:

$$\tau_{xy} \propto k\left(\frac{du}{dy}\right)^m, \qquad m \neq 1$$
$$\tau_{xy} = k\left(\frac{du}{dy}\right)^m,$$

where, k is the flow consistency coefficient, $\frac{du}{dy}$ is shear rate, and m is the flow behaviour index." [51]
Blood, toothpaste, colloidal suspensions, polymer solutions, and slurries are a few examples of non-Newtonian fluids.

Definition 2.2.5 (Ideal Plastic Fluid)
"A fluid, in which shear stress is more than the yield value and shear stress is proportional to the rate of shear strain (or velocity gradient) is known as ideal plastic fluid." [51]
For example blood and soap solution etc.

Definition 2.2.6 (Nanofluids)

"Nanofluids are engineered colloids made of a base fluid and nanoparticles. Nanofluids have higher thermal conductivity and single phase heat transfer coefficients than their base fluids metals, oxides, carbides, or carbon nanotubes are the typical nanoparticles which are used in nanofluids and oil, ethylene glycol and water are examples of common base fluids." [51]

Definition 2.2.7 (Hybrid Nanofluids)

"Hybrid nanofluids are advanced forms of nanofluids that have reportedly even better thermal properties than basic nanofluids. These special nanofluids are made of nanoparticles of two or more different materials of same or different size mixed in a traditional fluid." [4]

2.3 Types of Fluid Flow

In this section we have discussed the following types of fluid flow.

Definition 2.3.1 (Steady Flow)

"If the flow characteristics such as depth of flow, velocity of flow, rate of flow at any point in open channel flow do not change with respect to time, the flow is said to be steady flow. Mathematically,

$$\frac{\partial Q}{\partial t} = 0,$$

where Q is any fluid property." [55]

Some examples are pipes, nozzles, diffusers, pumps etc.

Definition 2.3.2 (Unsteady Flow)

"If at any point in open channel flow, the velocity of flow, depth of flow or rate of flow changes with respect to time, the flow is said to be unsteady.

Mathematically,

$$\frac{\partial Q}{\partial t} \neq 0,$$

where Q is any fluid property." [55]

Flood-wave movement is an example of unsteady flow.

Definition 2.3.3 (Internal Flow)

"Flows completely bounded by a solid surfaces are called internal or duct flows. The example of the internal flow is the flow through pipes or glass." [50]

Definition 2.3.4 (External Flow)

"Flows over bodies immersed in an unbounded fluid are said to be an external flow. The flow of water in the ocean or in the river is an example of the external flow." [50]

Definition 2.3.5 (Rotational Flow)

"Rotational flow is that type of flow in which the fluid particles while flowing along stream-lines, also rotate about their own axis." [51]

Laminar flow in a pipe is an example of rotational flow.

Definition 2.3.6 (Irrotational Flow)

"Irrotational flow is that type of flow in which the fluid particles while flowing along stream-lines, do not rotate about their own axis then this type of flow is called irrotational flow." [51]

The flow of water through a runner of the turbine.

Definition 2.3.7 (Compressible Flow)

"Compressible flow is that type of flow in which the density of the fluid changes from point to point or in other words the density (ρ) is not constant for the fluid. Mathematically,

$$\rho \neq k,$$

where k is constant." [51]

An air with high velocity like a flow around an airplane is a compressible fluid.

Definition 2.3.8 (Incompressible Flow)

"Incompressible flow is that type of flow in which the density is constant for the fluid. Liquids are generally incompressible while gases are compressible. Mathematically,

$$\rho = k,$$

where k is constant." [51]

An air flow with low velocity like breeze is an incompressible fluid.

2.4 Modes of Heat Transfer

This section is focused on different modes of heat transfer. As we know that energy is transferred from one point to another inside a medium or from one medium to another as a result of temperature differences. There are three modes of heat transfer.

Definition 2.4.1 (Conduction)

"The transfer of heat within a medium due to a diffusion process is called conduction." [52]

The process of heating a pan on a stove is an example of conduction.

Definition 2.4.2 (Convection)

"Convection heat transfer is usually defined as energy transport effected by the motion of a fluid. The convection heat transfer between two dissimilar media is governed by Newtons law of cooling." [52]

Hot air rising above a fire is an example of convection.

Definition 2.4.3 (Thermal Radiation)

"The process by which heat is transferred from a body by virtue of its temperature, without the aid of any intervening medium, is called thermal radiation. Sometimes radiant energy is taken to be transported by electromagnetic waves while at other times it is supposed to be transported by particle like photons. Radiation is found to travel at the speed of light in vacuum. The term electromagnetic radiation encompasses many types of radiation such as:

(i) Short wave radiation like gamma rays, x-rays and microwave.

(ii) Long wave radiation like radio wave and thermal radiation. The cause for the

emission of each type of radiation is different. Thermal radiation is emitted by a medium due to its temperature." [52]

2.5 Dimensionless Numbers

This section composses of some definitions of dimensionless numbers that will be used in next chapters.

Definition 2.5.1 (Nusselt Number)

"It is the relationship between the convective to the conductive heat transfer through the boundary of the surface. It is a dimensionless number which was first introduced by the German mathematician Nusselt. Mathematically, it is defined as:

$$Nu = \frac{qL}{k},$$

where q stands for convective heat transfer, L stands for characteristics length and k stands for thermal conductivity." [56]

Definition 2.5.2 (Skin Friction Coefficient)

"It expresses the dynamic friction resistance originating in viscous fluid flow around a fixed wall. The skin friction coefficient can be defined as

$$C_f = \frac{2\tau_w}{\rho U_w^2},$$

where τ_w denotes the shear stress on the wall, ρ the density and U_w the free-stream velocity." [56]

Definition 2.5.3 (Prandtl Number)

"It is the ratio between the momentum diffusivity ν and thermal diffusivity α. Mathematically, it can be defined as

$$Pr = \frac{\nu}{\alpha} = \frac{\frac{\mu}{\rho}}{\frac{k}{C_p \rho}} = \frac{\mu C_p}{k},$$

where μ represents the dynamic viscosity, Cp denotes the specific heat and k stands for thermal conductivity. The relative thickness of thermal and momentum

boundary layer is controlled by Prandtl number." [50]

Definition 2.5.4 (Reynolds Number)

"It is defined as the ratio of inertia force of a flowing fluid and the viscous force of the fluid. Mathematically,

$$Re = \frac{UL}{\nu},$$

where U denotes the free stream velocity, L is the characteristic length and ν stands for kinematic viscosity." [50]

Definition 2.5.5 (Grashof Number)

" The ratio of buoyancy to viscous forces acting on a fluid is roughly represented by the Grashof number, which is a dimensionless number. Similar to the Reynolds number, it frequently appears in the study of situations involving natural convection.

$$Gr = \frac{g\beta\rho^2(T_w - T)L^3}{\mu^2},$$

where g is the gravitational acceleration brought on by the Earth, $beta$ is the coefficient of thermal expansion, Tw is the surface temperature, T is the bulk temperature, and L is the vertical length." [56]

Definition 2.5.6 (Biot Number)

"The Biot number, abbreviated as (Bi), is a dimensionless quantity used in heat transfer calculations that provides a straightforward index of the ratio of thermal resistances present inside and outside of a body. This ratio determines whether a body's internal temperatures will vary widely in space as it warms or cools over time in response to a thermal gradient applied to its surface. The Biot number is defined as:

$$Bi = \frac{h_h L}{k},$$

where L is a characteristic length of the geometry under consideration, k is the body's thermal conductivity, and h_h is a convective heat transfer coefficient." [56]

2.6 Governing Laws

Definition 2.6.1 (Continuity Equation)

"The principle of conservation of mass can be stated as the time rate of change of mass in a fixed volume is equal to the net rate of flow of mass across the surface. The mathematical statement of the principle results in the following equation, known as the continuity (of mass) equation.

$$\frac{\partial \rho}{\partial t} + \nabla.(\rho \mathbf{v}) = 0$$

where ρ is the density $\mathtt{kgm}^{-3}$ of the medium, $\mathbf{v}$ the velocity vector $\mathtt{ms}^{-1}$, and ∇ is the nabla or del operator.

For steady-state conditions, the continuity equation becomes,

$$\nabla.(\rho \mathbf{v}) = 0,$$

When the density changes following a fluid particle are negligible, the continuum is termed incompressible. The continuity equation then becomes,

$$\nabla.\mathbf{v} = 0,$$

which is often referred to as the incompressibility condition or incompressibility constraint." [59]

Definition 2.6.2 (Momentum Equation)

"The momentum equation states that the time rate of change of linear momentum of a given set of particles is equal to the vector sum of all the external forces acting on the particles of the set, provided Newtons third law of action and reaction governs the internal forces. Mathematically, it can be written as:

$$\frac{\partial}{\partial t}(\rho \mathbf{u}) + \nabla.[(\rho \mathbf{u})\mathbf{u}] = \nabla.\mathbf{T} + \rho g,$$

The above equation is called momentum equation. Where $\mathbf{u}$ is velocity vector, g

is gravity." [52]

Definition 2.6.3 (Energy Equation)

"The law of conservation of energy states that the time rate of change of the total energy is equal to the sum of the rate of work done by the applied forces and change of heat content per unit time.

$$\frac{\partial \rho}{\partial t} + \nabla.\rho\mathbf{u} = -\nabla.\mathbf{q} + Q + \phi,$$

where ϕ is the dissipation function, $\mathbf{q}$ is heat flux vector , Q is the internal heat generation and ∇ is the nabla or del operator." [52]

2.7 Shooting Method

To elaborate the shooting method, consider the following nonlinear boundary value problem.

$$\left.\begin{aligned} y''(x) &= yy'(x) + 2y^2(x) \\ y(0) &= 0, \qquad y(S) = R. \end{aligned}\right\} \tag{2.1}$$

To reduce the order of the above boundary value problem, introduce the following notations.

$$y = Z_1, \qquad y' = Z_1' = Z_2, \qquad y'' = Z_2'. \tag{2.2}$$

As a result, (2.1) is converted into the following system of first order ODEs.

$$Z_1' = Z_2, \qquad Z_1(0) = 0, \tag{2.3}$$

$$Z_2' = Z_1 Z_2 + 2Z_1^2, \qquad Z_2(0) = m. \tag{2.4}$$

where m is the missing initial condition which will found by using the Newton method. The above IVP will be numerically solved by the order-4 Runge-Kutta method. The missing condition m is to be chosen such that.

$$Z_1(S, m) = R. \tag{2.5}$$

For convenience, now onward $Z_1(S, m)$ will be denoted by $Z_1(m)$.
Let us further denote $Z_1(m) - R$ by $H(m)$, so that (2.5) becomes.

$$H(m) = 0. \tag{2.6}$$

The above equation can be solved by using Newton's method with the following iterative formula.

$$m^{n+1} = m^n - \frac{H(m^n)}{\frac{\partial H(m^n)}{\partial m}}, \qquad n = 0, 1, 2, 3, \ldots$$

or

$$m^{n+1} = m^n - \frac{Z_1(m^n) - R}{\frac{\partial Z_1(m^n)}{\partial m}}, \qquad n = 0, 1, 2, 3, \ldots \tag{2.7}$$

To find $\frac{\partial Z_1(m^n)}{\partial m}$, introduce the following notations.

$$\frac{\partial Z_1}{\partial m} = Z_3, \quad \frac{\partial Z_2}{\partial m} = Z_4. \tag{2.8}$$

As a result of above new notations the Newton's iterative scheme, will then get the form.

$$m^{n+1} = m^n - \frac{Z_1(m) - R}{Z_3(m)}. \tag{2.9}$$

Now differentiating (2.3) and (2.4) with respect to m, we get the following two equations.

$$Z_3' = Z_4, \qquad Z_3(0) = 0. \tag{2.10}$$

$$Z_4' = Z_3 Z_2 + Z_1 Z_4 + 4 Z_1 Z_3, \qquad Z_4(0) = 1. \tag{2.11}$$

Writing all the four ODEs (2.3), (2.4), (2.10) and (2.11) together, we have the following initial value problem.

$$\begin{aligned} Z_1' &= Z_2, & Z_1(0) &= 0. \\ Z_2' &= Z_1 Z_2 + 2 Z_1^2, & Z_2(0) &= m. \\ Z_3' &= Z_4, & Z_3(0) &= 0. \\ Z_4' &= Z_3 Z_2 + Z_1 Z_4 + 4 Z_1 Z_3, & Z_4(0) &= 1. \end{aligned}$$

The above system will be solved numerically by Runge-Kutta method of order four. The stopping criteria for the Newton's technique is set as,

$$\mid Z_1(m) - R \mid < \epsilon,$$

where $\epsilon > 0$ is an arbitrarily small positive number.

Chapter 3

Assisting and Obstructing Flow of MHD Hybrid Nanofluid Flow

3.1 Introduction

This chapter is focused to study the numerical outcomes of of the MHD hybrid nanofluid flow past a permeable moving surface while being affected by thermal radiation, heat source/sink, slip and suction/injection. Using the appropriate transformations, the governing nonlinear PDEs are transformed into a system of dimensionless ODEs. The numerical solutions of velocity profile $f'(\eta)$ and temperature profile $\theta(\eta)$ are discussed at the end of this chapter. These investigations are depicted by the graphs. Results are validated by obtaining some already existing results in literature. The numerical results of skin friction coefficient and heat transfer coefficient are also presented through tables for different values of various parameters.

3.2 Mathematical Modeling

This fluid uses molybdenum disulfide (MoS_2) and silicon dioxide (SiO_2) (see for ref [45]) as nanoparticles. The flow is two dimensional and steady. Thermal

radiation, slip, suction/injection and heat source/sink effects are considered, to examine the hybrid nanofluid's capacity for heat transmission as it flows past a porous surface. The comparison of buoyancy opposing flow and buoyancy assisting flow of hybrid nanofluid is conducted.

3.2.1 Geometry of the Problem

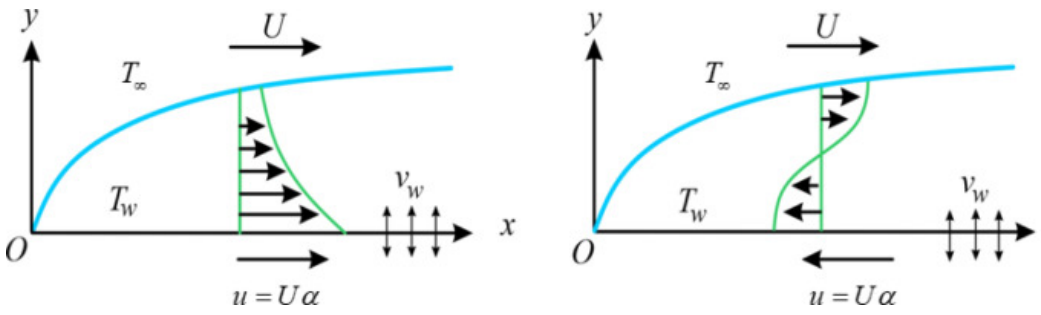

FIGURE 3.1: Physical representation of the problem.

Figure 3.1, displays the geometry and physical domain of the current model using the cartesian coordinates x and y. From figure, U represents the free stream velocity, whereas T_w and T_∞ represents the surface temperature and ambient temperature respectively. A fluctuating magnetic field $B = B_0(2x)^{-0.5}$ is applied perpendicularly to surface. Suction and injection are represented by the mass flux velocity $v_w(x)$ for positive and negative values, respectively. The following dependent quantities are considered in the problem:

- $Q_o^* = x^{-1}Q_o$ Heat source
- $h_f^* = x^{\frac{-1}{2}}h_f$ Heat transfer efficiency of a fluid under convection
- $k'^* = x^{\frac{1}{2}}k'$ length of the velocity slip
- $\beta^* = x^{-1}\beta$ Factor of thermal expansion.

One can see [46, 47] for reference. Water is used as base fluid and Molybdenum Disulfide (MoS_2) and Silicon Dioxide (SiO_2) are used as nanoparticles in the

problem. It is assumed that nanoparticles have uniform and same scale and their clustering on thermophysicals properties is ignored.

The governing equations for the flow with all above conventions are as follows [45]:

Continuity equation:

$$\frac{\partial u}{\partial x}+\frac{\partial v}{\partial y}=0, \tag{3.1}$$

Momentum Equation:

$$u\frac{\partial u}{\partial x}+v\frac{\partial u}{\partial y}=\frac{\mu_{hnf}}{\rho_{hnf}}\frac{\partial^2 u}{\partial y^2}+\frac{\sigma_{hnf}B^2}{\rho_{hnf}}(u_\infty-u)+\frac{(\rho\beta^*)_{hnf}\ g}{\rho_{hnf}}(T-T_\infty), \tag{3.2}$$

Energy Equation:

$$u\frac{\partial T}{\partial x}+v\frac{\partial T}{\partial y}=\frac{k_{hnf}}{(\rho C_p)_{hnf}}\left(\frac{\partial^2 T}{\partial y^2}\right)-\frac{1}{(\rho C_p)_{hnf}}\left(\frac{\partial q_r}{\partial y}\right)$$
$$+\frac{Q_o^*}{(\rho C_p)_{hnf}}(T-T_\infty), \tag{3.3}$$

where T stands for the temperature of the hybrid nanofluid, u and v respectively, are the components of flow velocity in the x and y directions. While μ_{hnf}, σ_{hnf}, $(\rho C_p)_{hnf}$, k_{hnf}, ρ_{hnf} and $(\beta^*)_{hnf}$ are the hybrid nanofluid's dynamic viscosity, electrical conductivity, heat capacity, thermal conductivity, density, and thermal expansion coefficient. Also q_r, k^* , Q_o and g are the radiative heat flux, the slip length, heat source/sink coefficient and acceleration due to gravity respectively. The subscripts f, hnf, and nf in this overview stand for the base fluid, hybrid nanofluid and nanofluid respectively.

The corresponding BCs have been considered as:

$$\left.\begin{aligned} &u=U\alpha+k'^*\frac{\partial u}{\partial y},\ v=v_w(x),\ \ -k_{hnf}\frac{\partial T}{\partial y}=h_f^*\ (T_w-T)\ at\ y=0,\\ &u=u_\infty\to U,\quad T\to T_\infty,\quad as\quad y\to\infty, \end{aligned}\right\} \tag{3.4}$$

where α is the moving parameter, α greater than or equal to 1 represents the downstream movement and α less than 1 represents upstream movement from origin.

The Rosseland approximation for the radiative heat flux is defined as (see for reference. [37]):

$$q_r = -\frac{4\sigma^*}{3k^*_{hnf}}\frac{\partial T^4}{\partial y}, \tag{3.5}$$

where σ^* is the Stefan-Boltzman constant and k^* is the absorption coefficient. If the temperature difference is very small, then the temperature T^4 can be expanded about T_∞ using Taylor series, as follows:

$$T^4 = T^4_\infty + 4T^3_\infty(T - T_\infty) + 6T^2_\infty(T - T_\infty)^2 + ...$$

Ignoring the higher order terms, we have

$$\begin{aligned} T^4 &= T^4_\infty + 4T^3_\infty(T - T_\infty), \\ T^4 &= T^4_\infty + 4T^3_\infty T - 4T^4_\infty, \\ T^4 &= -3T^4_\infty + 4T^3_\infty T, \\ T^4 &= 4T^3_\infty T - 3T^4_\infty. \end{aligned} \tag{3.6}$$

3.3 Thermophysical Properties of Hybrid Nanofluids

The following correlation for thermophysical properties are used, see for reference [22, 45, 48]:

$$\begin{aligned} \mu_{hnf} &= \frac{\mu_{water}}{(1-\phi_1)^{2.5}(1-\phi_2)^{2.5}}, \\ \rho_{hnf} &= \Big[\phi_2\rho_2 + (1-\phi_2)\Big(\phi_1\rho_1 + (1-\phi_1)\rho_{water}\Big)\Big], \end{aligned}$$

$$k_{hnf} = \left[\frac{(k_2 + 2k_{nf}) - 2\phi_2(k_{nf} - k_2)}{(k_2 + 2k_{nf}) + \phi_2(k_{nf} - k_1)}\right] * k_{nf},$$
$$k_{nf} = \left[\frac{(2k_w + k_1) - 2\phi_1(k_w - k_1)}{(2k_w + k_1) + \phi_1(k_w - k_1)}\right] * k_{water},$$
$$\sigma_{hnf} = \sigma_{nf}\left[\frac{\sigma_2(1 + 2\phi_2) + 2\sigma_{nf}(1 - \phi_2)}{\sigma_2(1 - \phi_2) + \sigma_{nf}(2 + \phi_2)}\right],$$
$$\sigma_{nf} = \sigma_w\left[\frac{\sigma_1(1 + 2\phi_1) + 2\sigma_w(1 - \phi_1)}{\sigma_1(1 - \phi_1) + \sigma_w(2 + \phi_1)}\right]$$
$$\beta_{hnf} = \left[\phi_2\beta_2 + (1 - \phi_2)\Big(\phi_1\beta_1 + (1 - \phi_1)\beta_{water}\Big)\right],$$
$$(\rho C_p)_{hnf} = \left[(1 - \phi_2)\Big(\phi_1(\rho C_p)_1 + (1 - \phi_1)(\rho C_p)_{water}\Big) + \phi_2(\rho C_p)_2\right],$$

where, the numbers 1 and 2 (in the subscript of ϕ, σ, ρ, β and ρCp) are used for SiO_2 and MoS_2 repectively for our convenience.

TABLE 3.1: Thermophysical properties of water, MoS_2 and SiO_2 nanoparticles [22, 45, 48]:

	$\rho(\frac{kg}{m^3})$	$C_p(\frac{J}{KgK})$	$k(\frac{W}{mK})$	$\beta(\frac{l}{K})$	$\sigma(\omega m)^{-1}$
Pure water	997.1	4179	0.613	21	0.05
MoS_2	5060	397.746	34.5	$2.8424 * 10^{-5}$	$2.09 * 10^4$
SiO_2	2650	730	1.5	42.7	$1.0 * 10^{-18}$

3.4 Transformation of Governing Equations into Dimensionless Form

Equation (3.3) is expressed as follows after using the (3.5) and (3.6):

$$u\frac{\partial T}{\partial x} + v\frac{\partial T}{\partial y} = \frac{k_{hnf}}{(\rho C_p)_{hnf}}\left(\frac{\partial^2 T}{\partial y^2}\right) + \frac{1}{(\rho C_p)_{hnf}}\left(\frac{16\sigma^* T_\infty^3}{3k^*_{hnf}}\right)\left(\frac{\partial^2 T}{\partial y^2}\right) + \frac{Q^*_o}{(\rho C_p)_{hnf}}(T - T_\infty). \tag{3.7}$$

For conversion of equations (3.1) to (3.3) into dimensionless form following transformation are used [45]:

$$\left.\begin{aligned} &u = Uf'(\eta)\ , \qquad \nu = \sqrt{\frac{U\nu_f}{2x}}(\eta f'(\eta) - f(\eta))\ , \qquad \theta(\eta) = \frac{T - T_\infty}{T_w - T_\infty}, \\ &\eta = y\sqrt{\frac{U}{2x\nu_f}}. \end{aligned}\right\} \tag{3.8}$$

The detailed method for transforming of equations (3.1)-(3.3) into the dimensionless form is discussed below.

Following derivatives are invovled in continuity equation:

$$\begin{aligned} \frac{\partial u}{\partial x} &= Uf''(\eta)\frac{\partial \eta}{\partial x}, \\ &= Uf''(\eta)\sqrt{\frac{U}{2\nu_f}}y\left(\frac{-1}{2}x^{\frac{-1}{2}-1}\right), \\ &= \frac{-U}{2}\sqrt{\frac{U}{2\nu_f}}yx^{\frac{-3}{2}}f''(\eta), \\ &= \frac{-U}{2}\sqrt{\frac{U}{2\nu_f}}yx^{\frac{-1}{2}}x^{-1}f''(\eta), \\ \frac{\partial u}{\partial x} &= \frac{-U}{2x}\eta f''(\eta), \end{aligned} \tag{3.9}$$

$$\begin{aligned} \frac{\partial v}{\partial y} &= \sqrt{\frac{U\nu_f}{2x}}\left(\eta f''(\eta)\frac{\partial \eta}{\partial y} + \frac{\partial \eta}{\partial y}f'(\eta) - f'(\eta)\frac{\partial \eta}{\partial y}\right), \\ &= \sqrt{\frac{U\nu_f}{2x}}\Big(\eta f''(\eta) + f'(\eta) - f'(\eta)\Big)\frac{\partial \eta}{\partial y}, \\ &= \sqrt{\frac{U\nu_f}{2x}}\eta f''\sqrt{\frac{U}{2x\nu_f}}, \\ \frac{\partial v}{\partial y} &= \frac{U}{2x}\eta f''(\eta). \end{aligned} \tag{3.10}$$

Hence equation (3.1) is easily satisfied by using (3.9) and (3.10), as follows:

$$\begin{aligned} \frac{\partial u}{\partial x} + \frac{\partial v}{\partial y} &= \frac{-U}{2x}\eta f''(\eta) + \frac{U}{2x}\eta f''(\eta), \\ &= 0. \end{aligned}$$

For dimensionless form of momentum equation the following conversions are necessary:

$$
\begin{aligned}
& u = Uf'(\eta), \qquad \nu = \sqrt{\frac{U\nu_f}{2x}}(\eta f'(\eta) - f(\eta)),\\
& \eta = y\sqrt{\frac{U}{2x\nu_f}},\\
& \frac{\partial u}{\partial x} = Uf''(\eta)\frac{\partial \eta}{\partial x},\\
& \qquad \frac{\partial u}{\partial x} = \frac{-yU^{\frac{3}{2}}}{x^{\frac{3}{2}}2^{\frac{3}{2}}\sqrt{\nu}_f}f''(\eta),\\
\Longrightarrow \quad & \qquad u\frac{\partial u}{\partial x} = \frac{-yU^{\frac{3}{2}}}{x^{\frac{3}{2}}2^{\frac{3}{2}}\sqrt{\nu}_f}f''(\eta)Uf'(\eta),\\
\Longrightarrow \quad & \qquad u\frac{\partial u}{\partial x} = \frac{-yU^{\frac{5}{2}}}{x^{\frac{3}{2}}2^{\frac{3}{2}}\sqrt{\nu}_f}f'(\eta)f''(\eta). \qquad (3.11)\\
Now, \quad & \qquad \frac{\partial u}{\partial y} = Uf''(\eta)\frac{\partial(\eta)}{\partial y},\\
\Longrightarrow \quad & \qquad \frac{\partial u}{\partial y} = Uf''(\eta)\sqrt{\frac{U}{2x\nu_f}},\\
\Longrightarrow \quad & \qquad \frac{\partial u}{\partial y} = U^{\frac{3}{2}}\sqrt{\frac{1}{2x\nu_f}}f''(\eta),\\
\Longrightarrow \quad & \qquad v\frac{\partial u}{\partial y} = U^{\frac{3}{2}}\sqrt{\frac{1}{2x\nu_f}}f''(\eta)\sqrt{\frac{U\nu_f}{2x}}(\eta f'(\eta) - f(\eta)),\\
\Longrightarrow \quad & \qquad v\frac{\partial u}{\partial y} = \frac{U^2}{2x}f''(\eta)\left(y\sqrt{\frac{U}{2x\nu_f}}f'(\eta) - f(\eta)\right),\\
\Longrightarrow \quad & \qquad v\frac{\partial u}{\partial y} = \frac{yU^{\frac{5}{2}}}{x^{\frac{3}{2}}2^{\frac{3}{2}}\sqrt{\nu}_f}f'(\eta)f''(\eta) - \frac{U^2}{2x}f(\eta)f''(\eta),\\
& \qquad u\frac{\partial u}{\partial x} + v\frac{\partial u}{\partial y} = -\frac{U^2}{2x}f(\eta)f''(\eta), \qquad (3.12)\\
& \qquad \frac{\partial^2 u}{\partial y^2} = \frac{U^{\frac{3}{2}}}{\sqrt{2x\nu_f}}f'''(\eta)\frac{\partial \eta}{\partial y},\\
\Longrightarrow \quad & \qquad = \frac{U^{\frac{3}{2}}}{\sqrt{2x\nu_f}}f'''(\eta)\sqrt{\frac{U}{2x\nu_f}},\\
\Longrightarrow \quad & \qquad \frac{\partial^2 u}{\partial y^2} = \frac{U^2}{2x\nu_f}f'''(\eta).
\end{aligned}
$$

Now, from (3.3),

$$
\begin{aligned}
-\frac{U^2}{2x}f(\eta)f''(\eta) &= \frac{\mu_{hnf}}{\rho_{hnf}}\frac{U^2}{2x\nu_f}f'''(\eta)+\frac{\sigma_{hnf}}{\rho_{hnf}}\frac{B_o^2}{2x}(u_\infty-u)+\frac{\beta_{hnf}g}{x}(T-T_\infty),\\
\implies\quad f(\eta)f''(\eta)&+\frac{\mu_{hnf}}{\rho_{hnf}}\frac{f'''(\eta)}{\nu_f}+\frac{\sigma_{hnf}}{\rho_{hnf}}\frac{B_o^2}{U^2}(U-Uf'\eta)+\frac{2\beta_{hnf}g}{U^2}(T-T_\infty)=0,\\
\implies\quad f(\eta)f''(\eta)&+\frac{\mu_{hnf}\rho_f f'''(\eta)}{\rho_{hnf}\mu_f}+\frac{\sigma_{hnf}}{\rho_{hnf}}\frac{B_o^2}{U^2}(U-Uf'\eta)+\frac{2\beta_{hnf}g}{U^2}(T-T_\infty)=0,\\
\implies f(\eta)f''(\eta)&+\frac{\mu_{hnf}f'''(\eta)\rho_f}{\rho_{hnf}\mu_f}+\frac{\rho_f}{\rho_f}\frac{\sigma_{hnf}}{\rho_{hnf}}\frac{\sigma_f}{\sigma_f}\frac{B_o^2}{U}(1-f'\eta)+\frac{\beta_f}{\beta_f}\frac{2\beta_{hnf}g}{U^2}\\
&(T-T_\infty)\frac{T_w-T_\infty}{T_w-T_\infty}=0,\\
&f(\eta)f''(\eta)+\frac{1}{AB}f'''(\eta)+\frac{C}{B}M(1-f'(\eta)+2D\lambda\theta=0,
\end{aligned}
\tag{3.13}
$$

where, $A=\dfrac{\mu_f}{\mu_{hnf}}$, $\quad B=\dfrac{\rho_{hnf}}{\rho_f}$, $\quad C=\dfrac{\sigma_{hnf}}{\sigma_f}$,
$D=\dfrac{\beta_{hnf}}{\beta_f}$, $M=\dfrac{\sigma_f}{\rho_f}\dfrac{B_o^2}{U}$, $\lambda=\dfrac{g\beta_f(T_w-T_\infty)}{U^2}$.

For the energy equation the following derivatives are required.

$$
\begin{aligned}
\theta(\eta)&=\frac{T-T_\infty}{T_w-T_\infty},\\
T-T_\infty&=(T_w-T_\infty)\theta,\\
T&=\theta(T_w-T_\infty)+T_\infty,\\
\frac{\partial T}{\partial x}&=(T_w-T_\infty)\frac{\partial\theta}{\partial\eta}\frac{\partial\eta}{\partial x},\\
\frac{\partial T}{\partial x}&=(T_w-T_\infty)\frac{\partial\theta}{\partial\eta}\frac{-y}{(2x)^{\frac{3}{2}}}\sqrt{\frac{U}{\nu_f}},\\
\implies u\frac{\partial T}{\partial x}&=-(T_w-T_\infty)\theta'U^{\frac{3}{2}}f'(\eta)\frac{y}{(2x)^{\frac{3}{2}}\sqrt{\nu}_f},
\end{aligned}
\tag{3.14}
$$

$$
\begin{aligned}
\frac{\partial T}{\partial y}&=(T_w-T_\infty)\frac{\partial\theta}{\partial\eta}\frac{\partial\eta}{\partial y},\\
\frac{\partial T}{\partial y}&=(T_w-T_\infty)\frac{\partial\theta}{\partial\eta}\sqrt{\frac{U}{2x\nu_f}},\\
\implies v\frac{\partial T}{\partial y}&=(T_w-T_\infty)\frac{\partial\theta}{\partial\eta}\frac{U}{2x}(\eta f'(\eta)-f(\eta)).
\end{aligned}
\tag{3.15}
$$

Using (3.14) and (3.15),

$$u\frac{\partial T}{\partial x}+v\frac{\partial T}{\partial y}=-(T_w-T_\infty)\ \frac{U}{2x}\ f\ \frac{\partial \theta}{\partial \eta}, \tag{3.16}$$

$$\Longrightarrow \frac{\partial^2 T}{\partial y^2}=(T_w-T_\infty)\theta''\ \sqrt{\frac{U}{2x\nu_f}}\ \frac{\partial \eta}{\partial y},$$

$$\Longrightarrow \frac{\partial^2 T}{\partial y^2}=(T_w-T_\infty)\theta''\ \sqrt{\frac{U}{2x\nu_f}}\ \ \sqrt{\frac{U}{2x\nu_f}},$$

$$\Longrightarrow \frac{\partial^2 T}{\partial y^2}=(T_w-T_\infty)\theta''\frac{U}{2x\nu_f}, \tag{3.17}$$

$$\Longrightarrow \frac{\partial}{\partial y}(q_r)=\frac{\partial}{\partial y}\Big[-(\frac{4\sigma^*}{3k^*_{hnf}})\frac{\partial T^4}{\partial y}\Big],$$

$$=\frac{\partial}{\partial y}\Big[-(\frac{4\sigma^*}{3k^*_{hnf}})\ \frac{\partial}{\partial y}\ (4T_\infty^3T-3T_\infty^4)\Big],$$

$$=\frac{\partial}{\partial y}\Big[-(\frac{4\sigma^*}{3k^*_{hnf}})\ 4T_\infty^3\ (T_w-T_\infty)\theta'\ \sqrt{\frac{U}{2x\nu_f}}\Big],$$

$$=-\frac{16\sigma^*}{3k^*_{hnf}}\ T_\infty^3\ (T_w-T_\infty)\theta''\ \sqrt{\frac{U}{2x\nu_f}}\ \frac{\partial \eta}{\partial y},$$

$$\Longrightarrow \frac{\partial}{\partial y}(q_r)=-\frac{16\sigma^*}{3k^*_{hnf}}\ T_\infty^3\ (T_w-T_\infty)\ \frac{U}{2x\nu_f}\ \theta''. \tag{3.18}$$

Consider, R.H.S. of energy equation (3.3) we have,

$$\frac{k_{hnf}}{(\rho C_p)_{hnf}}\ \frac{\partial^2 T}{\partial y^2}-\frac{1}{(\rho C_p)_{hnf}}\ \frac{\partial}{\partial y}(q_r)+\frac{Q_o^*\ (T-T_\infty)}{x\rho C_p)_{hnf}}, \tag{3.19}$$

$$\frac{k_{hnf}}{(\rho C_p)_{hnf}}(T_w-T_\infty)\frac{U}{2x\nu_f}\theta''+\frac{16\sigma^*T_\infty^3}{(\rho C_p)_{hnf}3k^*_{hnf}}(T_w-T_\infty)\frac{U}{2x\nu_f}\theta''+$$
$$\frac{Q_o(T-T_\infty)}{x(\rho C_p)_{hnf}},$$
$$\frac{(T_w-T_\infty)U}{(\rho C_p)_{hnf}2x\nu_f}\Big[k_{hnf}+\frac{16\sigma^*T_\infty^3}{3k^*_{hnf}}\Big]\theta''+\frac{Q_o(T-T_\infty)}{x(\rho C_p)_{hnf}}. \tag{3.20}$$

From (3.19) and (3.20) the equation (3.3) becomes:

$$-\frac{(T_w-T_\infty)Uf\theta'}{2x}=\frac{(T_w-T_\infty)U}{(\rho C_p)_{hnf}2x\nu_f}\Big[k_{hnf}+\frac{16\sigma^*T_\infty^3}{3k^*_{hnf}}\Big]\theta''+\frac{Q_o(T-T_\infty)}{x(\rho C_p)_{hnf}},$$

$$\Longrightarrow\ -f\theta'=\frac{1}{(\rho C_p)_{hnf}\nu_f}\Big[k_{hnf}+\frac{4}{3}\frac{4\sigma^*T_\infty^3}{k^*_{hnf}}\Big]\theta''+\frac{2Q_o\theta}{U(\rho C_p)_{hnf}},$$

$$\begin{aligned}
&\Longrightarrow \frac{1}{(\rho C_p)_{hnf}\nu_f}\left[k_{hnf}+\frac{4}{3}\frac{4\sigma^* T_\infty^3}{k^*_{hnf}}\right]\theta''+f\theta'+\frac{2Q_o\theta}{U(\rho Cp)_{hnf}}=0,\\
&\Longrightarrow \quad \frac{1}{\nu_f}\left[k_{hnf}+\frac{4}{3}\ \frac{4\sigma^* T_\infty^3}{k^*_{hnf}}\right]\theta''+(\rho C_p)_{hnf}\ f\theta'+\frac{2Q_o\theta}{U}=0,\\
&\left[k_{hnf}+\frac{4}{3}\ \frac{4\sigma^* T_\infty^3}{k^*_{hnf}}\right]\theta''+\frac{\mu_f}{\rho_f}(\rho C_p)_{hnf}\ f\theta'+\frac{2Q_o\theta}{U}\frac{\mu_f}{\rho_f}=0.
\end{aligned}$$

Dividing on both sides by k_f we have,

$$\begin{aligned}
&\left[\frac{k_{hnf}}{k_f}+\frac{4}{3}\ \frac{4\sigma^* T_\infty^3}{k^*_{hnf}k_f}\right]\theta''+\frac{\mu_f C_p}{\rho_f k_f C_p}(\rho C_p)_{hnf}\ f\theta'+\frac{2Q_o\theta}{U}\frac{\mu_f C_p}{\rho_f k_f C_p}=0,\\
\Longrightarrow &\left[\frac{k_{hnf}}{k_f}+\frac{4}{3}Rd\right]\theta''+\frac{(\rho C_p)_{hnf}}{(\rho C_p)_f}\frac{\mu_f(C_p)_f}{k_f}\ f\theta'+'+\frac{2Q_o}{U(\rho C_p)_f}\frac{\mu_f(C_p)_f}{k_f}\theta=0,\\
\Longrightarrow &\left[\frac{k_{hnf}}{k_f}+\frac{4}{3}Rd\right]\theta''+EPrf\theta'+2Q\ Pr\theta=0, \qquad (3.21)
\end{aligned}$$

where $R_d=\dfrac{4\sigma^* T_\infty^3}{k^*_{hnf}k_f}$, $E=\dfrac{(\rho C_p)_{hnf}}{(\rho C_p)_f}$, $Pr=\dfrac{\mu_f(C_p)_f}{k_f}$, $Q=\dfrac{2Q_o}{U(\rho C_p)_f}$.

3.5 Non-Dimensional Form of Boundary Conditions

In this section we focused on the dimensionaless form of the boundary conditions.

$$\begin{aligned}
&u=U\alpha+k'^*\frac{\partial u}{\partial y}, \quad v=v_w(x), \quad -k_{hnf}\frac{\partial T}{\partial y}=h^*_f(T_w-T) \quad at \quad y=0,\\
&u=u_\infty\to U, \quad T\to T_\infty, \quad as \quad y\to\infty.
\end{aligned}$$

From (3.8) we have,

$$\begin{aligned}
&u=Uf'(\eta) \qquad \text{and} \qquad \eta=y\sqrt{\frac{U}{2x\nu_f}},\\
&\frac{\partial u}{\partial y}=Uf''(\eta)\frac{\partial \eta}{\partial y},\\
\Longrightarrow\ &u=U\alpha+k'^*\ Uf''(\eta)\sqrt{\frac{U}{2x\nu_f}},
\end{aligned}$$

$$
\begin{aligned}
&\Longrightarrow u = Uf'(\eta),\\
&\quad Uf'(\eta) = U\alpha + k'^{*}\, Uf''(\eta)\sqrt{\frac{U}{2x\nu_f}},\\
&\quad Uf'(0) = U\alpha + k'^{*}\, Uf''(0)\sqrt{\frac{U}{2x\nu_f}} \qquad \text{at} \quad \eta = 0,\\
&\quad Uf'(0) = U\alpha + k'^{*}\, Uf''(0)\sqrt{\frac{U}{2x\nu_f}}. \qquad (3.22)\\
&\Longrightarrow f'(0) = \frac{U\alpha}{U} + \frac{k'^{*}}{U}Uf''(0)\sqrt{\frac{U}{2x\nu_f}},\\
\textit{then,}\quad &k' = \sqrt{x}k^{*},\\
&f'(0) = \frac{U\alpha}{U} + k'^{*}f''(0)\sqrt{\frac{U}{2\nu_f}}\frac{k'}{k'^{*}},\\
&f'(0) = \frac{U\alpha}{U} + k'\sqrt{\frac{U}{2\nu_f}}f''(0),\\
&f'(0) = \alpha + \gamma f''(0), \qquad (3.23)
\end{aligned}
$$

where $\gamma = k'\sqrt{\dfrac{U}{2\nu_f}}$.

The transformed boundary conditions are,

$$
\left.
\begin{aligned}
&f(\eta) = S, f'(0) = \alpha + \gamma f''(0), \frac{-k_{hnf}\theta'(\eta)}{k_f} = Bi(1-\theta(\eta)) \;\; at\ \eta = 0,\\
&f'(\eta) \to 1, \;\; \theta(\eta)) \to 0, \;\; as \quad \eta = 0.
\end{aligned}
\right\} \qquad (3.24)
$$

Different dimensionless parameters used in (3.13), (3.21) and (3.23) are formulated as follows:

$$
Re_x = \frac{U_x}{v_f}, \quad Rd = \frac{4\sigma^{*}T_{\infty}^{3}}{k_{hnf}^{*}k_f}.
$$

Finally we get the following boundary value problem:

$$
\begin{aligned}
&f(\eta)f''(\eta) + \frac{1}{AB}f'''(\eta) + \frac{C}{B}M(1 - f'(\eta) + 2D\lambda\theta = 0,\\
&\left[\frac{k_{hnf}}{k_f} + \frac{4}{3}Rd\right]\theta'' + EPrf\theta' + 2Q\ Pr\theta = 0,
\end{aligned}
$$

along with boundary conditions:

$$f(\eta) = S, f'(0) = \alpha + \gamma f''(0), \frac{-k_{hnf}\theta'(\eta)}{k_f} = Bi(1-\theta(\eta)) \text{ at } \eta = 0,$$
$$f'(\eta) \to 1, \quad \theta(\eta)) \to 0, \quad \text{at} \quad \eta = 0.$$

3.6 Important Physical Quantities

The skin friction coefficient, is given as follows:

$$C_f = \frac{\tau_w}{\rho_f U^2}, \qquad \tau_w = \mu_{hnf}\left(\frac{\partial u}{\partial y}\right)_{y=0}.$$

From (3.5) and put value of τ_w in (3.25) we have the following:

$$\begin{aligned}
C_f &= \frac{\mu_{hnf}\left(Uf''(\eta)\ \frac{\partial \eta}{\partial y}\right)}{\rho_f U^2}, \\
\implies C_f &= \frac{\mu_{hnf}\left(Uf''(\eta)\ \sqrt{\frac{U}{2xv_f}}\right)}{\rho_f U^2}, \\
\implies \sqrt{Ux}C_f &= \frac{\mu_{hnf}}{\rho_f}\ \frac{\mu_f}{\mu_f}\frac{1}{\sqrt{2}}\frac{1}{\sqrt{v_f}}f''(\eta), \\
\implies \sqrt{Ux}C_f &= \frac{\mu_{hnf}}{\mu_f}\ \frac{\mu_f}{\rho_f}\frac{1}{\sqrt{2}}\frac{1}{\sqrt{v_f}}f''(\eta), \\
\implies \sqrt{Ux}C_f &= \frac{\mu_{hnf}}{\mu_f}\ \sqrt{v_f}\frac{1}{\sqrt{2}}f''(\eta), \\
\implies \sqrt{Re_x}C_f &= \frac{1}{\sqrt{2}A}f''(0),
\end{aligned} \tag{3.25}$$

where, $Re_x = \sqrt{\frac{Ux}{v_f}}$ and $A = \frac{\mu_{hnf}}{\mu_f}$.

Nusselt number is given by following mathematical form:

$$Nu_x = \frac{x(q_w + q_r)}{k_f(T_w - T_\infty)}.$$

The radiative heat flux $(q_w + q_r)$ is defined as follows:

$$(q_w + q_r) = -\left(k_{hnf}\frac{\partial T}{\partial y} + \frac{4\sigma^*}{3k^*_{hnf}}\frac{\partial T^4}{\partial y}\right)\Bigg|_{y=0}. \tag{3.26}$$

Using (3.5) the quantity described in (3.26) we get the following form:

$$\frac{Nu_x}{Re_x} = \frac{-1}{\sqrt{2}}\left(\frac{k_{hnf}}{k_f} + \frac{4}{3}Rd\right)\theta'(0). \tag{3.27}$$

3.7 Numerical Method for Solution

Shooting method is used to solve the boundary value problem. To incorporate shooting technique we use the following notations:

$$f = y_1, \quad f' = y_1' = y_2, \quad f'' = y_1'' = y_2' = y_3, \quad f''' = y_3'.$$
$$\theta = y_4, \quad \theta' = y_4' = y_5, \quad \theta'' = y_5'.$$

As a result the momentum equation is transformed into the following system of first order ODEs:

$$\begin{aligned}
y_1' &= y_2, & y_1(0) &= S.\\
y_2' &= y_3, & y_2(0) &= \alpha + \gamma m,\\
y_3' &= -AB\left[-y_1y_3 - \frac{CM}{B}(1-y_2) - 2D\lambda y_4\right], & y_3(0) &= m,\\
y_4' &= y_5 & y_4(0) &= r,\\
y_5' &= \psi(-EPr\ y_1y_5 + 2Pr\ Qy_4), & y_5(0) &= -\frac{k_f}{k_{hnf}}\left(Bi(1-r)\right),
\end{aligned}$$

where m and r assumed missing conditions.

The Runge Kutta method of order four is used to solve the above IVP. The solution must satisfy the following equations:

$$\left.\begin{aligned} y_2(m, r, \eta = \infty) &= 1,\\ y_4(m, r, \eta = \infty) &= 0 \end{aligned}\right\}. \tag{3.28}$$

To solve the nonlinear algebraic equation (3.28) for m and r. This method has the following iterative scheme:

$$\begin{bmatrix} m \\ r \end{bmatrix}^{n+1} = \begin{bmatrix} m \\ r \end{bmatrix}^{n} - \left(\begin{bmatrix} \frac{\partial y_2}{\partial m} & \frac{\partial y_2}{\partial r} \\ \frac{\partial y_4}{\partial m} & \frac{\partial y_4}{\partial r} \end{bmatrix}^{-1} \begin{bmatrix} y_2 - 1 \\ y_4 - 0 \end{bmatrix} \right)^{n}.$$

To incorporate the above formula, we further need the following derivatives:

$$\frac{\partial y_1}{\partial m} = y_6, \quad \frac{\partial y_2}{\partial m} = y_7, \quad \frac{\partial y_3}{\partial m} = y_8, \quad \frac{\partial y_4}{\partial m} = y_9, \quad \frac{\partial y_5}{\partial m} = y_{10}$$

$$\frac{\partial y_1}{\partial r} = y_{11}, \quad \frac{\partial y_2}{\partial r} = y_{12}, \quad \frac{\partial y_3}{\partial r} = y_{13}, \quad \frac{\partial y_4}{\partial r} = y_{14}, \quad \frac{\partial y_5}{\partial r} = y_{15}.$$

The Newton's iterative scheme takes the following form as a result of these notations:

$$\begin{bmatrix} R \\ S \end{bmatrix}^{n+1} = \begin{bmatrix} R \\ S \end{bmatrix}^{n} - \left(\begin{bmatrix} y_7 & y_{12} \\ y_9 & y_{14} \end{bmatrix}^{-1} \begin{bmatrix} y_2 - 1 \\ y_4 - 0 \end{bmatrix} \right)^{n}.$$

Now, differentiating the system of five first ODEs with respect to each of the variables m and r to have another system of ten ODE's together. As a result following IVP is obtained:

$$\begin{aligned}
y_1' &= y_2, & y_1(0) &= s, \\
y_2' &= y_3, & y_2(0) &= \alpha + \gamma m, \\
y_3' &= AB\left[-y_1 y_3 - \frac{CM}{B}(1 - y_2) - 2D\lambda y_4\right], & y_3(0) &= m, \\
y_4' &= y_5 & y_4(0) &= r, \\
y_5' &= \psi(-EPr\ y_1 y_5 + 2Pr\ Q y_4) & y_5(0) &= -\frac{k_f}{k_{hnf}}\Big(Bi(1 - r)\Big), \\
y_6' &= y_7, & y_6(0) &= 0, \\
y_7' &= y_8, & y_7(0) &= r,
\end{aligned}$$

$$y_8' = AB\left[-y_1y_8 - y_3y_6 + \frac{CM}{B}(y_7) - 2D\lambda y_9\right], \qquad y_8(0) = 1,$$

$$y_9' = y_{10} \qquad y_9(0) = 0,$$

$$y_{10}' = \psi(-EPr\ y_1y_{10} - EPr\ y_5y_6 + 2Pr\ Qy_4) \qquad y_{10}(0) = 0,$$

$$y_{11}' = y_{12}, \qquad y_{11}(0) = 0,$$

$$y_{12}' = y_{13}, \qquad y_{12}(0) = m,$$

$$y_{13}' = AB\left[-y_1y_{13} - y_3y_{11} + \frac{CM}{B}(y_{12}) - 2D\lambda y_14\right], \qquad y_{13}(0) = 0,$$

$$y_{14}' = y_{15} \qquad y_{14}(0) = 1,$$

$$y_{15}' = \psi(-EPr\ y_1y_{15} - EPr\ y_5y_{11} + 2Pr\ Qy_{14}) \qquad y_{15}(0) = \frac{k_f}{k_{hnf}}\ Bi.$$

Where m and r as initial guesses, the above system of fifteen first order differential equations is solved by using Runge-Kutta method of order four.
The iterative procedure is continued until the following criteria is met:

$$\max |\ y_2(\eta, m, r) - 1\ |, |\ y_4(\eta, m, r)\ | < \epsilon,$$

for an arbitrarily small value of ϵ.

3.8 Code Validation

For testing the validity of flow problem we obtained results of Waini et al. [45] from our results. The results is done through the numerical scheme validation process.
Table 3 provides a comparison of the results for the special case with those published by Waini et al. [45]. The values of skin friction coefficient $(Re_x)^{\frac{1}{2}}C_f$ and heat transfer coefficient $(-(Re_x)^{\frac{-1}{2}}Nu_x)$ are contrasted for the flow of Cu-water nanofluid.
The use of the current numerical code is approved by the fact that our method produced outcomes that closely resembled those of Waini et al. [45].

TABLE 3.2: Code Validation $S = \phi_1 = R_d = M = L = Q = 0$

		Waini et al. [45]		Present results	
L	ϕ_2	$(Re_x)^{\frac{1}{2}}C_f$	$(Re_x)^{\frac{-1}{2}}Nu_x$	$(Re_x)^{\frac{1}{2}}C_f$	$(Re_x)^{\frac{-1}{2}}Nu_x$
-0.1	0.01	0.343018	0.513140	0.343018729	0.513140250
	0.05	0.410982	0.579437	0.410982095	0.579437325
	0.1	0.498390	0.657797	0.498390106	0.657796948
0	0.01	0.349380	0.637362	0.349380743	0.637361738
	0.05	0.418605	0.704281	0.418605021	0.704281645
	0.1	0.507634	0.784958	0.507634360	0.784957516

3.9 Representation of Tables and Graphs

This section contains a thorough discussion of $f'(\eta)$ and $\theta(\eta)$ using graphs and tables.

The impacts of different parameters on the hybrid nanofluid flow and heat transfer in the current model are also covered in this section. These parameters are ϕ_1 and ϕ_2 (the solid volume fractions), λ (mixed convection parameter), M (magnetic field parameter), γ (velocity slip parameter), Q (heat absorption/generation parameter) , R_d (thermal radiation parameter), S (suction/injection parameter), and Bi (Biot number).

The positive value of λ represents the case of assisting flow over the moving surface, and the negative value of λ represents the case of obstructing flow. In the current discussion, the value of λ is taken to be -0.1 for opposing flow and 0.1 for assisting flow.

The following values are found throughout the analysis when this parameter is assumed to remain constant:

$\phi_1 = 0.01$, $\phi_2 = 0.01$, $Rd = 2$, $Pr. = 6.2$, $M = 2$, $S = 1$, $Q = -0.1$, $\gamma = 0.1$, $Bi = 0.2$ and $\alpha = 1$. The impacts of various parameters on drag force coefficient

and Nusselt number is aslo depicted by virtue of tables.

3.9.1 Discussion of the Velocity Profiles of Hybrid Nanofluids

Figure 3.2, presents the profiles that how the mixed convection parameter (λ) affects velocity $f'(\eta)$. Additionally, we have demonstrated the suction and injection scenarios with $S = 1$ and $S = -1$, respectively, when the mixed convection parameter is changed.

When the mixed convection parameter is zero, neither the assisting flow nor the opposing flow exist. In the diagram, positive values of the parameter (λ) stand in for assisting flow, while negative values of the parameter (λ) stand in for opposing flow. This figure shows that a higher value for the mixed convection parameter causing the velocity to increase when both the suction and the injection parameters are present. During the flow, stronger buoyancy forces are associated as the mixed convection parameter's numerical value rises , which causes an increase in velocity profiles. The velocity profiles near the surface overshoot because of the favorable pressure gradient produced by the positive value of λ. Additionally, it is seen in figure that the velocity is greater when an injection is present. Compared to the suction case, the injection case exhibits higher positive peaks or lower negative peaks.

Figure 3.3, shows changes in velocity as suction/injection parameter is changed. When hybrid nanofluid is flowing in far field. The effects of suction and injection have been discussed for opposing flow as well as assisting flow. Suction is indicated when parameter S is positive, and injection applied at the surface is indicated when parameter S is negative. Suction and injection are not present when $S = 0$. Additionally, it has been discovered that the increment in S causes the velocity of an assisting flow to decrease (shown by solid lines), whereas increasing the numerical value of S causes the velocity of an opposing flow to increase (shown by dashed lines).

Figure 3.4, demonstrates the impact on velocity profiles $f'(\eta)$ by variation of magnetic parameter (M). The magentic field's value has increased in a positive way represent the strengthing of mgnetic field. The Lorentz force is produced by the magnetic field. The Lorentz force opposes the flow as the magnetic parameter is increased. Additionally, it can be seen in figure as the parameter's numerical value M rises the velocity is decreased for the case of assisting flow.
From Figure 3.5, it is noticed that the velocity profiles $f'(\eta)$ changes with the modification of Q.
We noticed that the capacity of the flow field to absorb heat is related to the heat generation within the flow field with the positive and negative values of Q . As seen in the figure, the velocity of an assisting flow enhances with the increment of Q, whereas the velocity of an opposing flow decreases with the increment of Q.

Figure 3.6, shows the change in the hybrid nanofluid flow's velocity profile $f'(\eta)$ with different radiation parameter's values. The results from both cases demonstrate that, while opposing flow behaves in the exact opposite way, assisting flow exhibits both an increase in velocity and an increase in the radiation parameter, which results in stronger buoyancy forces.

Figure 3.7, depicts the variation in $f'(\eta)$ with respect to the change in values of Bi. It has been noticed that for the case of assisting flow, the velocity enhances with increment in Bi, but for the case of opposing flow contrary results are observed.
Figure 3.8, shows how the variation in velocity profile as the velocity slip parameter (γ) changes. The figure clearly shows the relationship between slip parameter and hybrid nanofluid velocity is positive when flow is assisting, but if there is an opposite flow, the graph illustrates the inverse relationship between slip parameter and hybrid nanofluid velocity for increasing slip parameter's values.
The profiles drawn in Figures 3.9 and 3.10, display the variation in velocity $f'(\eta)$ with change in numerical values of nanoparticles with volume fractions (ϕ_1 and ϕ_2). The volume fraction of nanoparticles (ϕ_1 and ϕ_2) has been valued higher in

order to increase the concentration in the hybrid nanofluid's nanoparticles. This means that raising the numerical value of the nanoparticles (ϕ_1 and ϕ_2) correlates with raising the quantity of nanoparticles (ϕ_1) and (ϕ_2). From Figure 3.9, we witness the fact that in the scenario of an assisting flow with a rise in the volume fraction, velocity rises. However, results for an opposing flow are different. In the case of an assisting flow, the hybrid nanofluid's velocity decreases, while in the case of an obstructing flow, it increases, as shown in Figure 3.10.

Figure 3.11 shows the variation in $f'(\eta)$ for different values of α. The figure depicts the surface's movement downstream for α greater than or equal to 1 while it depicts the upstream changes in the surface for α less than 1. In this graph, we find that the surface tends to move downstream, which facilitates the velocity flow. Velocity increases when α values are greater than 1.

3.9.2 Discussion of Temperature Profiles of Hybrid Nanofluids

Figure 3.12, depicts the influence of parameter λ on the hybrid nanofluid's temperature profiles ($\theta(\eta)$). Both the suction ($S = 1$) and injection ($S = -1$) cases are presented by variation of λ. The temperature field is observed to decrease when the mixed convection parameter increases for both cases (suction/injuction). In contrast to when suction effect is used, it is discovered that temperature profiles are higher when injection effect is used. However, on the other hand, suction shows very low order variation in temperature profiles.

Figure 3.13, shows a variation in $\theta(\eta)$ as the suction/injection parameter changes meanwhile the hybrid nanofluid about far-field flow. Graph presents the impact of suction/injection for opposing flow as well as assisting flow cases for the comparison purpose. This figure displays that a rise in the suction/injection parameter causes a reduction in $\theta(\eta)$. It is also observed that with increasing numerical value for the suction/injection parameter (S) thermal boundary layer's thickness decreases. Figure 3.13, displays the same type of behaviour as in Figure 3.12. The difference in temperature between suction and absence of suction or injection is

found to be of very low order for both cases.

It is observed in Figure 3.14, that the heat source/sink parameter (Q) changes even with variation in $\theta(\eta)$. The positive value of Q generates heat within the system but the negative value of Q absorbs the heat during the flow of the system. It is noticed that the positive value of Q means heat generations and which eventually increase the hybrid nanofluid's temperature.

Figure 3.15, demonstrates the change in $\theta(\eta)$ with varying radiation parameter's values of hybrid nanofluid flow. This graph displays that the value of R_d increases as the temperature rises . The increasing radiation parameter (R_d) increase the temperature which corresponds to the circumstance where radiation during the flow of a hybrid nanofluid prevails over conduction. It has been discovered that the temperature of the hybrid nanofluid increases as it passes through the region of the boundary layer experiencing increased radiation-induced heat transfer.

Figure 3.16, depicts the changes in $\theta(\eta)$ of hybrid nanofluid flow with varying Biot number (Bi). Convective surface heating is related to the Biot number (Bi). The increase in the Biot number's numerical value corresponds to surface-level convective heating.

For $Bi = 0$, the isoflux wall condition is attained, and for $Bi \to \infty$ isothermal case is attained. Biot number (Bi) is used to analyse the relationship between surface convection and its solid conduction . The surface temperature ($\eta = 0$) is significantly changed as the Biot number (Bi) increases.

Additionally, by increasing Biot number (Bi) a rise in the $\theta(\eta)$ is observed. This is due to the thermal resistance of the surface due to increase in Biot number. The significant rise in surface temperature is because of the increase in convection.

The profiles drawn in Figures 3.17 and 3.18, display the temperature profile with different numerical values of ϕ_1 and ϕ_2 nanoparticles. The increase in the values of the nanoparticles ϕ_1 and ϕ_2 means that the ability of the hybrid nanofluid's nanoparticles to conduct heat is increasing, hence, it is noticed that there is an increase in temperature of nanofluid when volume fraction of any of the nanoparticles ϕ_1 or ϕ_2 is increased.

Figure 3.19, shows the changes in the temperature profile $\theta(\eta)$ of hybrid nanofluid

flow for the variation of α.

This figure depicts, the surface's upward motion frequently helps the temperature for α less than 1. Direct contact between the hybrid nanofluid layer and the surface experiences more friction due to its upstream movement. Hence, with increasing temperature it is observed that internal fluid layer friction rises which enhances the temperature.

TABLE 3.3: Numerical values of skin friction coefficient of HNF, ($Pr. = 6.2$)

									$\lambda = 0.1$	$\lambda = -0.1$
S	M	Q	R_d	γ	Bi	ϕ_1	ϕ_2	α	$(Re_x)^{\frac{1}{2}}C_f$	$(Re_x)^{\frac{1}{2}}C_f$
-1.0	2	-0.1	2	0.1	0.2	0.01	0.01	1.00	0.01711	-0.01731
0.0									0.00622	-0.00623
1.0									0.00242	-0.00243
	4.0								0.00209	-0.00209
	6.0								0.00186	-0.00186
		-0.5							0.00196	-0.00196
		0.5							0.00399	-0.00400
		1.0							0.01143	-0.01165
			4.0						0.00463	-0.00464
			6.0						0.00674	-0.00675
				0.5					0.00141	-0.00141
				0.9					0.00099	-0.00099
					0.6				0.00632	-0.00632
					1.0				0.00930	-0.00931
						0.05			0.00277	-0.00277
						0.10			0.00326	-0.00326
							0.05		0.00263	-0.00263
							0.10		0.00286	-0.00286
								0.90	0.13589	0.13094
								0.95	0.06928	0.06438

Table 3.3 is presented to display the numerical results of skin friction for different values of various parameters.

It is observed that skin friction coefficient decrease with increasing value of magnetic parameter, whereas the values of skin friction coefficient increases with increasing values of Biot number. From table We can also observed the impact of skin friction coefficient on the other parameters.

TABLE 3.4: Numerical values of heat transfer coefficient $(-(Re_x)^{\frac{-1}{2}}Nu_x)$ of HNF, $(Pr. = 6.2)$

									$\lambda = 0.1$	$\lambda = -0.1$
S	M	Q	R_d	γ	Bi	ϕ_1	ϕ_2	α	$H.T$	$H.T$
-1.0	2	-0.1	2	0.1	0.2	0.01	0.01	1.00	0.34256	0.34133
0.0									0.43531	0.43522
1.0									0.46937	0.46936
	4.0								0.46937	0.46936
	6.0								0.46937	0.46936
		-0.5							0.47413	0.47413
		0.5							0.45442	0.45438
		1.0							0.38885	0.38712
			4.0						0.77784	0.77780
			6.0						1.06978	1.06966
				0.5					0.46937	0.46936
				0.9					0.46937	0.46936
					0.6				1.22284	1.22271
					1.0				1.80114	1.80074
						0.05			0.45702	0.45701
						0.10			0.44238	0.44237
							0.05		0.44696	0.44695
							0.10		0.42278	0.42277
								0.90	0.46906	0.46905
								0.95	0.46921	0.46921

Table 3.4 is presented to display the numerical results of heat transfer coefficient (represented by H.T) for different values of various parameters. It is noticed that heat transfer coefficient nearly remains same with increment of M, whereas the values of heat transfer coefficient increases with increasing values of Biot number.

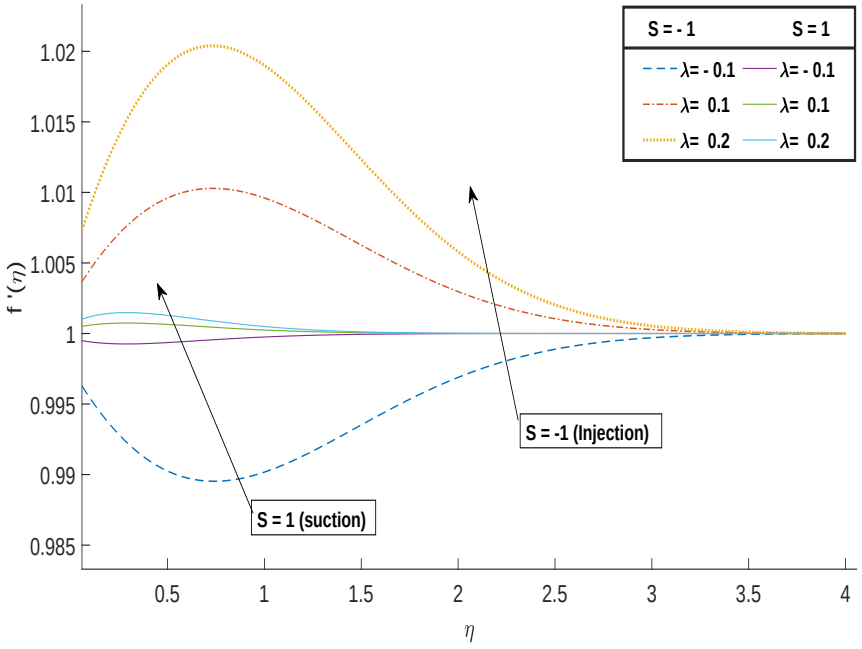

FIGURE 3.2: Variation in $f'(\eta)$ w.r.t. local mixed convection λ .

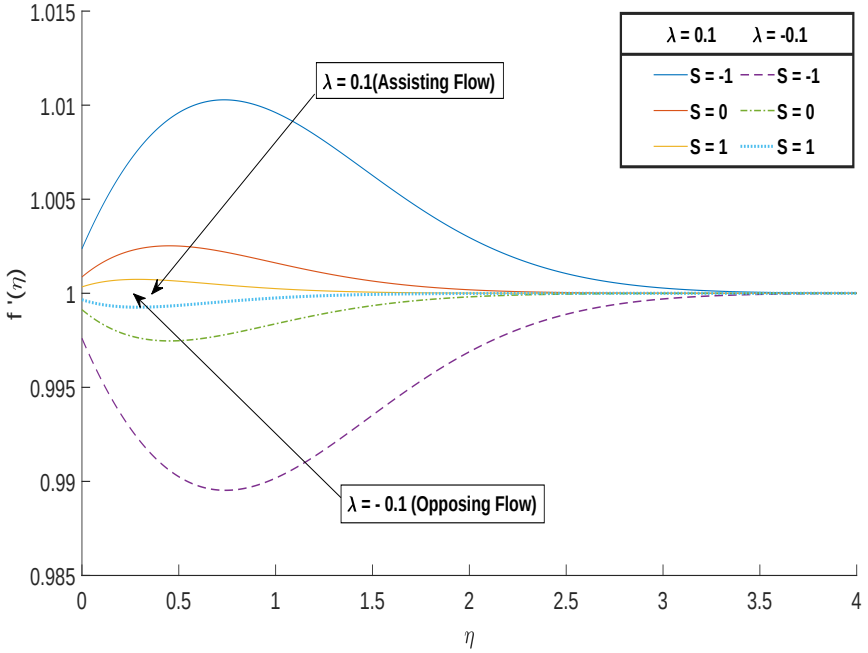

FIGURE 3.3: Variation in $f'(\eta)$ w.r.t. suction/injection parameter S .

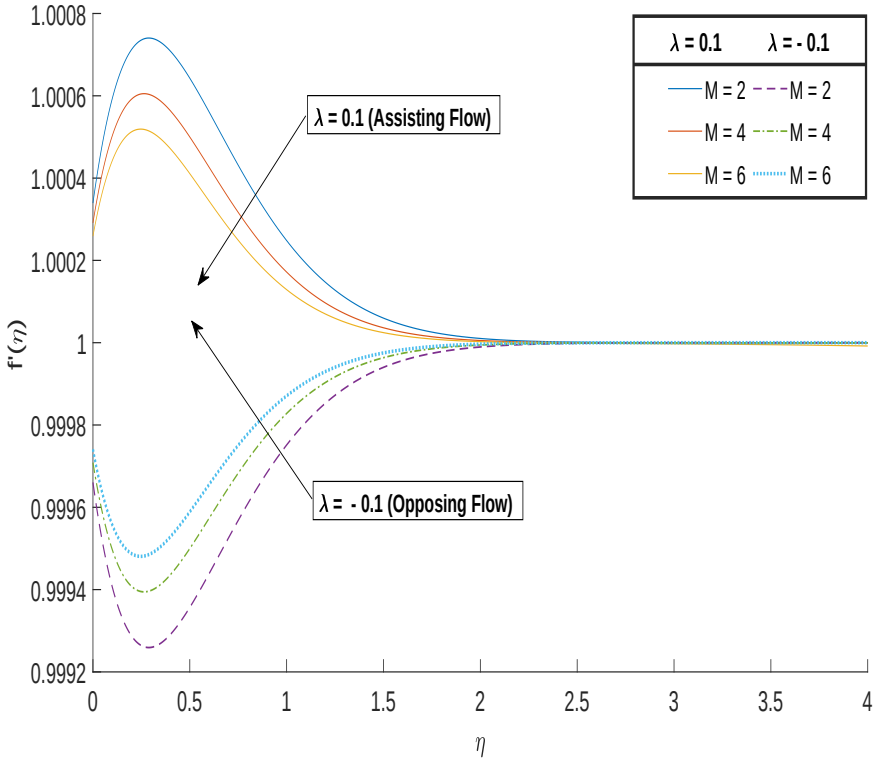

FIGURE 3.4: Variation in $f'(\eta)$ w.r.t. magnetic field parameter M .

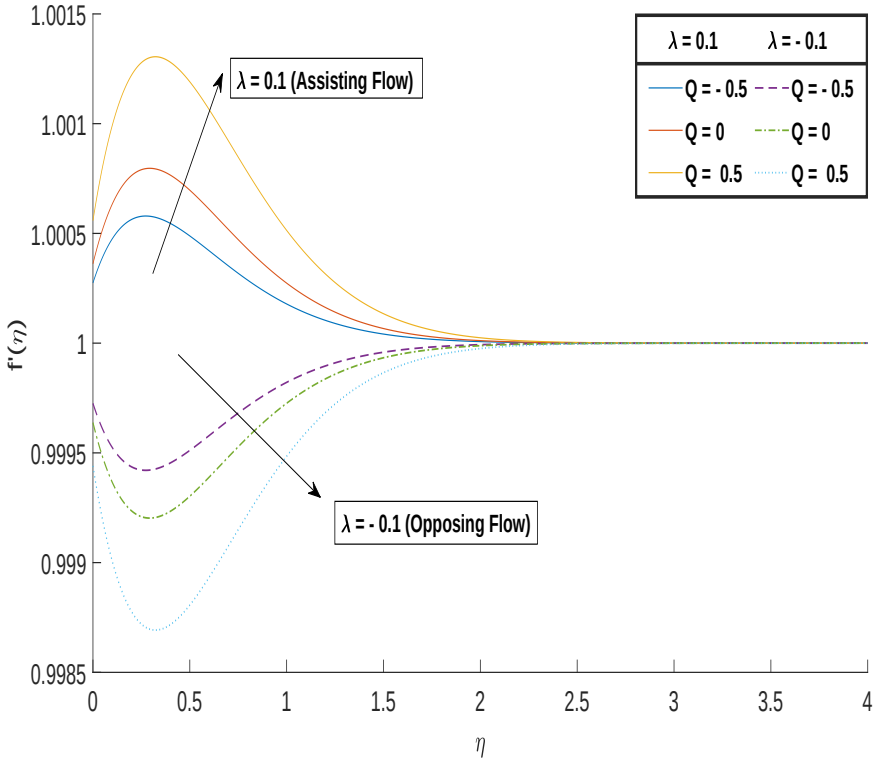

FIGURE 3.5: Variation in $f'(\eta)$ w.r.t. heat source/sink parameter Q.

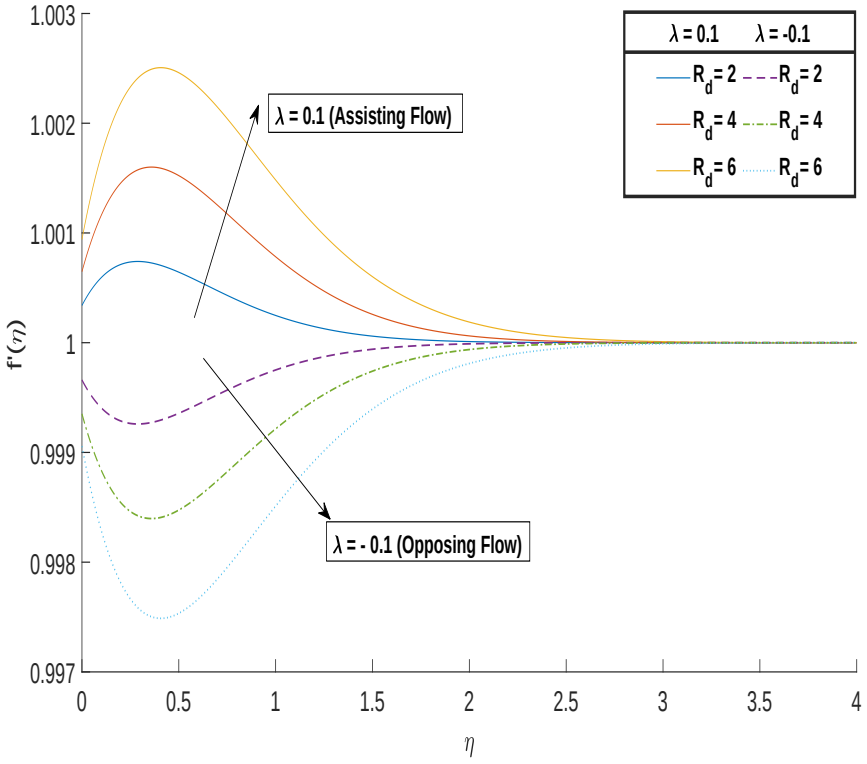

FIGURE 3.6: Variation in $f'(\eta)$ w.r.t. radiation parameter R_d .

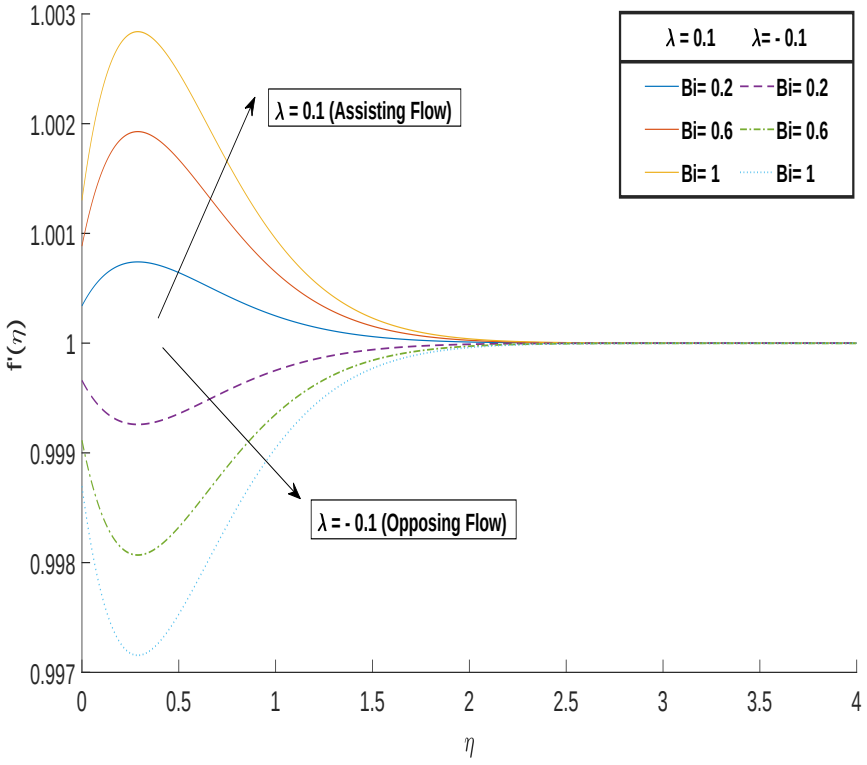

FIGURE 3.7: Variation in $f'(\eta)$ w.r.t. Biot number Bi.

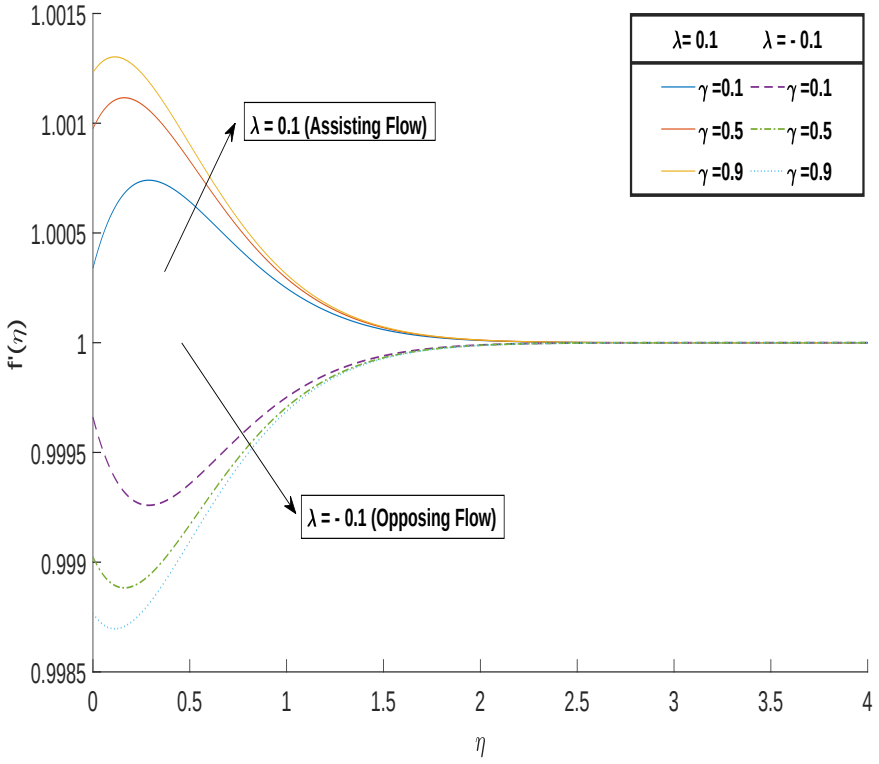

FIGURE 3.8: Variation in $f'(\eta)$ w.r.t. velocity slip parameter γ .

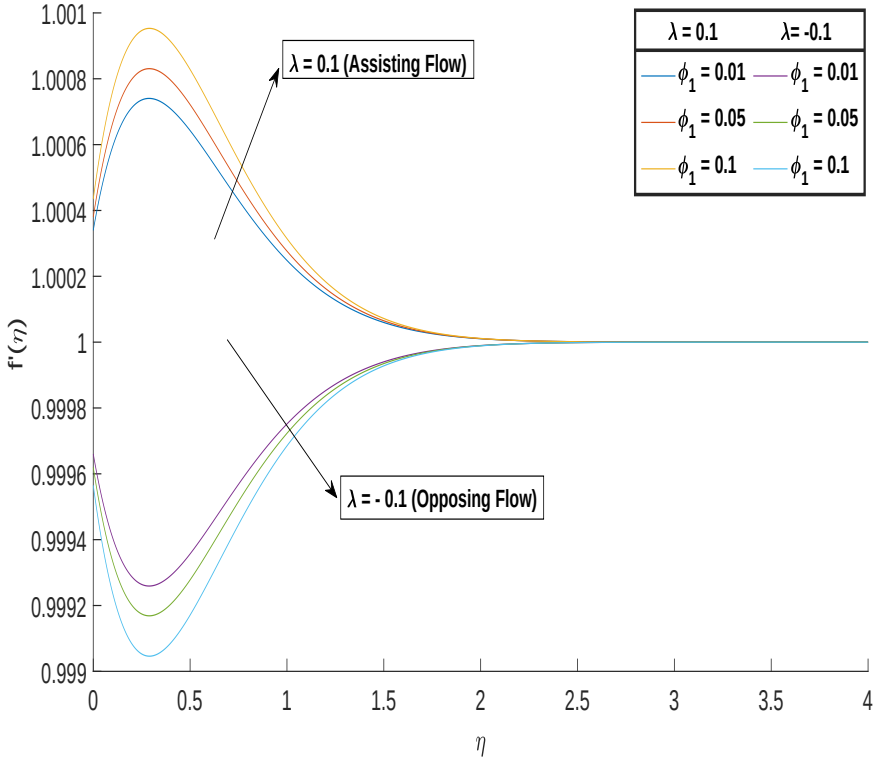

FIGURE 3.9: Variation in $f'(\eta)$ w.r.t. volume fraction of nanoparticles ϕ_1 .

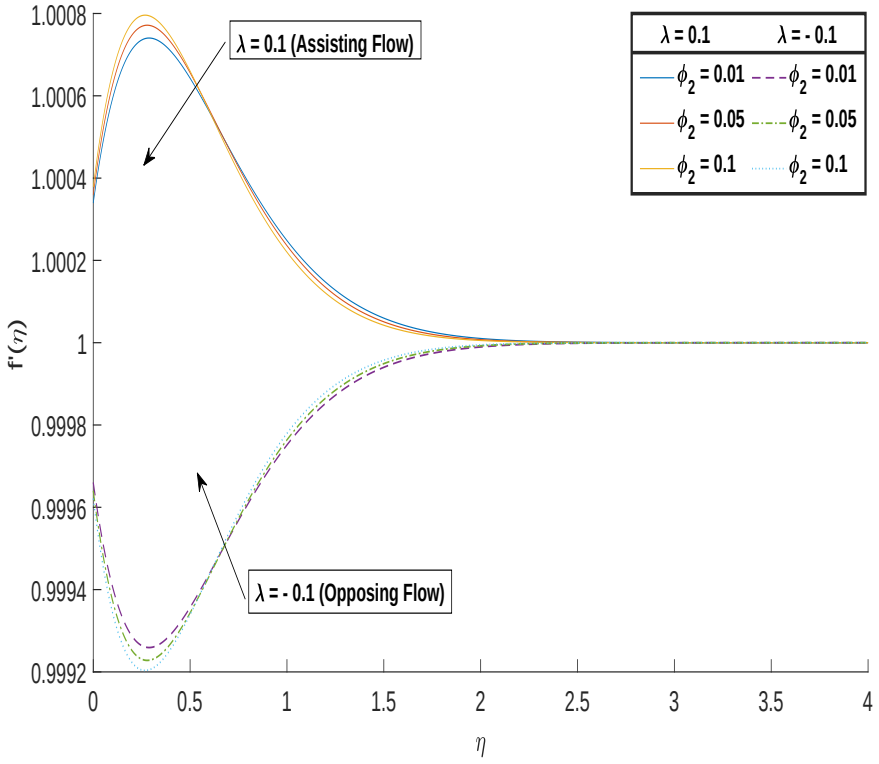

FIGURE 3.10: Variation in $f'(\eta)$ w.r.t. volume fraction of nanoparticles ϕ_2.

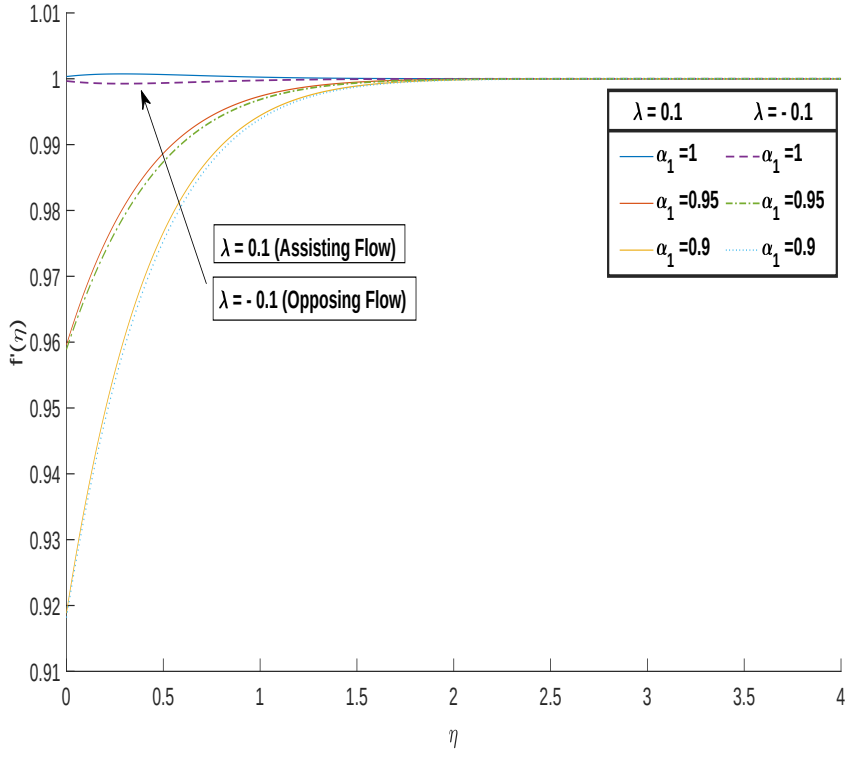

FIGURE 3.11: Variation in $f'(\eta)$ w.r.t. moving parameter α.

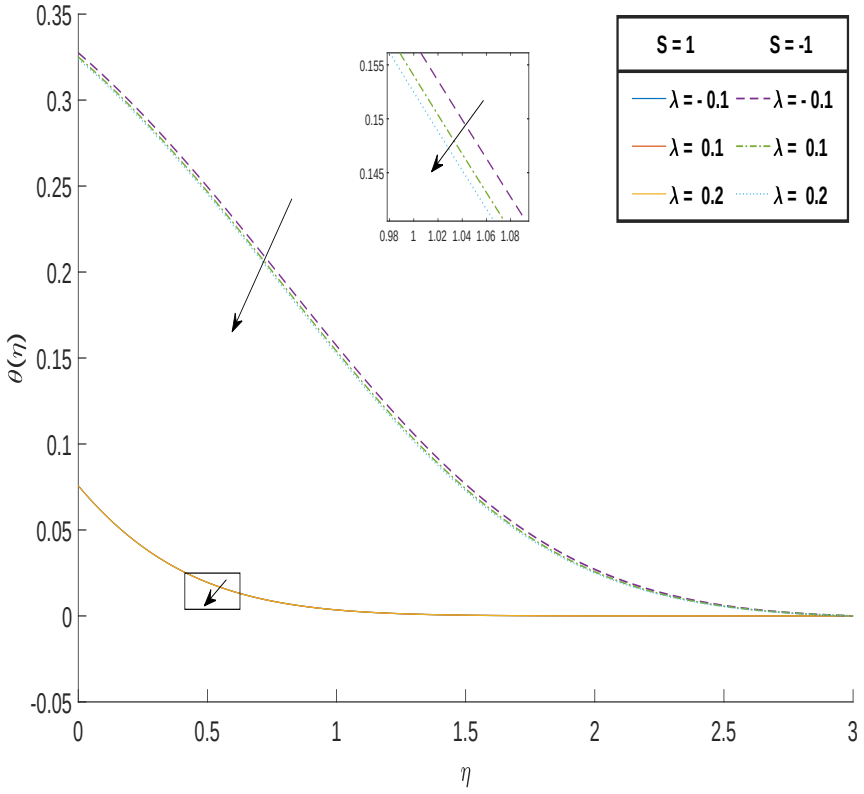

FIGURE 3.12: Variation in $\theta(\eta)$ w.r.t. local mixed convection λ.

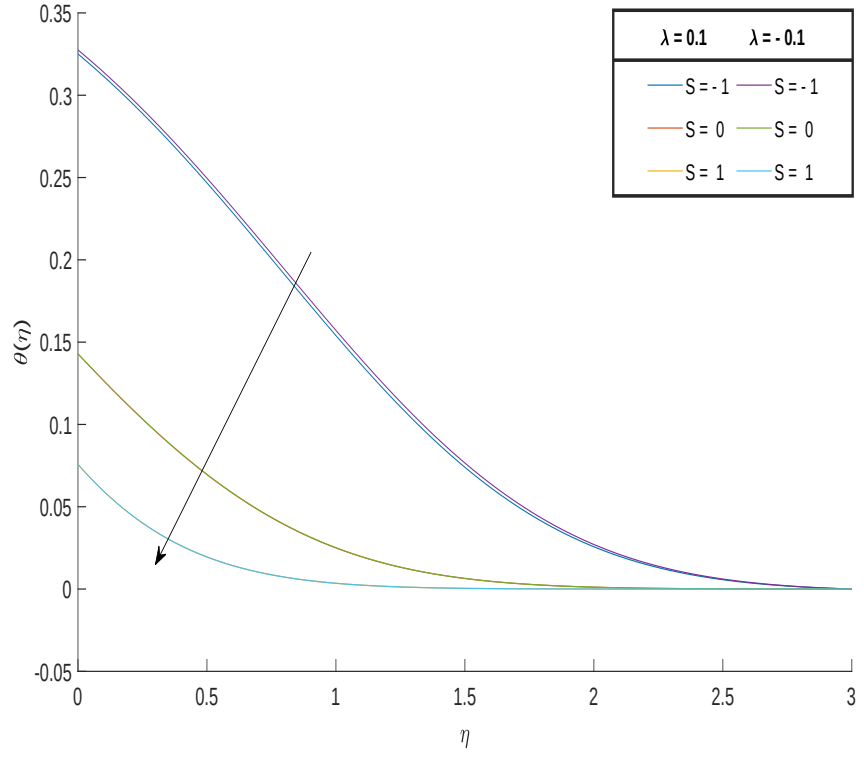

FIGURE 3.13: Variation in $\theta(\eta)$ w.r.t. suction/injuction parameter S.

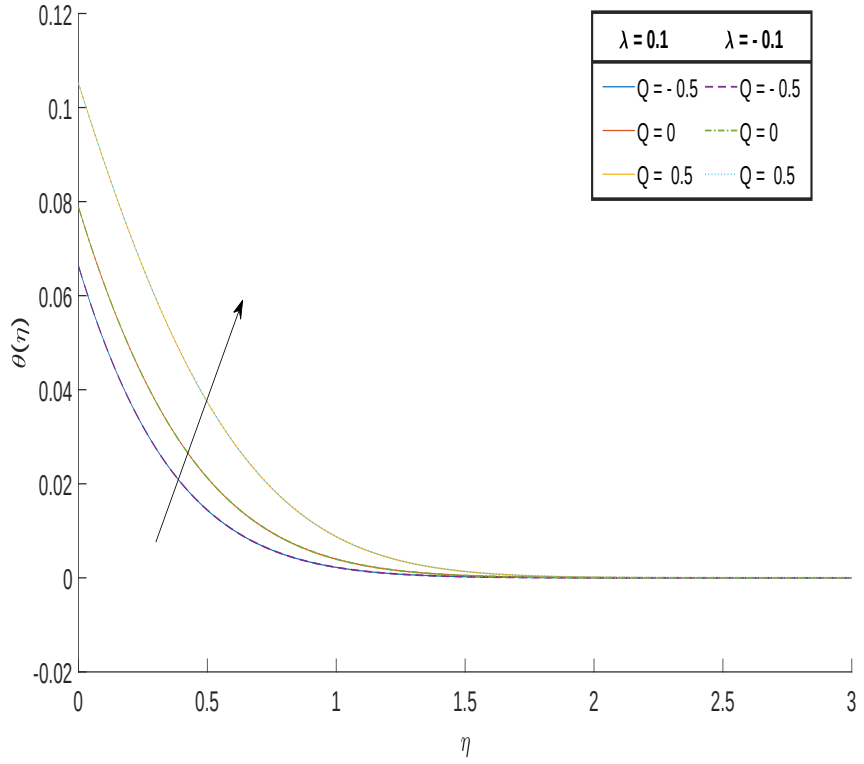

FIGURE 3.14: Variation in $\theta(\eta)$ w.r.t. heat source/sink parameter Q.

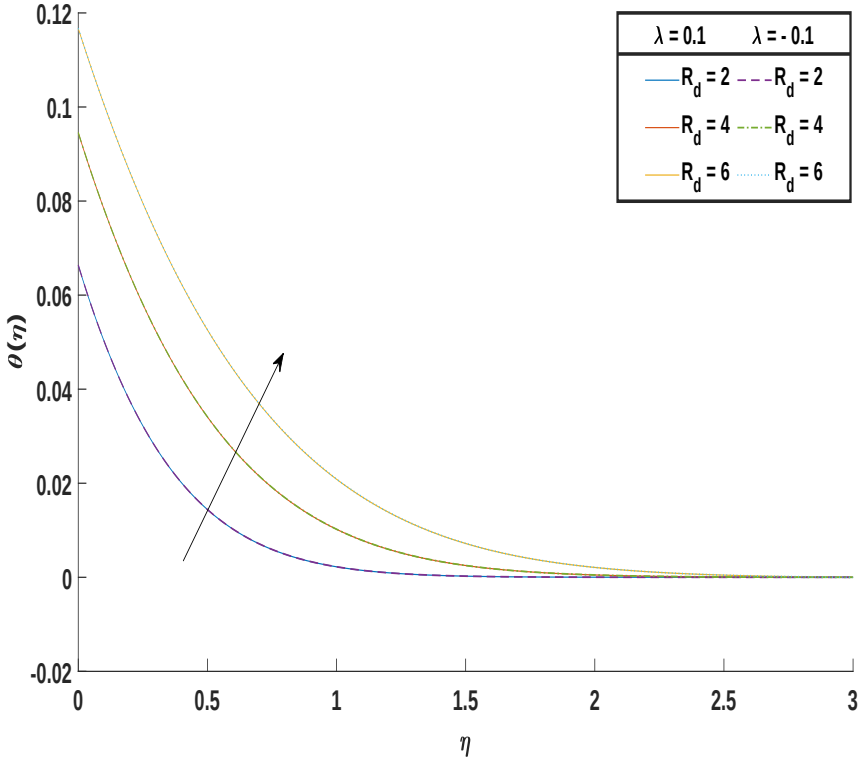

FIGURE 3.15: Impact on $\theta(\eta)$ w.r.t. R_d.

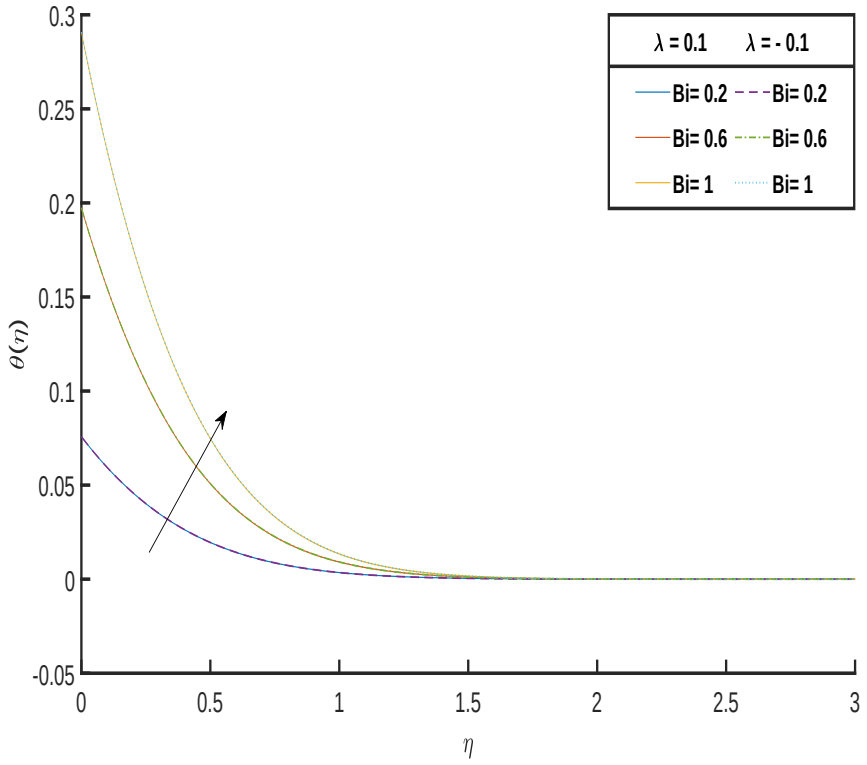

FIGURE 3.16: Variation in $\theta(\eta)$ w.r.t. Biot number Bi.

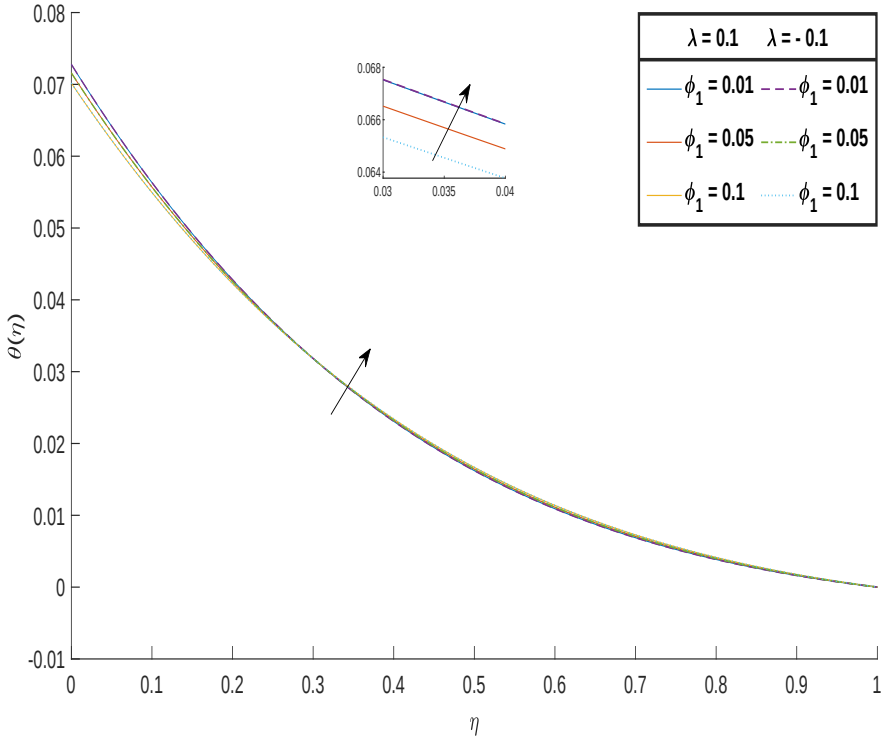

FIGURE 3.17: Variation in $\theta(\eta)$ w.r.t. volume fraction of nanoparticles ϕ_1 .

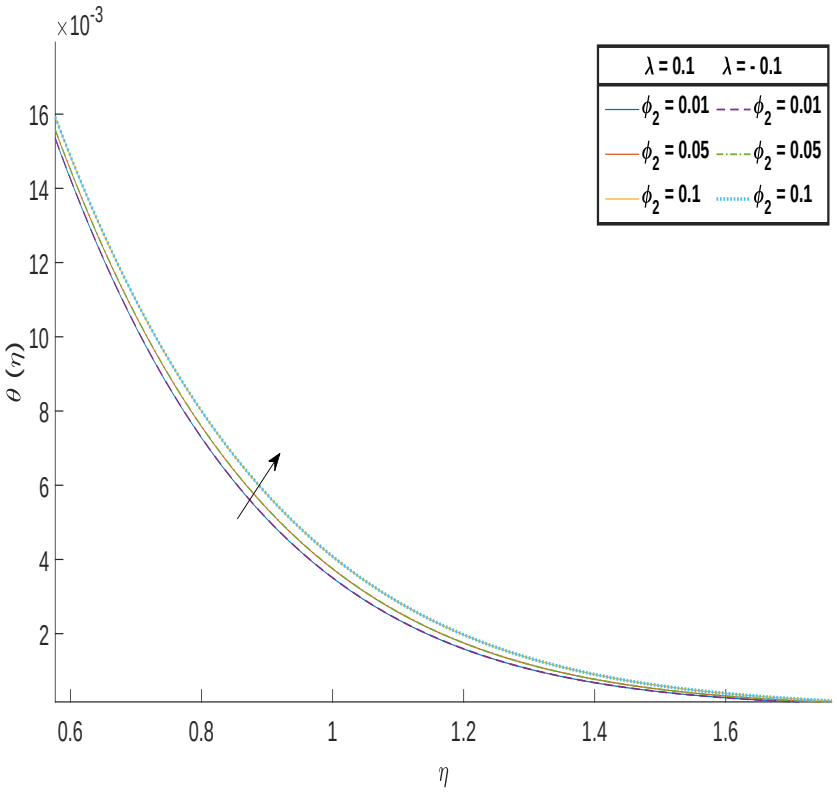

FIGURE 3.18: Variation in $\theta(\eta)$ w.r.t. volume fraction of nanoparticles ϕ_2.

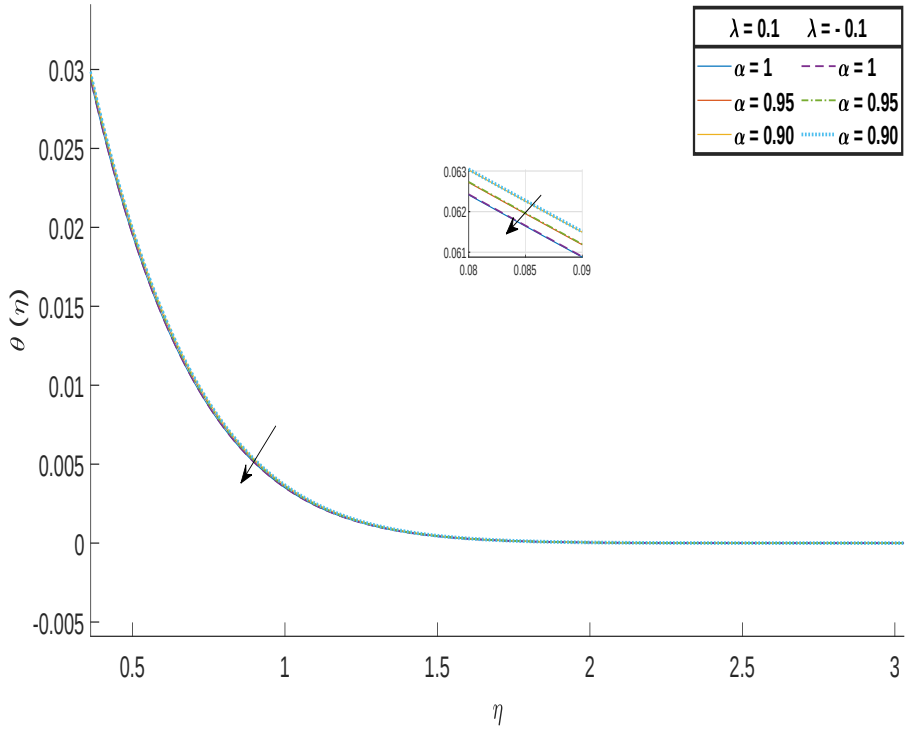

FIGURE 3.19: Variation in $\theta(\eta)$ w.r.t. moving parameter α.

Chapter 4

MHD Prandtl-Eyring Hybrid Nano-Fluid Flow

4.1 Introduction

This chapter provides an investigation of an assisting and opposing flow of Prandtl-Eyring hybrid nanofluid flow. The flow is over a moving surface under the effect of thermal radiation and velocity slip. Molybdenum disulfide (MoS_2) and Silicon dioxide (SiO_2) are used as nano particles with water as base fluid. The model of flow is a system of partial differential equation. Using the appropriate transformations, the governing nonlinear PDEs are transformed into a system of dimensionless ODEs. In order to solve the ODEs, the shooting technique is implemented in MATLAB. At the end of this chapter the numerical solutions for various parameters are discussed for the dimensionless velocity profile $f'(\eta)$ and temperature distribution $\theta(\eta)$.

4.2 Mathematical Modeling

The flow problem deals with the influence of Prandtl-Eyring fluid stress tensor over a permeable moving surface in two dimensions flow of a MHD hybrid nanofluid

with convection and containing a lot of silicon dioxide (SiO_2) and molybdenum disulfide (MoS_2) nanoparticles past a moving, permeable surface has been investigated. Molybdenum disulfide (MoS_2) and Silicon dioxide (SiO_2) are used as nano particles with water as base fluid. Thermal radiation, slip, suction/injection and heat source/sink effects are considered, to examine the hybrid nanofluid's capacity for heat transmission as it flows past a porous surface. The comparison of buoyancy opposing flow and buoyancy assisting flow of hybrid nanofluid is conducted.

4.2.1 Geometry of the Problem

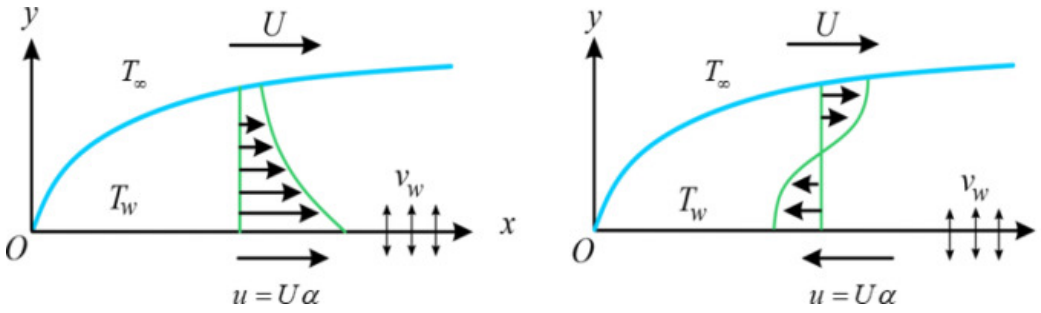

FIGURE 4.1: Physical representation of the problem.

The moving surface is heated by convection from a hot fluid at T_w temperature. The current model's geometry and physical domain are shown by Figure 4.1, where the cartesian coordinates x and y are used. The surface is assumed to be parallel to $x - axis$. The velocity of moving surface is replaced by U and the ambient temperature is denoted by T_∞. A variable magnetic field $B = B_o(2x)^{-0.5}$ is normally applied to a surface. Suction and injection are represented by the mass flux velocity $v_w(x)$ for positive and negative values, respectively. The following dependent quantities are considered in the problem:

- $Q_o^* = x^{-1}Q_o$ Heat source
- $h_f^* = x^{\frac{-1}{2}}h_f$ Heat transfer efficiency of a fluid under convection
- $k'^* = x^{\frac{1}{2}}k'$ length of the velocity slip

- $\beta^* = x^{-1}\beta$ Factor of thermal expansion.

One can see [46, 47] for reference. Molybdenum disulfide (MoS_2) and Silicon dioxide (SiO_2) are used as nano particles with water as base fluid. It is assumed that all the size of nanoparticles is consistent and constant and their clustering on thermophysicals properties is ignored.

4.2.2 Prandtl-Eyring Fluid Stress Tensor

Prandtl Eyring fluid stress tensor is given in the following mathematical form:

$$\tau = \frac{A_d \arcsin\left[\frac{1}{C}\left(\frac{\partial u}{\partial y}\right)^2 + \left(\frac{\partial u}{\partial y}\right)^{\sqrt{2}}\right]}{\left[\left(\frac{\partial u}{\partial y}\right)^2 + \left(\frac{\partial u}{\partial y}\right)^{\sqrt{2}}\right]}\left(\frac{\partial u}{\partial y}\right), \tag{4.1}$$

here the mechanisms is indicated by the curving velocity :

$\overline{u} = \Big[u(x,y,0), v(x,y,0), 0\Big]$. A_d and C represent fluid parameters.

The governing equations for the flow with all above conventions are as follows [45]:

Continuity equation:

$$\frac{\partial u}{\partial x} + \frac{\partial v}{\partial y} = 0 \tag{4.2}$$

Momentum Equation:

$$u\frac{\partial u}{\partial x} + v\frac{\partial u}{\partial y} = \frac{A_d}{C\ \rho_{hnf}}\frac{\partial^2 u}{\partial y^2} - \frac{A_d}{2C^3\ \rho_{hnf}}\frac{\partial^2 u}{\partial y^2}\left[\frac{\partial u}{\partial y}\right]^2 + \frac{\sigma_{hnf}B^2}{\rho_{hnf}}(u_\infty - u) + \frac{(\rho\beta^*)_{hnf}\ g}{\rho_{hnf}}(T - T_\infty) \tag{4.3}$$

Energy Equation:

$$u\frac{\partial T}{\partial x}+v\frac{\partial T}{\partial y}=\frac{k_{hnf}}{(\rho C_p)_{hnf}}\left(\frac{\partial^2 T}{\partial y^2}\right)-\frac{1}{(\rho C_p)_{hnf}}\left(\frac{\partial q_r}{\partial y}\right) + \frac{Q_o^*}{(\rho C_p)_{hnf}}(T-T_\infty), \tag{4.4}$$

where the components of flow velocity in the x- and y-directions are u and v respectively and T denotes the hybrid nanofluid's temperature. While μ_{hnf}, σ_{hnf}, $(\rho C_p)_{hnf}$, k_{hnf}, ρ_{hnf} and $(\beta^*)_{hnf}$ are the hybrid nanofluid's dynamic viscosity, electrical conductivity, heat capacity, thermal conductivity, density, and thermal expansion coefficient. Also q_r, k^* , Q_o and g are the radiative heat flux, the slip length, heat source/sink coefficient and acceleration due to gravity respectively. The subscripts f, hnf, and nf in this overview stand for the base fluid, the hybrid nanofluid, and the nanofluid respectively.

The associated BCs have been taken as:

$$\left.\begin{aligned} &u=U\alpha+k'^*\frac{\partial u}{\partial y},\ v=v_w(x),\ -k_{hnf}\frac{\partial T}{\partial y}=h_f^*\,(T_w-T)\ at\ y=0,\\ &u=u_\infty\to U,\quad T\to T_\infty,\quad as\quad y\to\infty, \end{aligned}\right\} \tag{4.5}$$

where α is the moving parameter, α greater than or equal to 1 represents the downstream movement and α less than 1 represents the upstream movement from origin.

4.3 Similarity Transformations

For conversion of equations (4.2) to (4.4) into dimensionless form following transformation are used [45].

$$\left.\begin{aligned} &u=Uf'(\eta)\ ,\qquad \nu=\sqrt{\frac{U\nu_f}{2x}}(\eta f'(\eta)-f(\eta))\ ,\qquad \theta(\eta)=\frac{T-T_\infty}{T_w-T_\infty},\\ &\eta=y\sqrt{\frac{U}{2x\nu_f}}. \end{aligned}\right\} \tag{4.6}$$

The detailed procedure for the conversion of continuity equation (4.2) has been already discussed in Chapter 3. So the continuity equation (4.2) can be seen satisfied under the same circumstances.

For dimensionless form of momentum equation the following conversions are necessary:

$$u = Uf'(\eta), \qquad \nu = \sqrt{\frac{U\nu_f}{2x}}(\eta f'(\eta) - f(\eta)), \qquad \eta = y\sqrt{\frac{U}{2x\nu_f}},$$

$$\frac{\partial u}{\partial x} = Uf''(\eta)\frac{\partial \eta}{\partial x},$$

$$\frac{\partial u}{\partial x} = \frac{-yU^{\frac{3}{2}}}{x^{\frac{3}{2}}2^{\frac{3}{2}}\sqrt{\nu}_f}f''(\eta),$$

$$\implies \quad u\frac{\partial u}{\partial x} = \frac{-yU^{\frac{3}{2}}}{x^{\frac{3}{2}}2^{\frac{3}{2}}\sqrt{\nu}_f}f''(\eta)Uf'(\eta),$$

$$\implies \quad u\frac{\partial u}{\partial x} = \frac{-yU^{\frac{5}{2}}}{x^{\frac{3}{2}}2^{\frac{3}{2}}\sqrt{\nu}_f}f'(\eta)f''(\eta), \tag{4.7}$$

$$\implies \quad \frac{\partial u}{\partial y} = Uf''(\eta)\frac{\partial(\eta)}{\partial y},$$

$$\implies \quad \frac{\partial u}{\partial y} = Uf''(\eta)\sqrt{\frac{U}{2x\nu_f}},$$

$$\implies \quad \frac{\partial u}{\partial y} = U^{\frac{3}{2}}\sqrt{\frac{1}{2x\nu_f}}f''(\eta),$$

$$\implies \quad v\frac{\partial u}{\partial y} = U^{\frac{3}{2}}\sqrt{\frac{1}{2x\nu_f}}f''(\eta)\sqrt{\frac{U\nu_f}{2x}}(\eta f'(\eta) - f(\eta)),$$

$$\implies \quad v\frac{\partial u}{\partial y} = \frac{U^2}{2x}f''(\eta)\left(y\sqrt{\frac{U}{2x\nu_f}}f'(\eta) - f(\eta)\right)$$

$$v\frac{\partial u}{\partial y} = \frac{yU^{\frac{5}{2}}}{x^{\frac{3}{2}}2^{\frac{3}{2}}\sqrt{\nu}_f}f'(\eta)f''(\eta) - \frac{U^2}{2x}f(\eta)f''(\eta),$$

$$u\frac{\partial u}{\partial x} + v\frac{\partial u}{\partial y} = -\frac{U^2}{2x}f(\eta)f''(\eta), \tag{4.8}$$

$$\frac{\partial^2 u}{\partial y^2} = \frac{U^{\frac{3}{2}}}{\sqrt{2x\nu_f}}f'''(\eta)\frac{\partial \eta}{\partial y},$$

$$\implies \quad = \frac{U^{\frac{3}{2}}}{\sqrt{2x\nu_f}}f'''(\eta)\sqrt{\frac{U}{2x\nu_f}},$$

$$\implies \quad \frac{\partial^2 u}{\partial y^2} = \frac{U^2}{2x\nu_f}f'''(\eta),$$

$$\implies \frac{A_d}{C\rho_{hnf}}\frac{\partial^2 u}{\partial y^2} - \frac{A_d}{2C^3\rho_{hnf}}\frac{\partial^2 u}{\partial y^2}\left[\frac{\partial u}{\partial y}\right]^2 + \frac{\sigma_{hnf}}{\rho_{hnf}}B^2(u_\infty - u) + \frac{(\rho\beta^*)_{hnf}g}{\rho_{hnf}}(T - T_\infty),$$

$$\implies \frac{A_d}{C\rho_{hnf}}\frac{U^2}{2xv_f}f''' - \frac{A_d}{2C^3\rho_{hnf}}\frac{U^2}{2xv_f}f'''[\frac{U^3}{2xv_f}f''^2] + \frac{\sigma_{hnf}}{\rho_{hnf}}\frac{B_o^2}{2x}(u_\infty - u)$$
$$+ \frac{\rho_{hnf}\beta_{hnf}g}{\rho_{hnf}x}(T - T_\infty),$$

$$\implies -\frac{U^2}{2x}f(\eta)f''(\eta) = \frac{A_d}{C\rho_{hnf}}\frac{U^2}{2xv_f}f''' - \frac{A_d}{2C^3\rho_{hnf}}\frac{U^2}{2xv_f}f'''[\frac{U^3}{2xv_f}f''^2]$$
$$+ \frac{\sigma_{hnf}}{\rho_{hnf}}\frac{B_o^2}{2x}(u_\infty - u) + \frac{\beta_{hnf}g}{x}(T - T_\infty),$$
$$-\frac{U^2}{2x}f(\eta)f''(\eta) = \frac{A_d}{C\rho_{hnf}}\frac{1}{v_f}f''' - \frac{A_d}{2C^3\rho_{hnf}}\frac{1}{v_f}f'''[\frac{U^3}{2xv_f}f''^2]$$
$$+ \frac{\sigma_{hnf}}{\rho_{hnf}}\frac{B_o^2}{U^2}(U - Uf'\eta) + \frac{2\beta_{hnf}g}{U^2}(T - T_\infty) = 0, \tag{4.9}$$

put, $\nu_f = \dfrac{\mu_f}{\rho_f}$ in (4.9) we get,

$$f(\eta)f''(\eta) + \frac{A_d}{C\rho_{hnf}\frac{\mu_f}{\rho_f}}f''' - \frac{A_d}{2C^3\rho_{hnf}\frac{\mu_f}{\rho_f}}f'''[\frac{U^3}{2xv_f}f''^2] + \frac{\sigma_{hnf}}{\rho_{hnf}}\frac{B_o^2}{U^2}(U - Uf'\eta) +$$
$$\frac{2\beta_{hnf}g}{U^2}(T - T_\infty) = 0. \tag{4.10}$$

Now in (4.10) 4th term is divide and multiply by ρ_f and σ_f whereas 5th term is divide and multiply by β_f, so we have:

$$f(\eta)f''(\eta) + \frac{A_d}{\mu C}\frac{1}{\frac{\rho_{hnf}}{\rho_f}}f''' - \frac{A_d}{\mu C}\frac{1}{\frac{\rho_{hnf}}{\rho_f}}f'''[\frac{U^3}{4C^2xv_f}f''^2] + \frac{\rho_f}{\rho_f}\frac{\sigma_{hnf}}{\rho_{hnf}}\frac{\sigma_f}{\sigma_f}\frac{B_o^2}{U}(1 - f'\eta) +$$
$$\frac{2\beta_{hnf}g}{U^2}\frac{\beta_f}{\beta_f}(T - T_\infty)\frac{T_w - T_\infty}{T_w - T_\infty} = 0,$$
$$f(\eta)f''(\eta) + \frac{A1}{B}f''' - \frac{A1}{B}f'''A2f''^2 + \frac{\sigma_{hnf}}{\sigma_f}\frac{1}{\frac{\rho_{hnf}}{\rho_f}}\frac{\sigma_f}{\rho_f}\frac{B_o^2}{U}(1 - f'\eta)$$
$$+ \frac{2\beta_{hnf}}{\beta_f}\frac{g\beta_f(T_w - T_\infty)}{U^2}\frac{(T - T_\infty)}{(T_w - T_\infty)} = 0,$$
$$f(\eta)f''(\eta) + \frac{A1}{B}f'''(\eta)(1 - A2f''^2) + \frac{C}{B}M(1 - f'(\eta) + 2D\lambda\theta = 0, \tag{4.11}$$

where, $A1 = \dfrac{A_d}{\mu C}$, $\quad$ A2=$\dfrac{U^3}{4C^2xv_f}$.

Where, A_1 and A_2 denotes the Prandtl Eyring parameter-I and Prandtl Eyring parameter-II respectively. The detailed procedure for the conversion of energy

equation (4.4) has been already discussed in Chapter 3. The already worked out derivatives (3.14) to (3.20) in Chapter 3, will be directly used here.

$$\left[\frac{k_{hnf}}{k_f}+\frac{4}{3}Rd\right]\theta''+EPrf\theta'+2Q\ Pr\theta=0. \tag{4.12}$$

4.4 Numerical Method for Solution

The shooting method has been used to solve the ordinary differential equations (4.11) and (4.12). The following notations have been considered:

$$f=y_1,\qquad f'=y_1'=y_2,\qquad f''=y_1''=y_2'=y_3,\qquad f'''=y_3'.$$
$$\theta=y_4,\qquad \theta'=y_4'=y_5,\qquad \theta''=y_5'.$$

As a result the momentum and energy equations are converted into the following system of first order ODEs:

$$\begin{aligned}
y_1' &= y_2, & y_1(0) &= s,\\
y_2' &= y_3, & y_2(0) &= \alpha+\gamma m,\\
y_3' &= [A1(1-A2y_3^2)]^{-1}\left[-By_1y_3-CM(1-y_2)-2BD\lambda y_4\right], & y_3(0) &= m,\\
y_4' &= y_5, & y_4(0) &= r,\\
y_5' &= \psi(-EPr\ y_1y_5+2Pr\ Qy_4), & y_5(0) &= -\frac{k_f}{k_{hnf}}\Big(Bi(1-r)\Big),
\end{aligned}$$

where m and r assumed missing conditions.

The above IVP is solved by using Runge Kutta method of oder four.

$$\left.\begin{aligned} y_2(m,r,\eta=\infty)&=1,\\ y_4(m,r,\eta=\infty)&=0. \end{aligned}\right\} \tag{4.13}$$

Newton's method is used to solve the non linear algebraic equation (4.13) for m and r.

This method has the following iterative scheme:

$$\begin{bmatrix} m \\ r \end{bmatrix}^{n+1} = \begin{bmatrix} m \\ r \end{bmatrix}^{n} - \left(\begin{bmatrix} \frac{\partial y_2}{\partial m} & \frac{\partial y_2}{\partial r} \\ \frac{\partial y_4}{\partial m} & \frac{\partial y_4}{\partial r} \end{bmatrix}^{-1} \begin{bmatrix} y_2 - 1 \\ y_4 - 0 \end{bmatrix} \right)^{n}.$$

To incorporate the above formula, we further need the following derivatives:

$$\frac{\partial y_1}{\partial m} = y_6, \qquad \frac{\partial y_2}{\partial m} = y_7, \qquad \frac{\partial y_3}{\partial m} = y_8,$$

$$\frac{\partial y_4}{\partial m} = y_9, \qquad \frac{\partial y_5}{\partial m} = y_{10},$$

$$\frac{\partial y_1}{\partial r} = y_{11}, \qquad \frac{\partial y_2}{\partial r} = y_{12}, \qquad \frac{\partial y_3}{\partial r} = y_{13},$$

$$\frac{\partial y_4}{\partial r} = y_{14}, \qquad \frac{\partial y_5}{\partial r} = y_{15}.$$

As the result of these notations, the Newton's iterative scheme gets the form:

$$\begin{bmatrix} R \\ S \end{bmatrix}^{n+1} = \begin{bmatrix} R \\ S \end{bmatrix}^{n} - \left(\begin{bmatrix} y_7 & y_{12} \\ y_9 & y_{14} \end{bmatrix}^{-1} \begin{bmatrix} y_2 - 1 \\ y_4 - 0 \end{bmatrix} \right)^{n}$$

Now, differentiating the system of five first ODEs with respect to each of the variables m and r to have another system of ten ODE's together. As a result

following IVP is obtained:

$$
\begin{aligned}
y_1' &= y_2, & y_1(0) &= s,\\
y_2' &= y_3, & y_2(0) &= \alpha + \gamma m,\\
y_3' &= [A1(1 - A2y_3^2)]^{-1}\left[-By_1y_3 - CM(1 - y_2) - 2BD\lambda y_4\right], & y_3(0) &= m,\\
y_4' &= y_5, & y_4(0) &= r,\\
y_5' &= \psi(-EPr\ y_1y_5 + 2Pr\ Qy_4), & y_5(0) &= -\frac{k_f}{k_{hnf}}\Big(Bi(1 - r)\Big),\\
y_6' &= y_7, & y_6(0) &= 0,\\
y_7' &= y_8, & y_7(0) &= r,\\
y_8' &= [A1(1 - A2y_3^2)]^{-2}[2A1A2y_3y_8]\left[-By_1y_3 - CM(1 - y_2) - 2BD\lambda y_4\right] +\\
&\left[A1(1 - A2y_3^2)\right]^{-1}[-By_1y_8 - By_3y_6 + CM(y_7) - 2BD\lambda y_9], & y_8(0) &= 1,\\
y_9' &= y_{10}, & y_9(0) &= 0,\\
y_{10}' &= \psi(-EPr\ y_1y_{10} - EPr\ y_5y_6 + 2Pr\ Qy_4), & y_{10}(0) &= 0,\\
y_{11}' &= y_{12}, & y_{11}(0) &= 0,\\
y_{12}' &= y_{13}, & y_{12}(0) &= m,
\end{aligned}
$$

$$
\begin{aligned}
y_{13}' &= [A1(1 - A2y_3^2)]^{-2}[2A1A2y_3y_{13}]\left[-By_1y_3 - CM(1 - y_2) - 2BD\lambda y_4\right] +\\
&\left[A1(1 - A2y_3^2)\right]^{-1}[-By_1y_{13} - By_3y_{11} + CM(y_{12}) - 2BD\lambda y_{14}], & y_{13}(0) &= 0,\\
y_{14}' &= y_{15}, & y_{14}(0) &= 1,\\
y_{15}' &= \psi(-EPr\ y_1y_{15} - EPr\ y_5y_{11} + 2Pr\ Qy_{14}), & y_{15}(0) &= \frac{k_f}{k_{hnf}}\ Bi.
\end{aligned}
$$

The Runge Kutta method of order four is used to solve the above system of fifteen first order differential equations with m and r as initial guess. The iterative process is repeated until the criteria listed below is met:

$$\max\left[\mid y_2(\eta, m, r) - 1 \mid, \mid y_4(\eta, m, r) \mid\right] < \epsilon,$$

for an arbitrarily small positive value of ϵ.

4.5 Representation of Tables and Graphs

Examining the effects of various dimensionless parameters on the velocity profiles $f'(\eta)$ and temperature profiles $\theta(\eta)$ of hybrid nanofluid flow is the primary goal of this section.

In the current discussion, the value of λ is taken as -0.1 to represents the case of obstructing flow and as 0.1 to represents the case of assisting flow. During the whole analysis we find the following values when this parameter assumed to be unchanged:

$\phi_1 = 0.01$, $\phi_2 = 0.01$, $Rd = 2$, $Pr. = 6.2$, $M = 2$, $S = 1$, $Q = -0.1$, $\gamma = 0.1$, $Bi = 0.2$ and $\alpha = 1$.

4.5.1 Discussion of the Velocity Profiles of Hybrid Nanofluids

Figure 4.2, demonstrates the impact on velocity profiles $f'(\eta)$ by the variation of mixed convection parameter (λ). Where, $S = 1$ and $S = -1$ represents the suction and injection scenarios respectively.

We observe neither the assisting flow nor the opposing flow exist for λ=0. Diagram depicts that the positive values of the parameter λ stand in for assisting flow, while negative values of the parameter λ stand in for opposing flow.

This figure shows that a higher value for the mixed convection parameter causing the velocity to increase when both the suction and the injection parameters are present. During the flow, stronger buoyancy forces are associated as the mixed convection parameter's numerical value rises, which causes an increase in velocity profiles. The velocity profiles near the surface overshoot because of the favorable pressure gradient produced by the positive value of λ. As compared to the suction case, the injection case exhibits higher positive peaks or lower negative peaks.

Figure 4.3, shows that velocity varies with change in suction/injection parameter, if the hybrid nanofluid flow about far field. Suction is indicated when parameter

S is positive, and injection applied at the surface is indicated when parameter S is negative. For $S = 0$ suction and injection are not present. It is noticed that the increasing value of S causes the velocity of an assisting flow to decrease (shown by solid lines), whereas the increasing value of S causes the velocity of an opposing flow to increase.

Figure 4.4, demonstrates the variation of magnetic parameter on velocity profiles $f'(\eta)$. Increasing the value of M means strengthing of mgnetic field. The Lorentz force is produced by the magnetic field. The Lorentz force opposes the flow as the magnetic parameter is increased. It can be seen in figure that as the parameter's numerical value rises the velocity is decreased for assisting flow (shown by solid lines) and in case of opposing flow velocity is increased (shown by dotted lines).

From figure 4.5, displays the variation in velocity by changing the value of Q, the source/sink parameter. We note that the capacity of the flow field to absorb heat is related to the heat generation within the flow field with the positive and negative values of Q . It is noticed that the velocity of an assisting flow increases as the value of the parameter (Q) increases, whereas the velocity of an opposing flow decreases as the value of the parameter (Q) increases.

Figure 4.6, shows the variation in velocity profile $f'(\eta)$ with different radiation parameter's values. In both cases (opposing and assisting flow) velocity profile increases with increasing values of radiation parameter R_d.

Figure 4.7, demonstrates the variation in velocity profile $f'(\eta)$ with respect to different values of Biot number (Bi). It is noticed that in the case of assisting flow, the velocity enhances with increasing values of Biot number (Bi), but for the case of opposing flow contrary results are observed.

Figure 4.8, shows the changes in velocity profiles as the values of velocity slip parameter (γ) changes. The figure clearly shows the direct relationship between

slip parameter and hybrid nanofluid velocity with assisting flow, but if there is an opposite flow, the graph illustrates the inverse relationship between slip parameter and hybrid nanofluid velocity.

The profiles drawn in figures 4.9 and 4.10, represent the impact in velocity profiles $f'(\eta)$ with an increase in numerical values of nanoparticles with volume fractions ϕ_1 and ϕ_2. Increasing the values of ϕ_1 and ϕ_2 mean to enhance the concentration of hybrid nano-fluid.
This means that raising the numerical value of the nanoparticles ϕ_1 and ϕ_2 correlates with raising the quantity of nanoparticles ϕ_1 and ϕ_2.
From Figure 4.9, we observed that for scenario of an assisting flow velocity rises with a rise in the values of volume fraction where as for an opposing flow velocity decreases. From Figure 4.10, we noticed that in the case of an assisting flow, the velocity decreases, while in the case of an obstructing flow, it increases.

Figure 4.11, shows the variation in the velocity profile for different values of α. The figure depicts the surface's movement downstream for α greater than or equal to 1 while it depicts the upstream changes in the surface for α less than 1. In this graph, we find that the surface tends to move downstream, which aids the velocity flow. Velocity enhances when α is greater than 1.

4.5.2 Discussion of Temperature Profiles of Hybrid Nanofluids

Figure 4.12, depicts the variation in temperature profiles $\theta(\eta)$ for mixed convection parameter (λ).
The temperature field is observed to decrease when the mixed convection parameter increases for both cases (suction/injection). It is discovered that temperature profiles are higher when injection effect is used. However, on the other hand, suction shows very low order variation in temperature profiles.

Figure 4.13, shows changes in $\theta(\eta)$ as the suction/injection parameter changes. This figure displays that a rise in the suction/injection parameter causes a reduction in $\theta(\eta)$. It is also observed that by increasing numerical values for the suction/injection parameter (S) thermal boundary layer thickness decreases. Figure 4.13, displays the same type of behaviour as in Figure 4.12. The difference in temperature between suction and absence of suction or injection is found to be of very low order for both cases.

Figure 4.14, displays the variation in temperature profiles $\theta(\eta)$ with respect to source/sink parameter Q. The positive value of Q generates heat within the system but the negative value of Q absorbs the heat during the flow of the system. It is observed that the positive value of Q means heat generations which eventually increase the hybrid nanofluid's temperature.

Figure 4.15, shows the impact on $\theta(\eta)$ with various values of radiation parameter R_d.
This diagram shows that the temperature rises with increasing values of R_d. The increasing radiation parameter (R_d) increase the temperature which corresponds to the circumstance where radiation during the flow of a hybrid nanofluid prevails over conduction.
It has been noticed that the temperature of the hybrid nanofluid increases as it passes through the region of the boundary layer experiencing increased radiation-induced heat transfer.

Figure 4.16, shows the variation in $\theta(\eta)$ with varying Biot number (Bi). The increase in the Biot number's numerical value corresponds to surface-level convective heating.
For $Bi = 0$, the isoflux wall condition is attained, and for $Bi \to \infty$ isothermal case is attained. Biot number (Bi) is used to analyse the relationship between surface convection and its solid conduction.

The surface temperature ($\eta = 0$) is significantly different as the Biot number (Bi) increases.
Additionally, by increasing Biot number (Bi) a rise in $\theta(\eta)$ is observed. Physically, when the Biot number (Bi) upsurges, the surface thermal resistance significantly decrease. The upsurge in convection lead to a rise in surface temperature.

The profiles drawn in Figures 4.17 and 4.18, display variation in $\theta(\eta)$ with different numerical values of volume fraction ϕ_1 and ϕ_2 of nanoparticles. The increase in the values of ϕ_1 and ϕ_2 represented the enhancement in the ability of field to conduct heat.
Hence temperatue is increased when volume fraction of any nanoparticle is increased.

Figure 4.19, shows the changes in $\theta(\eta)$ for the variation in (α), the moving parameter . This figure depicts, the surface's upward motion frequently helps the temperature for (α) less than 1.

Direct contact between the hybrid nanofluid layer and the surface experiences more friction due to its upstream movement.
Hence, with increasing temperature it is observed that internal fluid layer friction rises which enhances the temperature.

4.5.3 Graphical Represenation of Prandtl-Eyring Parameters

Figure 4.20, presents that how Prandtl Eyring parameter (A_1) affects velocity profiles $f'(\eta)$.
It has been noticed in the case of assisting flow , the velocity decreases as the value of parameter A_1 increases, whereas for an opposing flow velocity increases as the value of parameter A_1 increases.

Figure 4.21, depicts that for different values of Prandtl Eyring parameter (A_2) the velocity profiles remains same.

TABLE 4.1: Numerical values of skin friction coefficient of hybrid nanofluid when $Pr. = 6.2$

									$\lambda = 0.1$	$\lambda = -0.1$
S	M	Q	R_d	γ	Bi	ϕ_1	ϕ_2	α	$(Re_x)^{\frac{1}{2}}C_f$	$(Re_x)^{\frac{1}{2}}C_f$
-1.0	2	-0.1	2	0.1	0.2	0.01	0.01	1.00	0.01753	-0.01773
0.0									0.00644	-0.00646
1.0									0.00252	-0.00252
	4.0								0.00216	-0.00216
	6.0								0.00192	-0.00192
		-0.5							0.00203	-0.00203
		0.5							0.00415	-0.00415
		1.0							0.01186	-0.01209
			4.0						0.00480	-0.00481
			6.0						0.00696	-0.00697
				0.5					0.00144	-0.00145
				0.9					0.00101	-0.00101
					0.6				0.00657	-0.00657
					1.0				0.00967	-0.00969
						0.05			0.00313	-0.00313
						0.10			0.00409	-0.00410
							0.05		0.00296	-0.00296
							0.10		0.00357	-0.00357
								0.90	0.14010	0.13491
								0.95	0.07127	0.06616

Table 4.1 is presented to display the numerical results of skin friction coefficient for different values of various parameters.

It is observed that with increasing values of magnetic parameter skin friction coefficient decreases for assisting flow and increases for obstructing flow.

It is also observed that with increasing values of Biot number the values of skin friction coefficient increases for assisting flow and decreases for obstructing flow.

TABLE 4.2: Numerical values of heat transfer coefficient $-(Re_x)^{\frac{-1}{2}} Nu_x$ of hybrid nanofluid, when $Pr. = 6.2$

									$\lambda = 0.1$	$\lambda = -0.1$
S	M	Q	R_d	γ	Bi	ϕ_1	ϕ_2	α	$H.T$	$H.T$
-1.0	2	-0.1	2	0.1	0.2	0.01	0.01	1.00	0.34276	0.34152
0.0									0.43531	0.43522
1.0									0.46936	0.46936
	4.0								0.46936	0.46936
	6.0								0.46936	0.46936
		-0.5							0.47413	0.47412
		0.5							0.45442	0.45438
		1.0							0.38892	0.38715
			4.0						0.77785	0.77781
			6.0						1.07001	1.06989
				0.5					0.46937	0.46935
				0.9					0.46937	0.46935
					0.6				1.22283	1.22270
					1.0				1.80114	1.80072
						0.05			0.45701	0.45700
						0.10			0.44238	0.44237
							0.05		0.44695	0.44695
							0.10		0.42278	0.42277
								0.90	0.46906	0.46905
								0.95	0.46921	0.46921

Table 4.2 is presented to display the numerical results of heat transfer coefficient for different values of various parameters.

It is noticed that heat transfer coefficient nearly remains same with increasing values of magnetic parameter for both cases.

Whereas the values of heat transfer coefficient increases with increasing values of Biot number for both cases.

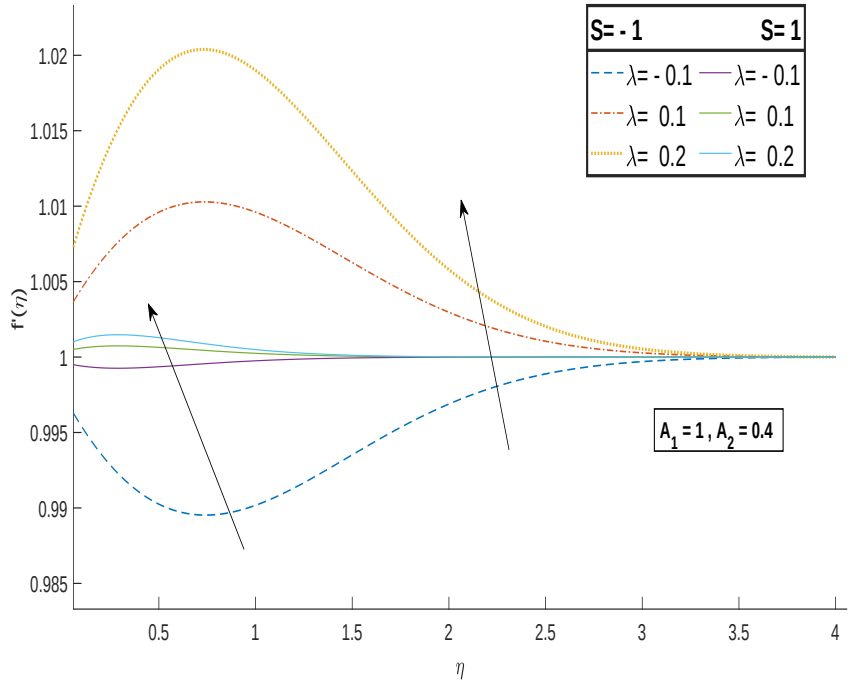

FIGURE 4.2: Variation in $f'(\eta)$ w.r.t. local mixed convection λ.

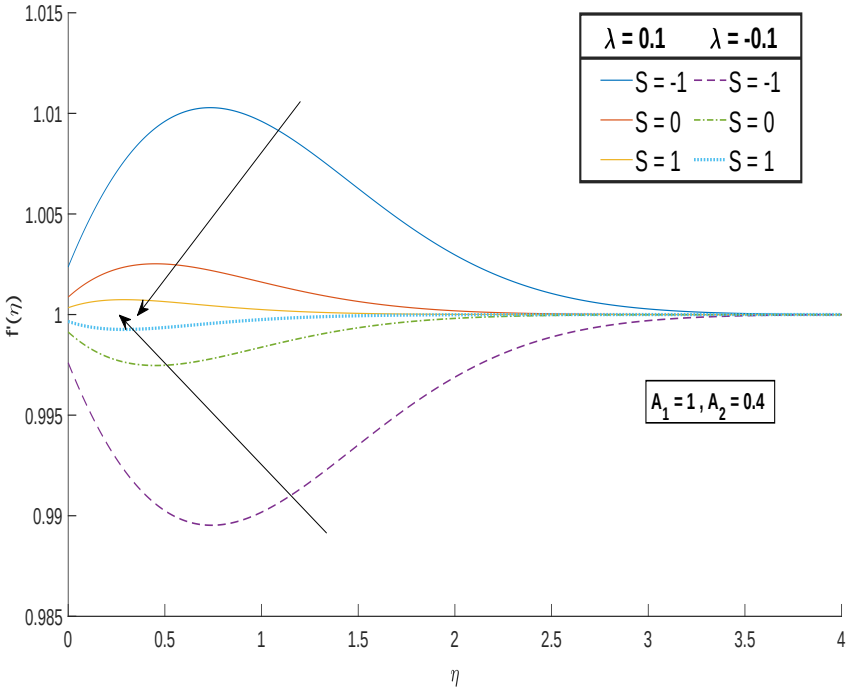

FIGURE 4.3: Variation in $f'(\eta)$ w.r.t. suction/injuction parameter S.

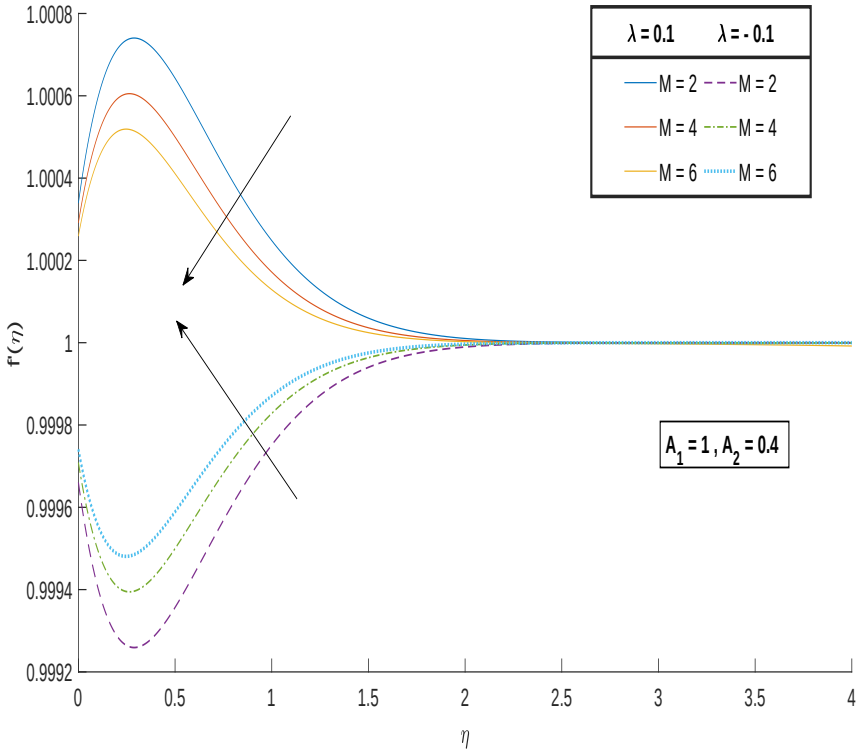

FIGURE 4.4: Variation in $f'(\eta)$ w.r.t. magnetic field parameter M .

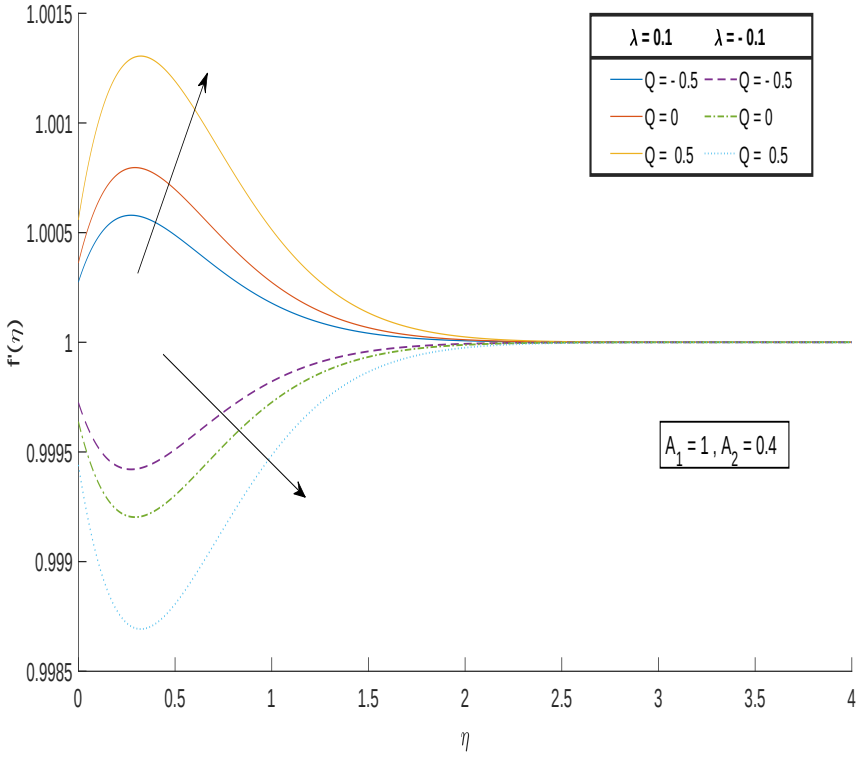

FIGURE 4.5: Variation in $f'(\eta)$ w.r.t. heat source/sink parameter Q .

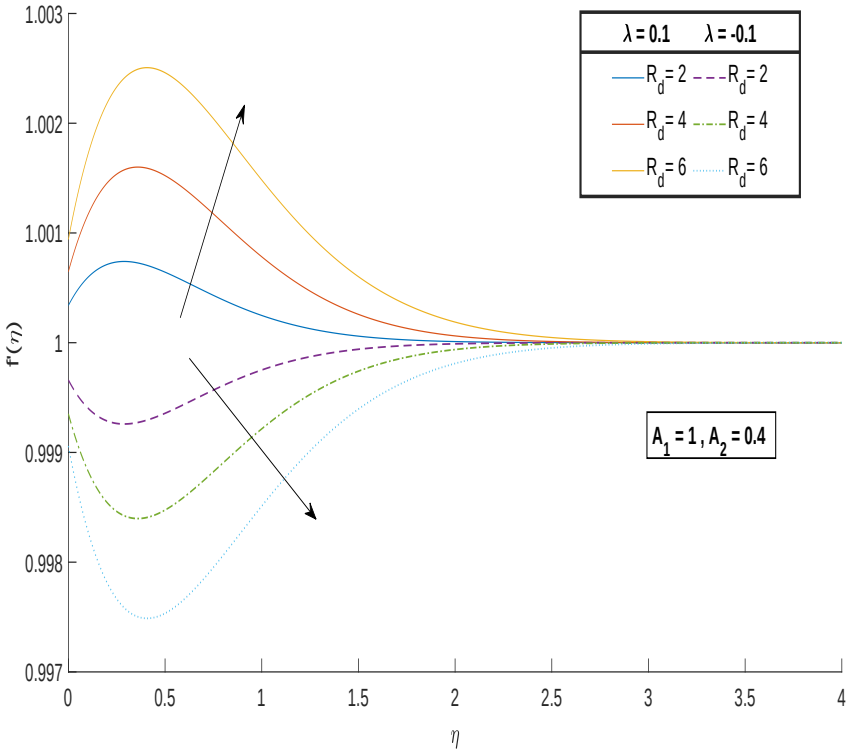

FIGURE 4.6: Variation in $f'(\eta)$ w.r.t. radiation parameter R_d.

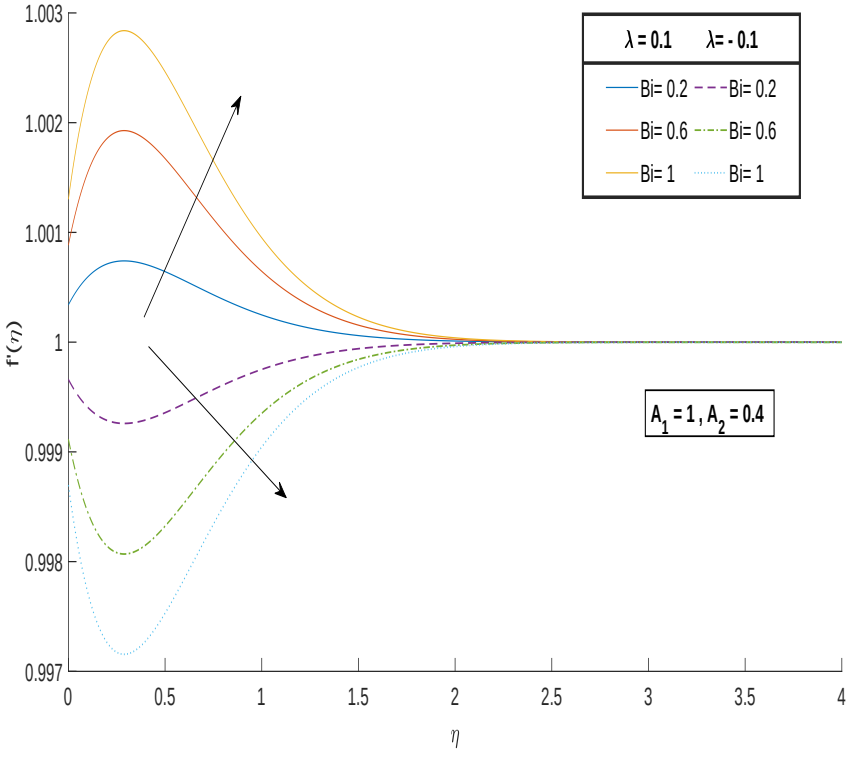

FIGURE 4.7: Variation in $f'(\eta)$ w.r.t. Biot number Bi.

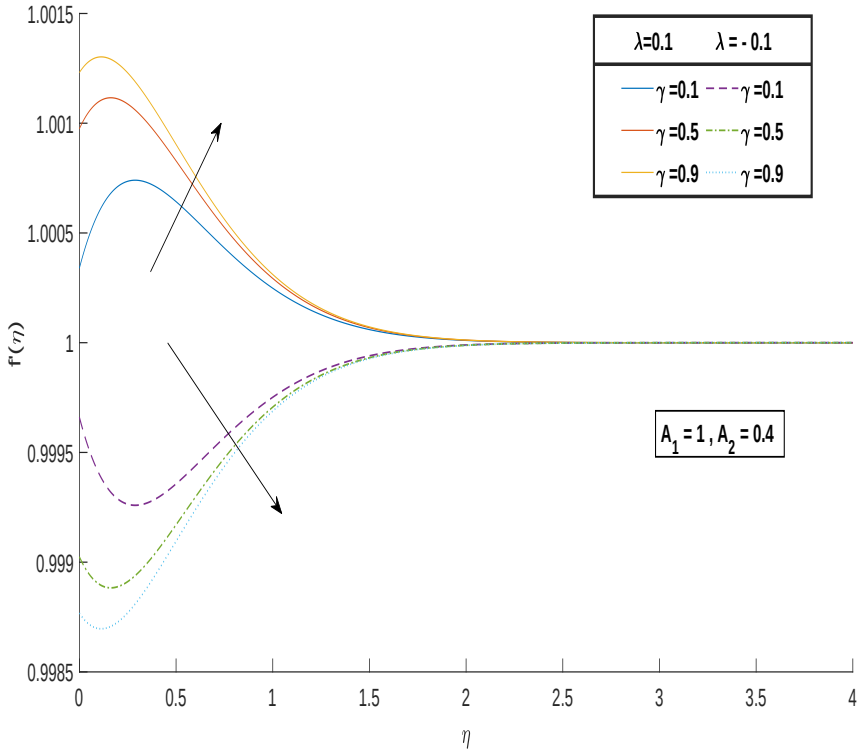

FIGURE 4.8: Variation in $f'(\eta)$ w.r.t. velocity slip parameter γ.

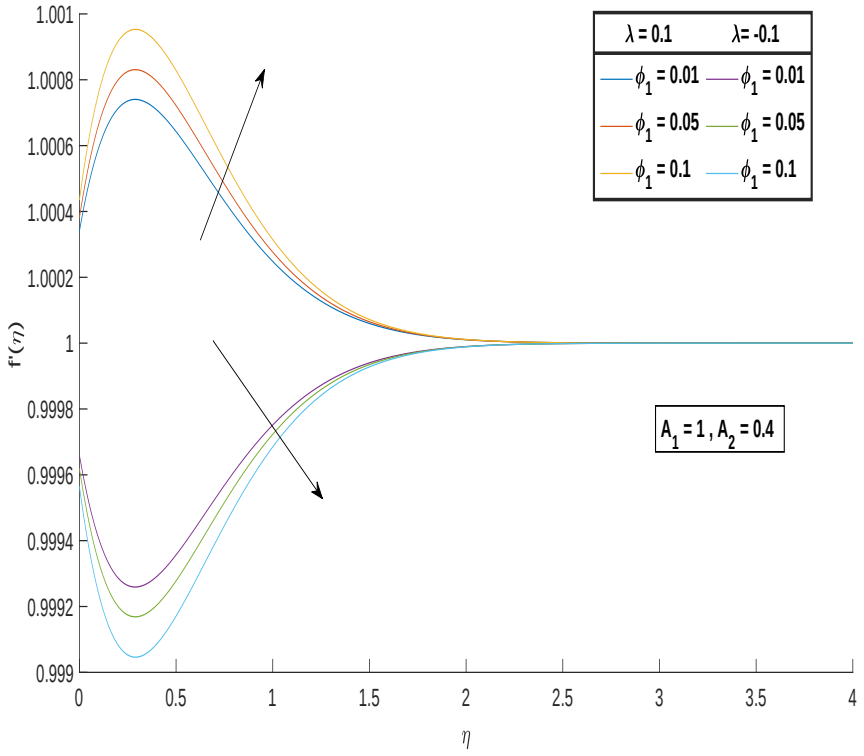

FIGURE 4.9: Variation in $f'(\eta)$ w.r.t. volume fraction of nanoparticles ϕ_1.

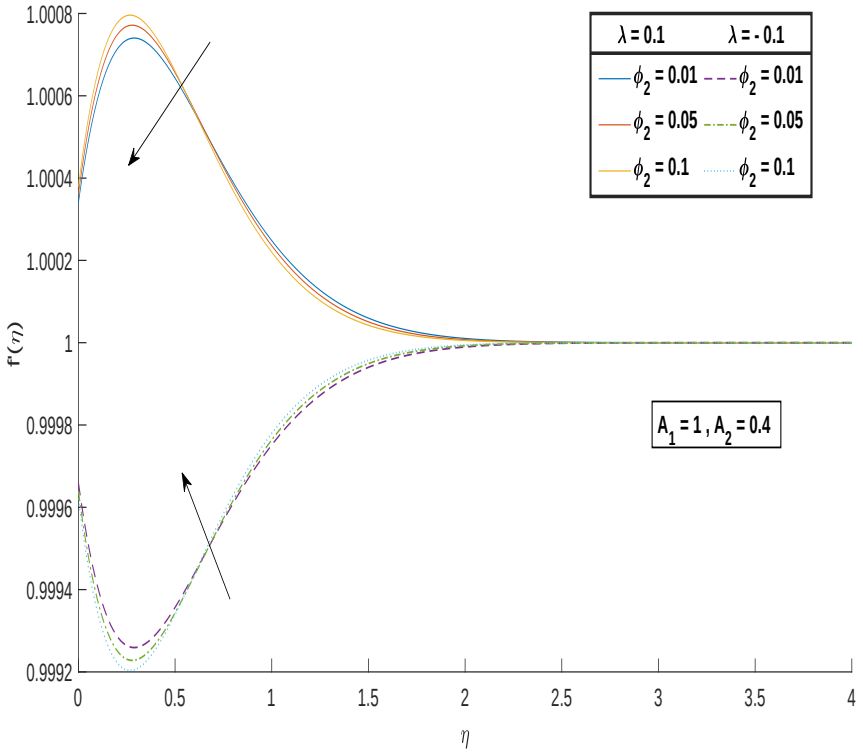

FIGURE 4.10: Variation in $f'(\eta)$ w.r.t. volume fraction of nanoparticles ϕ_2.

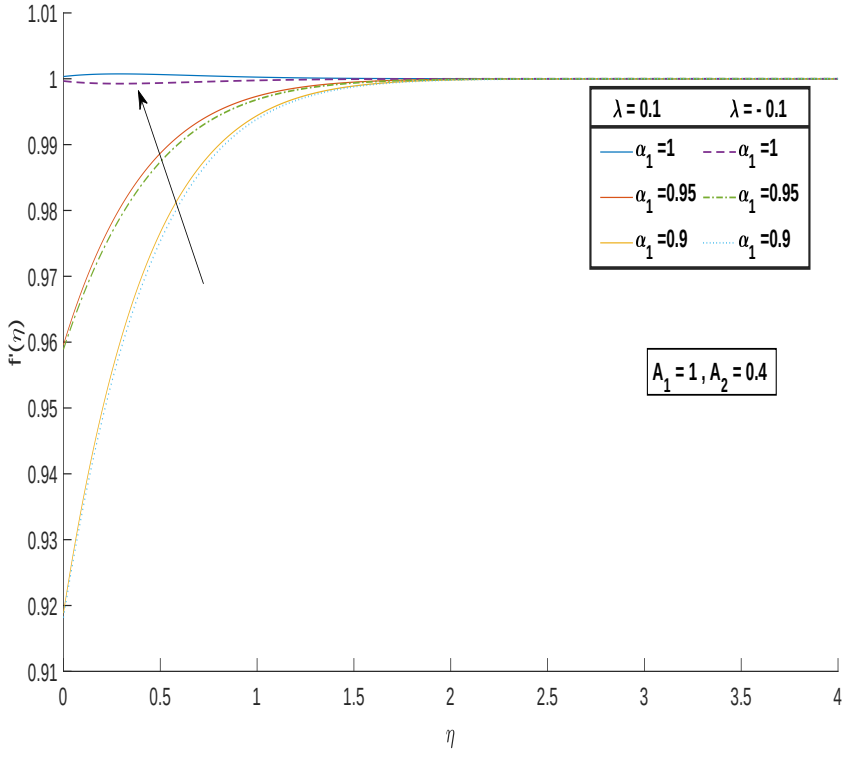

FIGURE 4.11: Variation in $f'(\eta)$ w.r.t. moving parameter α.

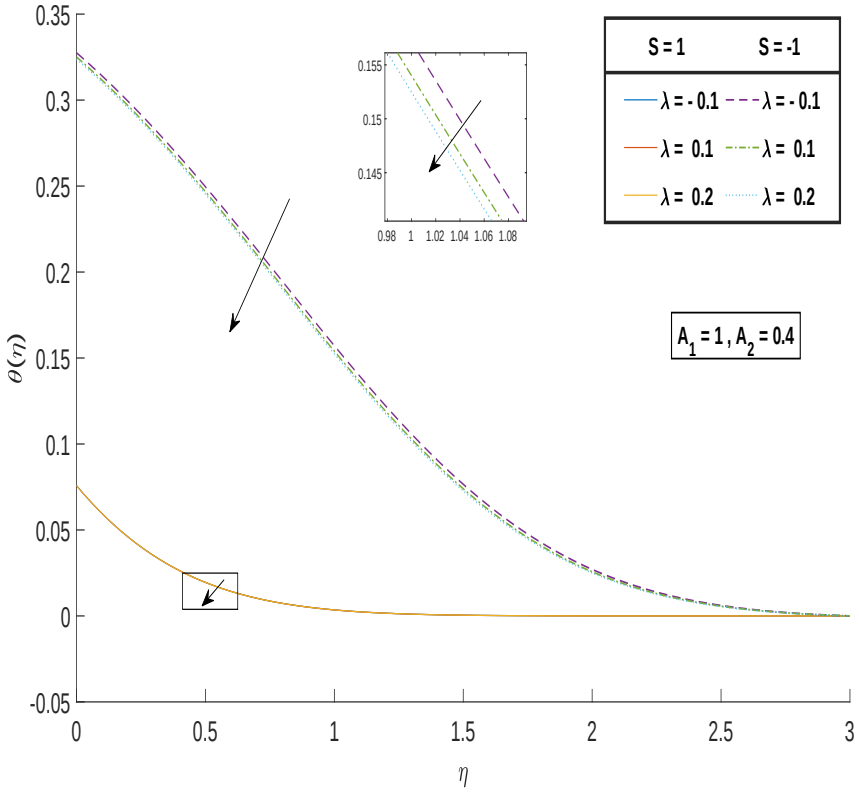

FIGURE 4.12: Variation in $\theta(\eta)$ w.r.t. local mixed convection λ .

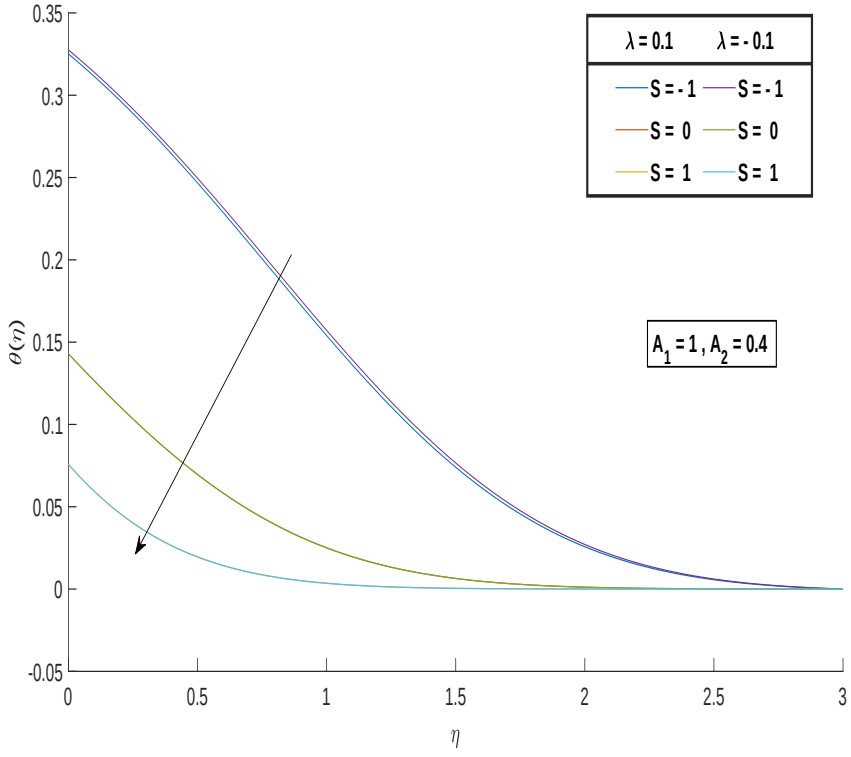

FIGURE 4.13: Variation in $\theta(\eta)$ w.r.t. suction/injuction parameter S.

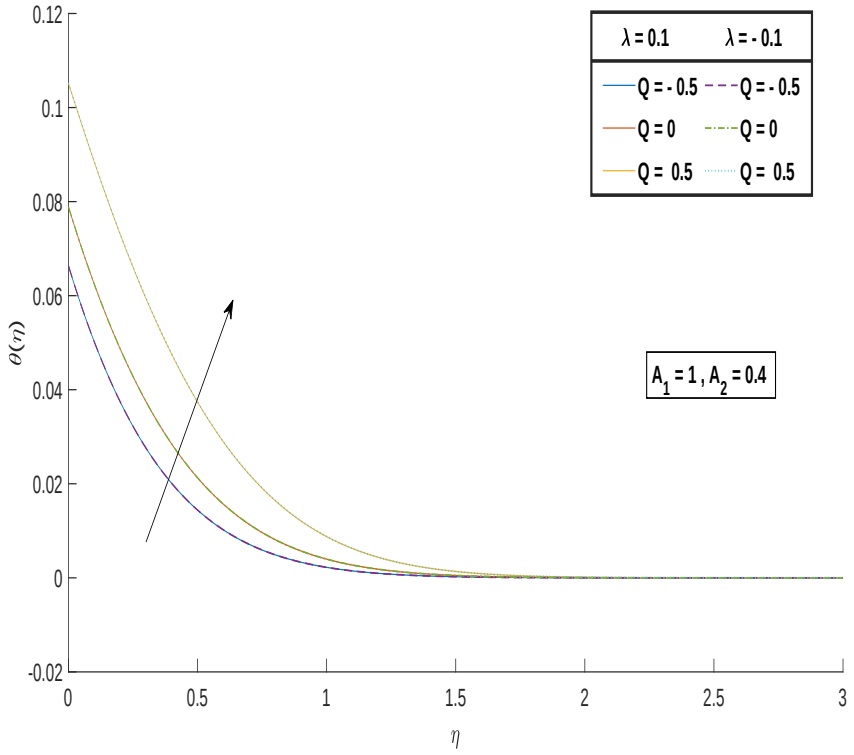

FIGURE 4.14: Variation in $\theta(\eta)$ w.r.t. heat source/sink parameter Q.

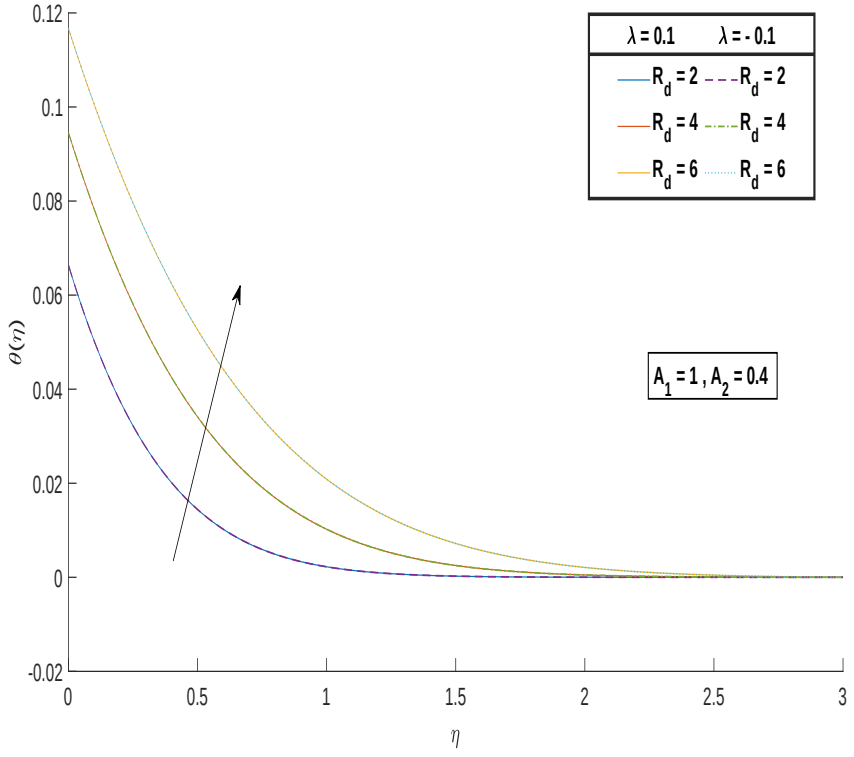

FIGURE 4.15: Variation in $\theta(\eta)$ w.r.t. radiation parameter R_d.

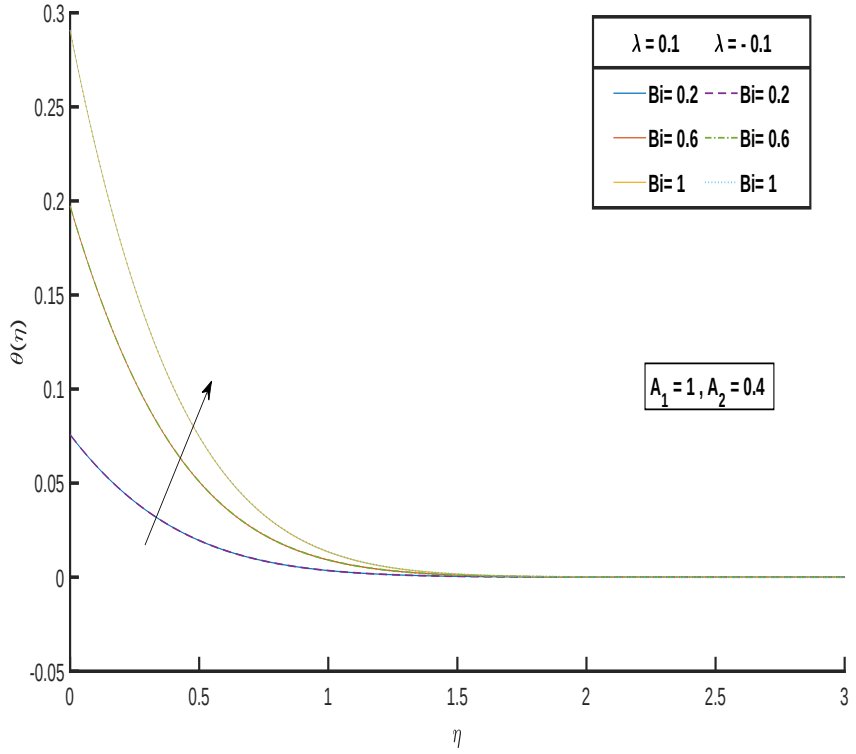

FIGURE 4.16: Variation in $\theta(\eta)$ w.r.t. Biot number Bi.

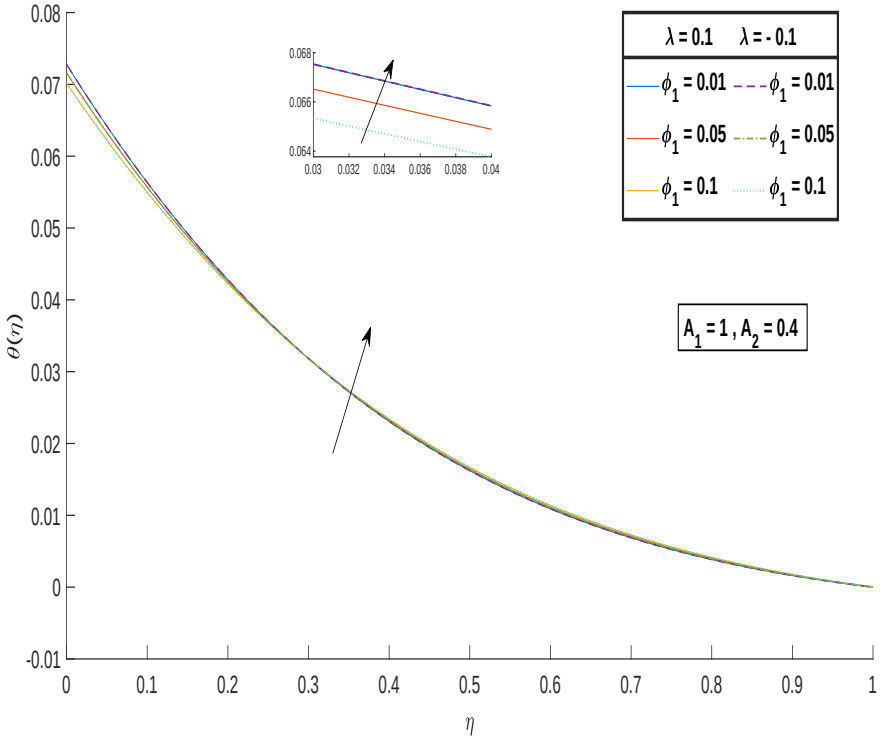

FIGURE 4.17: Variation in $\theta(\eta)$ w.r.t. volume fraction of nanoparticles ϕ_1.

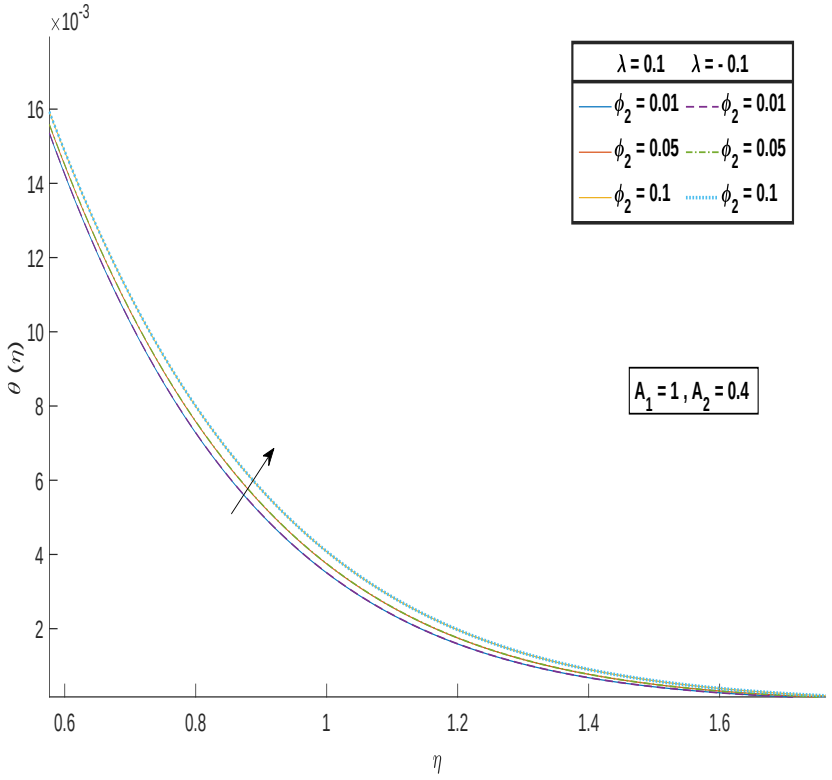

FIGURE 4.18: Variation in $\theta(\eta)$ w.r.t. volume fraction of nanoparticles ϕ_2.

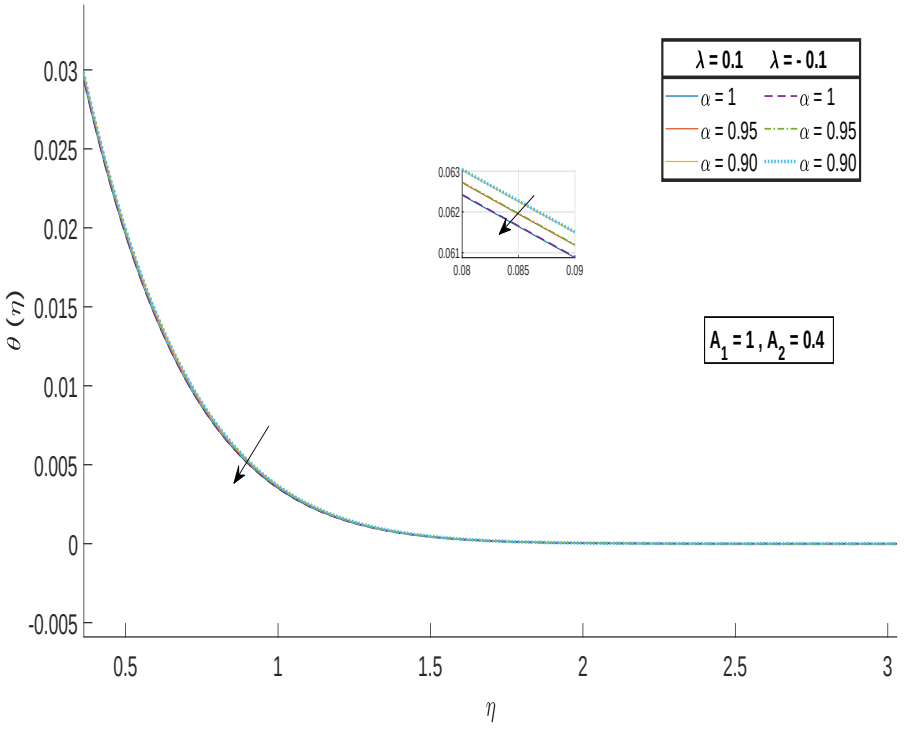

FIGURE 4.19: Variation in $\theta(\eta)$ w.r.t. α.

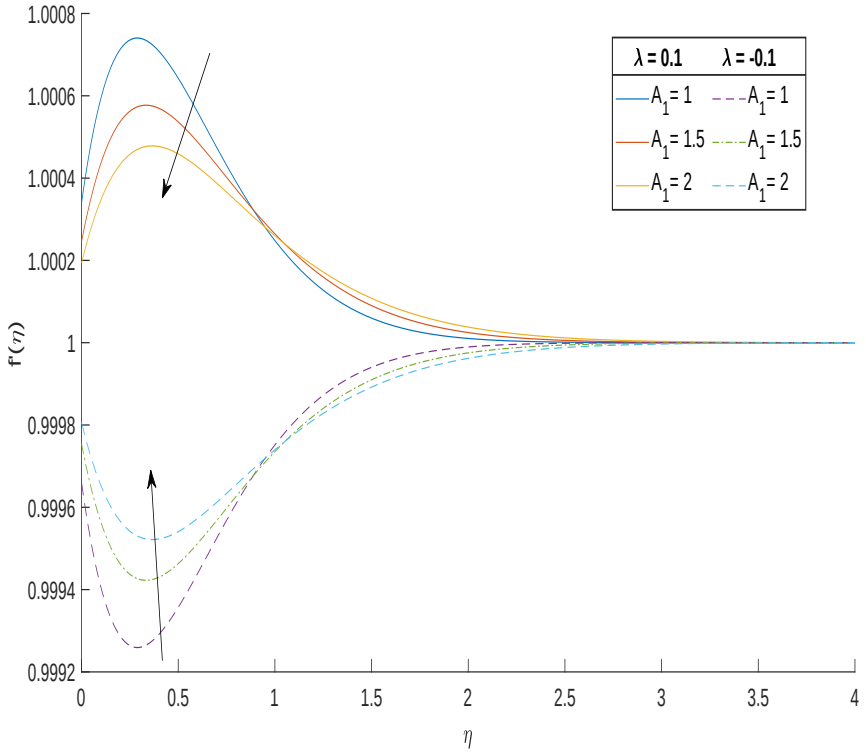

FIGURE 4.20: Variation in $f'(\eta)$ w.r.t. Prandtl Eyring parameter A_1.

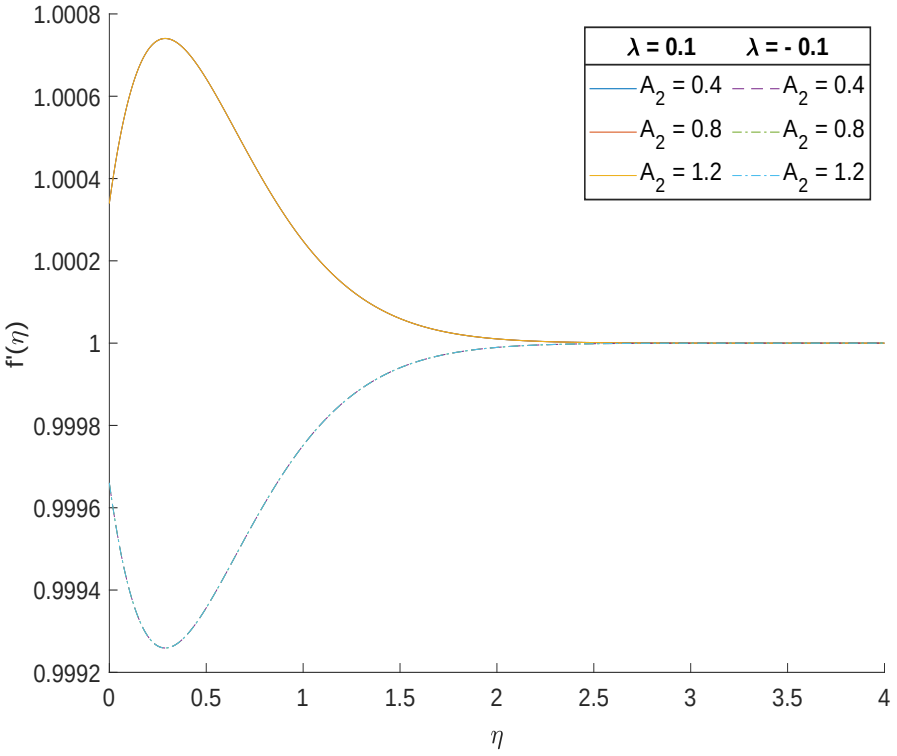

FIGURE 4.21: Variation in $f'(\eta)$ w.r.t. Prandtl Eyring parameter A_2.

Chapter 5

Conclusions

In this study, a model is created to examine the Prandtl-Eyring hybrid nanofluid flow on a moving surface with the impacts of thermal radiation and heat generation/abosorption. Velocity slip, suction/injection effects, and convective heating of the surface are further factors that affect boundary layer flow.
The prandle-Eyring hybrid nanofluid that is the subject of this work has thermophysical characteristics that are dependent on the volume fraction of nanoparticles ($SiO2 - MoS_2$/water). The following important conclusions were drawn from this study:

- The hybrid nano-fluid velocity is observed to be higher for assisting flow as compared to opposing flow.
- The temperature of the hybrid nanofluid is increased during flow by the volume fraction of both nanoparticles.
- For both assisting and opposing flow, slip parameter has opposite impacts on skin fraction coefficient and heat transfer coefficient.
- The increase in Q and Bi increases the temperature and heat transfer rate of the ($SiO2 - MoS_2$/water) hybrid nanofluid flow at the surface.
- Suction is observed to assist the process of heat transfer of hybrid nano-fluid ($SiO2 - MoS_2$/water) at the surface.

- It is noticed that the increment in Biot number enhances the value of skin friction coefficient.
- By increasing the magnetic parameter, the values of skin friction coefficient decreases.
- It is noticed that heat transfer coefficient nearly remains with increment in M.
- It is observed that heat transfer coefficient increase when values of Biot number increase.
- For the case of assisting flow , the velocity decreases as the values of Prandtl Eyring parameter-I increases, whereas for opposing flow the velocity increases as the values of Prandtl Eyring parameter-I increase.
- For different values of Prandtl Eyring parameter-II, the velocity profile remains same.

Bibliography

[1] Choi SUS. “Enhancing thermal conductivity of fluids with nanoparticles”, year 1995, institution Argonne National Lab.(ANL), Argonne, IL (United States).

[2] Tiwari RK, Das MK. “Heat transfer augmentation in a two-sided lid-driven differentially heated square cavity utilizing nanofluids”, International Journal of heat and Mass transfer, volume 50, number 9-10, pages 2002–2018, year 2007, publisher Elsevier.

[3] Buongiorno J. “Convective transport in nanofluids”, 2006; 128(3): 240-250.

[4] Safaei MR, Gooarzi M, Akbari OA, Shadloo MS, Dahari M. “Performance evaluation of nanofluids in an inclined ribbed microchannel for electronic cooling applications”, Electronics cooling, volume 832, year 2016, publisher InTech Croatia.

[5] Anderson Jr. JD. “Fundamentals of aerodynamics”, Forth Edittion, year2010, publisher Tata McGraw-Hill Education.

[6] Falodun BO, Fadugba SE. “Effects of heat transfer on unsteady magnetohydrodynamics (MHD) boundary layer flow of an incompressible fluid a moving vertical plate”, journal:World Scientific News, volume 88, number 2, pages 118–137, year 2017.

[7] Bachok N, Ishak A, Pop I. “Flow and heat transfer characteristics on a moving plate in a nanofluid”, International Journal of Heat and Mass Transfer, volume 55, number 4, pages 642–648, year 2012, publisher Elsevier.

[8] Najib N, Bachok N, Arifin NM, Senu N. "Boundary layer flow and heat transfer of nanofluids over a moving plate with partial slip and thermal convective boundary condition: Stability analysis", International Journal of Mechanics, volume 11, number 1, pages 18–24, year 2017.

[9] Rawat SK, Kumar M. "Cattaneo–Christov heat flux model in flow of copper water nanofluid through a stretching/shrinking sheet on stagnation point in presence of heat generation/absorption and activation energy", International Journal of Applied and Computational Mathematics, volume 6, pages 1–26, year 2020, publisher Springer.

[10] Shankar GB, Pramod KP, Malga BS. "Effect of heat source on an unsteady MHD free convection flow of Casson fluid past a vertical oscillating plate in porous medium using finite element analysis", journal:Partial Differential Equations in Applied Mathematics, volume 2, pages 100015, year 2020, publisher Elsevier.

[11] Waini I, Ishak A, Pop I. "Hybrid nanofluid flow and heat transfer over a nonlinear permeable stretching/shrinking surface", International Journal of Numerical Methods for Heat & Fluid Flow, volume 29, number 9, pages 3110–3127, year 2019, publisher:Emerald Publishing Limited.

[12] Waini I, Ishak A, Pop I. "Unsteady flow and heat transfer past a stretching/shrinking sheet in a hybrid nanofluid", International journal of heat and mass transfer, volume 136, pages 288–297, year 2019, publisher:Elsevier.

[13] Waini I, Ishak A, Pop I. "Hybrid nanofluid flow and heat transfer past a vertical thin needle with prescribed surface heat flux", International Journal of Numerical Methods for Heat & Fluid Flow, volume 29, number 12, pages 4875–4894, year 2019, publisher Emerald Publishing Limited.

[14] Waini I, Ishak A, Pop I. "Transpiration effects on hybrid nanofluid flow and heat transfer over a stretching/shrinking sheet with uniform shear flow", Alexandria Engineering Journal, volume 59, number 1, pages 91–99, year 2020, publisher:Elsevier.

[15] Waini I, Ishak A, Pop I. "MHD flow and heat transfer of a hybrid nanofluid past a permeable stretching/shrinking wedge", journal:Applied Mathematics and Mechanics, volume 41, number 3, pages 507–520, year 2020, publisher: Springer.

[16] , Waini I, Ishak A, Pop I. "Hybrid nanofluid flow and heat transfer over a nonlinear permeable stretching/shrinking surface", International Journal of Numerical Methods for Heat & Fluid Flow, volume 30, number 7, pages 3110–3127, year 2019, publisher: Emerald Publishing Limited.

[17] Waini I, Ishak A, Groan T, Pop I. "Mixed convection of a hybrid nanofluid flow along a vertical surface embedded in a porous medium", journal: International Communications in Heat and Mass Transfer, volume 114, pages 104565, year 2020, publisher: Elsevier.

[18] Kumar TS. "Hybrid nanofluid slip flow and heat transfer over a stretching surface", journal: Partial Differential Equations in Applied Mathematics, volume 4, pages 100070, year 2021, publisher: Elsevier.

[19] Kumar KG, Hani EHB, Assad MEH, Rahimi-Gorji M, Nadeem S. "A novel approach for investigation of heat transfer enhancement with ferromagnetic hybrid nanofluid by considering solar radiation", journal: Microsystem Technologies, volume 27, pages 97–104, year 2021, publisher Springer.

[20] Shoaib M, Raja MAZ, Sabir MT, et al. "Numerical investigation for rotating flow of MHD hybrid nanofluid with thermal radiation over a stretching sheet", journal: Scientific Reports, volume 10, number 1, pages 18533, year 2020, publisher: Nature Publishing Group UK London.

[21] Roy NC, Saha LK, Sheikholeslami M. "Heat transfer of a hybrid nanofluid past a circular cylinder in the presence of thermal radiation and viscous dissipation", journal: AIP Advances, volume 10, number 9, pages 095208, year 2020, publisher: AIP Publishing LLC.

[22] Khan U, Shafiq A, Zaib A, Baleanu D "Hybrid nanofluid on mixed convective radiative flow from an irregular variably thick moving surface with convex and

concave effects", journal: Case Studies in Thermal Engineering, volume 21, pages 100660, year 2020, publisher Elsevier.

[23] Subhani M, Nadeem S. "Numerical analysis of micropolar hybrid nanofluid", journal: Applied Nanoscience, volume 9, number 4, pages 447–459, year 2019, publisher: Springer.

[24] Khashiie NS, Arifin NM, Nazar R EH, Wahi N, Pop I. "Magnetohydrodynamics (MHD) axisymmetric flow and heat transfer of a hybrid nanofluid past a radially permeable stretching/shrinking sheet with Joule heating", Chinese Journal of Physics, volume 64, pages 251–263, year 2020, publisher: Elsevier.

[25] Khashiie NS, Arifin NM, Wahi N, Pop I, Nazar R, Hafidzuddin EH. "Thermal Marangoni flow past a permeable stretching/shrinking sheet in a hybrid Cu-Al", journal: Sains Malaysiana, volume 49, number 1, pages 211–222, year 2020.

[26] Shojaie Chahregh H, Dinarv S. "TiO2-Ag/blood hybrid nanofluid flow through an artery with applications of drug delivery and blood circulation in the respiratory system", International Journal of Numerical Methods for Heat & Fluid Flow, volume 30, number 11, pages 4775–4796, year 2020, publisher: Emerald Publishing Limited.

[27] Muhammad K, Hayat T, Alsaedi A, Ahmad B. "Numerical study of entropy production minimization in Bödewadt flow with carbon nanotubes", journal: Physica A: Statistical Mechanics and its Applications, volume 550, pages 123966, year 2020, publisher: Elsevier.

[28] Shafee A, Sheikholeslami M, Jafaryar M, Babazadeh H. "Irreversibility of hybrid nanoparticles within a pipe fitted with turbulator", Journal of Thermal Analysis and Calorimetry, volume 143, pages 715–723, year 2021, publisher: Springer.

[29] Davidson PA, Belova EV. "An introduction to magnetohydrodynamics", year 2002, publisher: American Association of Physics Teachers.

[30] Kumar KA, Sugunamma V, Sandeep N, Mustafa MT. "Simultaneous solutions for first order and second order slips on micropolar fluid flow across a convective surface in the presence of Lorentz force and variable heat source/sink", journal: Scientific reports, volume 9, number 1, pages 14706, year 2019, publisher: Nature Publishing Group UK London.

[31] Tlili I, Mustafa MT, Kumar KA, Sandeep N. "Effect of asymmetrical heat rise/fall on the film flow of magnetohydrodynamic hybrid ferrofluid" journal: Scientific reports, volume 10, number 1, pages 1–11, year 2020, publisher Springer.

[32] Mishra A, Kumar M. "Thermal performance of MHD nanofluid flow over a stretching sheet due to viscous dissipation, Joule heating and thermal radiation", International Journal of Applied and Computational Mathematics, volume 6, number 4, pages 123, year 2020, publisher Springer.

[33] Akolade MT. "Thermophysical impact on the squeezing motion of non-Newtonian fluid with quadratic convection, velocity slip, and convective surface conditions between parallel disks", journal: Partial differential equations in applied mathematics, volume 4, pages 100056, year 2021, publisher: Elsevier.

[34] Anantha KK, R Reddy JV, Sandeep N. "Magnetohydrodynamic Cattaneo-Christov flow past a cone and a wedge with variable heat source/sink", Alexandria Eng, journal J, volume 57, pages 435–443, year 2018.

[35] Kempannagari AK, Buruju RR, Naramgari S, Vangala S. "Effect of Joule heating on MHD non-Newtonian fluid flow past an exponentially stretching curved surface", journal: Heat Transfer, volume 49, number 6, pages 3575–3592, year 2020, publisher: Wiley Online Library.

[36] Ahmad S, Nadeem S. "Thermal analysis in buoyancy driven flow of hybrid nanofluid subject to thermal radiation", International Journal of Ambient Energy, volume 43, number 1, pages 3868–3876, year 2022, publisher: Taylor & Francis.

[37] Anantha KK, Sugunamma V, Sandeep N. "Influence of viscous dissipation on MHD flow of micropolar fluid over a slendering stretching surface with modified heat flux model", Journal of Thermal Analysis and Calorimetry, volume 139, pages 3661–3674, year 2020, publisher Springer.

[38] Alharbi SO, Nawaz M, Nazir U. "Thermal analysis for hybrid nanofluid past a cylinder exposed to magnetic field", journal: AIP Advances, volume 9, number 11, pages 115022, year 2019, publisher: AIP Publishing LLC.

[39] Anantha KK, Sugunamma V, Sandeep N. "Effect of thermal radiation on MHD Casson fluid flow over an exponentially stretching curved sheet", Journal of Thermal Analysis and Calorimetry, volume 140, pages 2377–2385, year 2020, publisher: Springer.

[40] Venkateswarlu B, S Narayana PV. "Cu-Al2O3/H2O hybrid nanofluid flow past a porous stretching sheet due to temperatue-dependent viscosity and viscous dissipation", journal Heat Transfer, volume 50, number 1, pages 432–449, year 2021, publisher: Wiley Online Library.

[41] Kumar A, Sugunamma V, Sandeep N. "Impact of non-linear radiation on MHD non-aligned stagnation point flow of micropolar fluid over a convective surface", Journal of Non-Equilibrium Thermodynamics, volume 43, number 4, pages 327–345, year 2018, publisher De Gruyter.

[42] Anantha KK, Sugunamma V, Sandeep N. "Physical aspects on unsteady MHD-free convective stagnation point flow of micropolar fluid over a stretching surface", journal: Heat TransferAsian Research, volume 48, number 8, pages 3968–3985, year 2019, publisher: Wiley Online Library.

[43] Anantha KK, Sugunamma V, Sandeep N, Ramana RJV. "Numerical examination of MHD nonlinear radiative slip motion of non-newtonian fluid across a stretching sheet in the presence of a porous medium", journal: Heat Transfer Research, volume 50, number 12, year 2019, publisher: Begel House Inc.

[44] Zainal NA, Pop I, Nazar R, Naganthran K. "MHD flow and heat transfer of hybrid nanofluid over a permeable moving surface in the presence of thermal

radiation", International Journal of Numerical Methods for Heat & Fluid Flow, volume 31, number 3, pages 858–879, year 2021, publisher: Emerald Publishing Limited.

[45] Waini I, Ishak A, Pop I. "Flow and heat transfer of a hybrid nanofluid past a permeable moving surface", Chinese Journal of Physics", volume 66, pages 606–619, year 2020, publisher: Elsevier.

[46] Aziz A. "A similarity solution for laminar thermal boundary layer over a flat plate with a convective surface boundary condition", Commun Nonlinear Sci Numer Simul pages 1064-1068, volume 14, number 4, year 2009.

[47] Rana P, Mahanthesh B, Mackolil J, Al-Kouz W. "Nanofluid flow past a vertical plate with nanoparticle aggregation kinematics, thermal slip and significant buoyancy force effects using modified Buongiorno model", journal: Waves in Random and Complex Media, pages 1–25, year 2021, publisher Taylor & Francis.

[48] Yaseen M, Rawat SK, Kumar M. "Hybrid nanofluid (MoS2–SiO2/water) flow with viscous dissipation and Ohmic heating on an irregular variably thick convex/concave-shaped sheet in a porous medium", journal: Heat Transfer, volume 51, number 1, pages 789–817, year 2022, publisher: Wiley Online Library.

[49] Shampine LF, Gladwell I, Thompson S. "Solving ODEs with MATLAB", year 2003, publisher Cambridge University Press.

[50] RW Fox, A McDonald, and P Pitchard. Introduction to Fluid Mechanics, 2004, year 2006, publisher: John Wiley & Sons, Inc.

[51] R Bansal. "A textbook of fluid mechanics", year 2005, publisher: Firewall Media.

[52] JN Reddy and DK Gartling. "The finite element method in heat transfer and fluid dynamics", year 2010, publisher CRC press.

[53] PA Davidson and A Thess. "Magnetohydrodynamics", volume 418, year 2002, publisher: Springer Science & Business Media.

[54] RW Fox, AT McDonald, and PJ Pritchard. "Introduction to fluid mechanics", john wiley&sons, journal: Inc., New York, year 1994.

[55] Y Cengel and J Cimbala. EBOOK: Fluid Mechanics Fundamentals and Applications (SI units), year 2013, publisher: McGraw Hill.

[56] J Kunes. "Dimensionless physical quantities in science and engineering", year 2012, publisher: Elsevier.

[57] Sanders CJ, Holman JP. "Franz Grashof and the Grashof number", International Journal of Heat and Mass Transfer, volume 15, number 3, pages 562–563, year 1972, publisher: Pergamon.

[58] M Yaseen, SK Rawat, Sawan K and M Kumar. "Assisting and opposing flow of a MHD hybrid nanofluid flow past a permeable moving surface with heat source/sink and thermal radiation", journal: Partial Differential Equations in Applied Mathematics, volume 4, pages 100168, year 2021, publisher: Elsevier.

[59] Versteeg HK and Malalasekera. "Computational fluid dynamics", journal: The finite volume method, pages 1–26, year 1995.

[60] J Wasim, D Baleanu, M Nasir, F Shahzad, KS Nisar, M Shoaib, S Ahmad, Sohail,KA Ismail. "The improved thermal efficiency of Prandtl–Eyring hybrid nanofluid via classical Keller box technique", journal: Scientific reports, volume 11, number 1, pages 23535, year 2021, publisher Nature Publishing Group UK London.